AER/AGS Special Report 126

Alberta Energy Regulator

Analysis of Hyperspectral Imagery Collected from Drillcore from Alberta Using the Lithotype™ Method

AGS
ALBERTA GEOLOGICAL SURVEY

AER/AGS Special Report 126

Analysis of Hyperspectral Imagery Collected from Drillcore from Alberta Using the Lithotype™ Method

M.C. Tappert, D.M. Rogge and R. Tappert

Hyperspectral Intelligence Inc.

August 2025

ISBN 978-1-4601-5730-5

Tappert, M.C., Rogge, D.M. and Tappert, R. (2025): Analysis of hyperspectral imagery collected from drillcore from Alberta using the Lithotype™ method; Alberta Energy Regulator / Alberta Geological Survey, AER/AGS Special Report 126, 57 p.

Authors address:
M.C. Tappert, D.M. Rogge and R. Tappert
Hyperspectral Intelligence Inc.
Box 851
Gibsons, BC V0N 1V0
Canada

Tel: 604.399.0019
Email: michelle@hyperspectral-intelligence.com

Published August 2025 by:
Alberta Energy Regulator
Alberta Geological Survey
Suite 205
4999 – 98 Avenue NW
Edmonton, AB T6B 2X3
Canada

Tel: 780.638.4491
Email: AGS-Info@aer.ca
Website: ags.aer.ca

Contents

Foreword

The Alberta Geological Survey (AGS) contracted Hyperspectral Intelligence Inc. (HII) to process and analyze an existing dataset of hyperspectral imagery of archived mineral drillcores stored at the AGS Mineral Core Research Facility in Edmonton, Alberta. Hyperspectral Intelligence Inc. analyzed a total scan length of 50 842.61 m from 805 drillcores. These cores were drilled during previous mineral exploration projects to target a variety of commodities and intervals of interest, including gold, diamonds, lithium brines, uranium, base metals, polymetallic shale, potash, evaporites, kimberlite-indicator minerals, titanium, platinum, silver, copper, zinc, lead, oil sands, and zones of potential mineralization or hydrothermal alteration. The drillcores selected for this project intersect a variety of lithologies and stratigraphic intervals from the Precambrian basement, Paleozoic carbonate rocks and evaporites, Mesozoic fine- and coarse-grained siliciclastic rocks, through to Quaternary sediments. The core locations are distributed across the Athabasca Basin, Canadian Shield, and Western Canada Sedimentary Basin within Alberta. The hyperspectral imagery analyzed for this project was originally collected between November 2021 and February 2022 for a project under the AGS Mineral Mapping Program, in which the AGS contracted Spectrum Geosciences Ltd. to scan the drillcores using TerraCore Geospectral Imaging's hyperspectral core imaging system. In 2024, the resultant hyperspectral imagery dataset was reprocessed by HII using its proprietary tools and Lithotype™ method. To effectively apply the Lithotype method to meaningfully related subsets of drillcore, this large dataset was subdivided into seven categories, based on allocations to the AGS's Geological Framework of Alberta: (1) Archean and Paleoproterozoic - Athabasca Basin; (2) Archean and Paleoproterozoic - Canadian Shield; (3) Cambrian, Lower Ordovician, and Silurian; (4) Devonian; (5) Carboniferous to Jurassic; (6) Cretaceous; (7) Paleogene to Quaternary.

The Lithotype method was applied separately to each subset of cores to produce outputs that can be used to better understand the compositional characteristics of Alberta's geological units in a mineral exploration and stratigraphic context.

This work was completed under the Mineral Grant provided by the Government of Alberta dated June 22, 2021.

Analysis of hyperspectral imagery collected from drill core from Alberta (Canada) using the Lithotype™ Method

Michelle Tappert, Derek Rogge, Ralf Tappert

Hyperspectral Intelligence, Gibsons, BC, Canada

E-mail: michelle@hyperspectral-intelligence.com

Abstract

Hyperspectral imaging techniques are currently being applied to overcome challenges associated with traditional visual drill core logging, which is a highly subjective process. However, hyperspectral imaging systems typically produce very large data volumes, and their outputs often lack sufficient sensitivity and can be difficult to integrate into existing workflows. Therefore, a novel method of data processing has been developed to reduce the data volumes of hyperspectral imaging datasets by >97% to make them easier to manage and analyze. For this project, hyperspectral imagery collected from 805 drill cores from Alberta, totalling approximately 50,840 meters, were divided into seven chronostratigraphic intervals of interest for data reduction and analysis using the Lithotype™ Method. This method identifies compositional groups to produce spectral logs that can be used to generate more accurate correlations between drill cores, minimizing the subjective challenges of visual drill core logging. The resulting spectral logs can also be used to better understand the compositional characteristics of rocks in the context of mineral exploration and mining. The primary goal of this project was to generate additional value from hyperspectral imagery that was previously collected from drill core.

1. Introduction

To help mineral exploration and mining companies accurately and rapidly identify rocks, Hyperspectral Intelligence Inc. (HII) has developed a novel method of processing hyperspectral data called the Lithotype™ Method that identifies distinct, mappable rock compositions, where each unique composition is referred to as a lithotype. A lithotype represents a combination of the original lithology, and alteration and mineralization that has occurred. The main benefit of using the Lithotype™ Method is that it identifies distinct rock compositions at a much higher sensitivity level than typical mineral mapping methods, while also producing outputs that allow for the straightforward correlation of distinct compositional units between drill cores. Overall, the outputs produced using the Lithotype™ Method allow for more effective resource identification.

For this project, hyperspectral imagery was collected from 805 drill cores, with a total scan length of 50,842.61 meters, by Spectrum Geosciences Ltd. using the TerraCore Hyperspectral Core Imaging system between November 2021 and February 2022 for a project under the AGS Mineral Mapping Program. This hyperspectral imagery was reprocessed by HII in 2024 using its proprietary tools and Lithotype™ Method. To effectively apply the Lithotype™ Method, the province of Alberta was divided into seven chronostratigraphic intervals of

interest. The Lithotype™ Method was applied separately to each chronostratigraphic interval to produce outputs that can be used to better understand the compositional characteristics of Alberta in the context of critical mineral identification and exploration. The primary goal of this project was to generate additional value from existing hyperspectral imagery that had been previously collected from drill core.

1.1 Chronostratigraphic Intervals of Interest

The seven chronostratigraphic intervals of interest for Alberta are listed in Table 1-1. These intervals were generated by the AGS for the purpose of this project and are based on intersections of the boreholes with surfaces in the Geological Framework of Alberta. The Target Commodities listed for each interval were also provided by the AGS.

Table 1-1. Chronostratigraphic intervals used to process hyperspectral data from Alberta using the Lithotype™ Method. In total, 805 drill cores and approximately 50,840 meters of hyperspectral data were analyzed for this project.

Chronostratigraphic Interval	No. of Drill Cores	Meters Analyzed	Location	Target Commodities*
Archean and Paleoproterozoic	145	24,321	Athabasca Basin	Unconformity-Associated Uranium, Li-Brine Source Regions, Potential Mineralization, and Diamonds
Archean and Paleoproterozoic	27	970	Canadian Shield	Li-Brine Source Regions, Potential Mineralization and Sources of Mineralization, and Diamonds
Cambrian, Lower Ordovician, Silurian	18	990	WCSB	Base Metal Mineralization, Potential Mineralization/Sources of Mineralization, and Uranium
Devonian	145	5,201	WCSB	Diamonds, Gold, Li Brine Source Regions, Potash/Evaporites, Base Metal Mineralization, Hydrothermal Alteration/Mineralization, Polymetallic Shales, Silver, Platinum, Copper, Zinc, Lead, Uranium, and Oil Sands
Carboniferous-Jurassic	32	616	WCSB	Li Brine Source Regions, Potential Hydrothermal Alteration/Mineralization, and Polymetallic Shales
Cretaceous	285	11,972	WCSB	Hydrothermal Alteration/Mineralization, Li Brine Source Regions, Polymetallic Shales, Base Metal Mineralization, Gold, Diamonds, Oil Sands, Titanium, and Uranium (Sandstone-Hosted and Unconformity-Related)
Paleogene-Quaternary	153	6,770	WCSB	Polymetallic Shales, Gold, Diamonds, Kimberlite Indicator Minerals, Titanium, Oil Sands, and Uranium

*Information, including target commodities, were provided by the AGS

1.2 Data Collection

Hyperspectral data were collected at the Spectrum Geosciences facilities in Calgary, Alberta, between November 2021 and February 2022 using the TerraCore Hyperspectral Core Imaging system, which has three hyperspectral imaging cameras:

SPECIM FX10 - Visible to Near-Infrared
(VNIR: 400-1000 nm)

- Wavelength Range: 400 nm – 1000 nm
- Spectral Bands (collected): 93
- Spectral Bands (output): 112
- Spectral resolution: 5.5 nm (mean)
- Spatial resolution (pixel size): 0.45 mm (resampled to 1.13 mm)
- Light Source: Halogen lamp illumination

SPECIM SWIR3 - Short-Wave Infrared
(SWIR: 1000-2500 nm)

- Wavelength Range: 1000 nm – 2500 nm
- Spectral Bands (collected): 288
  Spectral Bands (output): 251
- Spectral Resolution: 12 nm
- Spatial resolution (pixel size): 1.13 mm
- Light Source: Halogen lamp illumination

SPECIM OWL - Long-Wave Infrared
(LWIR: 8000-12000 nm)

- Wavelength Range: 8000 nm – 12000 nm
- Spectral Bands (collected): 100
- Spectral Bands (output): 288
- Spectral resolution: 100 nm
- Spatial resolution (pixel size): 1.13 mm
- Light Source: Thermal heating bar illumination

During data collection by Spectrum Geosciences, standard system corrections were applied to from radiance to reflectance to all camera image data using the white and dark reference files. Data were subset to their active wavelength ranges, and the data were converted produce hyperspectral image cubes in a BIL format (Band Interleaved by Line) with associated ENVI-compatible header files. Data QA/QC by Spectrum Geosciences included daily camera reviews, image data reviews for quality, focus, geometry, and scan completion.

1.3 Hyperspectral Data Processing

To efficiently analyze hyperspectral imagery collected from drill core, HII used several in-house tools to accomplish the following tasks:

(1) Data Reduction, wherein data volumes are reduced by >97%, making the resulting files much easier to store, manage, transfer, and process.

(2) Library Creation, wherein the VNIR, SWIR, and LWIR imagery is converted to downhole reflectance profile libraries so that ~900 spectra are output for each meter of drill core, which equates to a ~1 mm spatial resolution (pixel size).

(3) Library Conversion, wherein the three reflectance profile libraries generated for each drill core (VNIR, SWIR, and LWIR) are merged to produce a single spectral library file for each drill core. Each spectrum is labelled with relevant information, such as the drill core box, drill core row, and depth. The libraries are saved as ENVI-formatted spectral libraries using the 16-bit unsigned integer data type.

(4) Lithotype Identification, wherein a spectral library is created for each geographical region of interest which is organized according to lithotype.

(5) Lithotype Mapping, wherein the lithotype spectral library is used to classify the hyperspectral data from that same geographical region to produce a spectral log, which is presented as a sorted, stacked, horizontal bar graph with a depth binning interval of one meter. The spectral logs show the relative frequency of each lithotype between 0 and 1 for each one-meter depth interval, with the outputs provided in three data formats (PNG, EPS, and CSV).

1.4 Deliverables and Disclaimer

The primary goals of this work are to increase the accessibility of existing hyperspectral data, improve the efficiency of resource identification and mapping, and enhance the public understanding of Alberta's mineral resources. Although the spectral logs produced using the Lithotype™ Method are reproducible and can be validated using auxiliary data, it is the responsibility of the qualified geologist working on a project to ensure that the results of all data sources have been reviewed and considered. Therefore, it is strongly suggested that the spectral logs generated by the Lithotype™ Method be used in combination with other data sources to validate and critique the spectral results, with the goal of ensuring that all outputs are robust and reproducible.

To assist with this task, HII has provided its deliverable files in a variety of easy-to-use output formats and file types that allow the downstream user to have several options when it comes to further use, analysis, and presentation.

Each drillhole folder uploaded to the AER cloud contains per box and full drill hole spectral profile libraries (ENVI Spectral Library, Unsigned integer 16-bit) for VNIR, SWIR and LWIR data:

- Box depths are included in a separate depth file
- Box libraries are labeled as:
  specrange_drillhole_boxnumber_spec
- Full drill hole libraries are labeled as:
  specrange_drillhole_spec

- Depths file labeled as:
  specrange_drillhole_depths.csv

Each deliverables folder contains drillhole spectral logs including:

- *_llog.eps - drill hole spectral log image with legend in eps format
- *_llog.png - drill hole spectral log image with legend in png format
- *_log.csv - drill hole spectral log tabular data in csv format
- *_log.eps - drill hole spectral log image in eps format
- *_log.png - drill hole spectral log image in png format
- *_log_LithXX.eps - lithotype X profile log image in eps format
- *_log_LithXX.png - lithotype X profile log image in png format

2. Archean and Paleoproterozoic - Athabasca Basin

2.1 Overview

The Athabasca Basin is a globally recognized source for uranium deposits. It is a Paleoproterozoic sedimentary basin that consists of a sequence of unmetamorphosed sandstones, conglomerates, and associated sedimentary rocks that were deposited in a relatively shallow marine to fluvial environment (e.g., Kupsch and Catuneanu, 2002; Ramaekers, 2004; and references therein). Sedimentary rocks overlie the crystalline basement, and high-grade unconformity-related uranium deposits are typically found at the unconformity between the basin sandstones and the basement rocks (Collier, 2004). In northeastern Alberta, the basin contains sedimentary rocks from the Quaternary, Devonian, and Paleoproterozoic (i.e., Athabasca Group), which are underlain by Paleoproterozoic and Archean basement rocks that have been identified as granitoids, gneisses, and mylonites (Wilson, 1986).

Table 2-1. Drill cores of Archean and Paleoproterozoic rocks of the Athabasca Basin analyzed in this study.

Borehole ID	Number of Boxes	Start Depth (m)	End Depth (m)	Total Length (m)
DDH-1	20	62	125	63
DDH-2	28	25.908	91.44	65.53
FC-001	10	63.1	346.4	283.3
FC-002	13	46.2	264.3	218.1
FC-003	59	38.5	906.7	868.2
FC-004	105	26.2	919.2	893
FC-005	393	30.5	847.6	817.1
FC-006	82	28.8	922.6	893.8
FC-007	582	3.7	1255	1251.3
FC-008	140	37.2	1160.3	1123.1
FC-009	162	2.4	359	356.6
FC-014	90	35.1	252.8	217.7
FC-015	100	17.4	233.9	216.5
FC-016	15	47.9	183.3	135.4
FC-017	27	34.8	227.8	193
FC-024	14	58.5	117.9	59.4
FC-026	22	58.5	151.5	93
FC-027	100	58.2	276.4	218.2
FC-028	114	54	307	253
FC-029	65	64	206.3	142.3
FC-030	106	55.5	291.6	236.1
FC-031	35	31.9	118	86.1
FC-032	26	49.1	105.3	56.2
FC-033	68	27.7	181.9	154.2
FC-035	37	59.7	145.6	85.9
FC-037	62	33.5	173.1	139.6
FC-039	92	15.8	214.5	198.7
FC-041	31	36.5	108.8	72.3
FC-042	9	49.5	87.5	38
FC-043	37	54.9	163.4	108.5
FC-044	20	27.4	115.5	88.1
FC-045	32	34.3	124	89.7
FC-046	21	47	117.3	70.3
FC-048	40	37.5	149.7	112.2

Table 2-1 continued.

Borehole ID	Number of Boxes	Start Depth (m)	End Depth (m)	Total Length (m)
FC-049	7	13.7	153	139.3
FC-050	5	26.2	213.5	187.3
FC-051	6	8.2	231.5	223.3
FC-052	105	16.1	245.9	229.8
FC-053	1	75.3	76.5	1.2
FC-054	1	36.2	37.85	1.65
FC-055	12	14.3	62.4	48.1
FC-056	12	14.4	43.5	29.1
FC-057	6	16.37	29.7	13.33
FC-058	15	7.9	41.7	33.8
FC-059	14	7.9	36.5	28.6
FC-060	17	6	41.7	35.7
FC-061	11	7.5	29.5	22
FC-062	7	11.9	26.5	14.6
FC-063	9	7	26.5	19.5
FC-064	14	9	38.7	29.7
FC-065	11	10.9	38.7	27.8
FC-066	11	6.4	31.9	25.5
FC-067	8	6.4	29.6	23.2
FC-070	1	49.9	50.9	1
FC-071	71	61.2	215.5	154.3
FC-072	42	29.7	197.8	168.1
FC-075	47	93.9	191.1	97.2
FC-081	5	13	27	14
FC-082	7	20.6	35	14.4
FC-083	3	15.4	20	4.6
FC-084	10	15.7	38	22.3
FC-085	11	15.2	42.5	27.3
FC-100	123	12	293.94	281.94
FC-101A-1	53	104.2	220	115.8
FC-101A-2	16	58.65	124.28	65.63
FC-101	14	60.3504	103.9368	43.59
MR-01	31	33.5	167	133.5
MR-02	64	33.5	180.5	147
MR-03	37	36.7	191	154.3
MR-04	48	39.9	248	208.1
MR-05	32	50	188	138
MR-06	36	36.5	191	154.5
MR-07	33	38	185	147
MR-08	33	35	197	162
MR-09	63	34.7	172.5	137.8
MR-100	43	46.2	230	183.8
MR-102-C	31	91.5	230	138.5
MR-103-A	39	61.5	227	165.5
MR-105-A	46	47.1	245.3	198.2
MR-106	44	23.1	215	191.9
MR-10	32	46.2	194	147.8
MR-11	37	47.3	209	161.7
MR-13	32	35	164	129
MR-14	29	62.6	185	122.4
MR-15	55	39.6	192	152.4
MR-16	29	49.5	170	120.5
MR-17	36	36.5	188	151.5
MR-18	69	33.7	182.2	148.5
MR-19	34	25.5	179	153.5
MR-21	29	58	188	130
MR-22	58	27.9	260	232.1

Table 2-1 continued.

Drill Core ID	Number of Boxes	Start Depth (m)	End Depth (m)	Total Length (m)
MR-23	58	40	166.8	126.8
MR-24	32	27.5	167	139.5
MR-26	59	27.7	284	256.3
MR-27	57	34.8	278	243.2
MR-28	96	30.6	238	207.4
MR-29	109	37.2	272	234.8
MR-30	49	19.2	224	204.8
MR-32	80	18.5	362	343.5
MR-35	66	24.6	314.5	289.9
MR-36	66	43	326	283
MR-37	89	68	380	312
MR-39	50	34.6	251	216.4
MR-44	53	22.3	254	231.7
MR-45	54	24.7	260	235.3
MR-48	47	21	224	203
MR-49	48	44.8	269	224.2
MR-50	111	46.6	282.6	236
MR-51	57	49.3	296	246.7
MR-53	47	24.9	230	205.1
MR-54	70	37.8	338	300.2
MR-56	50	35.4	251	215.6
MR-57	49	34.8	239	204.2
MR-58	54	37	263	226
MR-59	59	22.2	272	249.8
MR-60	53	21.3	249	227.7
MR-61	43	70.7	255.3	184.6
MR-64	57	28	270.3	242.3
MR-65	186	14	433.7	419.7
MR-66	100	18.2	449	430.8
MR-67	13	15.2	75	59.8
MR-70	78	78.4	417.3	338.9
MR-71	66	58.1	349.6	291.5
MR-72	96	48.8	460.1	411.3
MR-73	47	34	237.3	203.3
MR-74X	36	40.5	188	147.5
MR-75	51	35	257	222
MR-76	23	37.5	137	99.5
MR-77X	86	18	204	186
MR-78	22	28.9	83	54.1
MR-79	54	30	260	230
MR-80	54	27.5	257	229.5
MR-81	91	36.5	233	196.5
MR-82	53	35.5	260	224.5
MR-83	38	22.1	182	159.9
MR-85	55	35.4	317.7	282.3
MR-87	86	44.5	299	254.5
MR-88	73	30.5	251	220.5
MR-89	115	25.1	371.8	346.7
MR-90	113	37	377	340
MR-92	46	43.8	248	204.2
MR-97	41	40.9	215	174.1
MR-99	41	40	230	190
MT-1	81	70.1	419.7	349.6
MT-2	52	58.1	281	222.9

In this chronostratigraphic interval of interest, the primary exploration target is uranium, which is typically associated with faults and sheer zones within graphite-rich metapelites (Ramaekers, 2004). In general, it is the interaction between oxidizing fluids derived from the basin and the reducing conditions of the basement that leads to the precipitation of uranium ores at or near the unconformity (Kupsch and Catuneanu, 2002).

2.2 Results

In total, 12 lithotypes were identified in hyperspectral data collected from 145 drill cores from the Athabasca Basin, totalling 24,321 meters (Table 2-1**)**. A representative spectrum for each lithotype is provided in Figure 2-1. Each spectrum is a composite of data collected from three different hyperspectral imaging cameras (VNIR, SWIR, and LWIR). The straight line between 2450 and 7500 nm is due to a gap in sensor coverage. Vertical lines at 1415, 1930, 2200, 8200, and 9200 nm show the locations of important spectral features (e.g., troughs or peaks). Although there are numerous features observed in these spectra, there are six spectral regions of interest that provide important compositional information: 400-1000, 1415, 1930, 2200, 8200, and 9200 nm:

- 400-1000 nm: Referred to as the visible and near-infrared (VNIR), troughs and peaks observed in this range relate primarily to the electronic processes of transition elements, such as iron. Spectral variability in this wavelength region typically correlates with changes in colour.
- 1415 nm: Troughs observed in this wavelength region are produced by the overtones of the -OH stretch of hydroxyl and indicate the presence of the hydroxyl anion.
- 1930 nm: Troughs observed in this wavelength region are produced by the overtones of the -OH stretch and HOH bend of water and indicate the presence of molecular water.
- 2200 nm: Troughs observed near 2200 nm are produced by the combination band involving the -OH fundamental stretch of hydroxyl bound to aluminum and indicate the presence of white micas such as muscovite and phengite, and clays such as montmorillonite.
- 8200 nm: Peaks observed near 8200 nm are produced by the fundamental vibration modes of the Si-O asymmetrical stretch. The wavelength position of these peaks indicates the presence of minerals like quartz.
- 9200 nm: Peaks observed near 9200 nm are produced by the fundamental vibration modes of the Si-O asymmetrical stretch. The wavelength position of these peaks indicates the presence of white micas and chlorites, for example.

The infrared-active minerals identified in this dataset are included in the lithotype legend (Figure 2-2). It is critical to note that reflectance spectroscopy is not a quantitative mineralogical technique, and other non-infrared-active minerals can be present in these rocks. Many minerals do not produce intense infrared spectral features that can be easily detected. Therefore, the legend provided for the lithotypes describes only those minerals that produce obvious diagnostic spectral absorption features. For a comprehensive mineralogical assessment of the different lithotypes, other analytical techniques, such as microscopy, X-Ray Diffractometry (XRD), Scanning Electron Microscopy (SEM), and/or Wavelength- or Energy-Dispersive X-Ray Spectroscopy (WDS/EDS), should be employed.

A spectral log was produced for each drill core showing the frequency and distribution of the twelve different lithotypes at one-meter depth intervals. These spectral logs allow for the visualization of compositional change along the surface of the drill core. For the purpose of this project, observations of compositional change were used to manually generate spectral strip logs for a subset of drill cores to identify large-scale compositional domains. For this project, the spectral logs and spectral strip logs for MR-54 and MR-102C are plotted alongside pXRF-derived elemental concentrations of Si, Al, Fe, Mg, K, S, Th, and U (Figures 2-3A and 2-3B). For MR-54, a lithologic log generated by Orr (1989) was added for comparison (Figure 2-4A).

2.3 Discussion

As observed in the reflectance spectra, the rocks from the Athabasca Basin are dominated by felsic, silicic compositions (Figures 2-1 and 2-2). For example, muscovitic illite and quartz are observed in all lithotypes, as indicated by the presence of troughs at ~2200 nm, and peaks at 8200 and 9200 nm. Although carbonate is observed in Lithotype 12, this lithotype was extracted from Devonian rocks overlying the Paleoproterozoic sediments.

Using the spectral logs generated from this study, in conjunction with the auxiliary data collected by other analytical methods and published lithologic logs, the following three zones were identified:

Zone 1: Quaternary, Devonian, and Paleoproterozoic sediments that extend to the base of the Manitou Falls Formation. This zone does not show evidence of alteration and, consequently, does not have a high potential for uranium mineralization. In many drill cores, the upper parts of the Fair Point Formation can also be included in Zone 1. This zone is dominated by Lithotypes 1 through 4, 11, and 12.

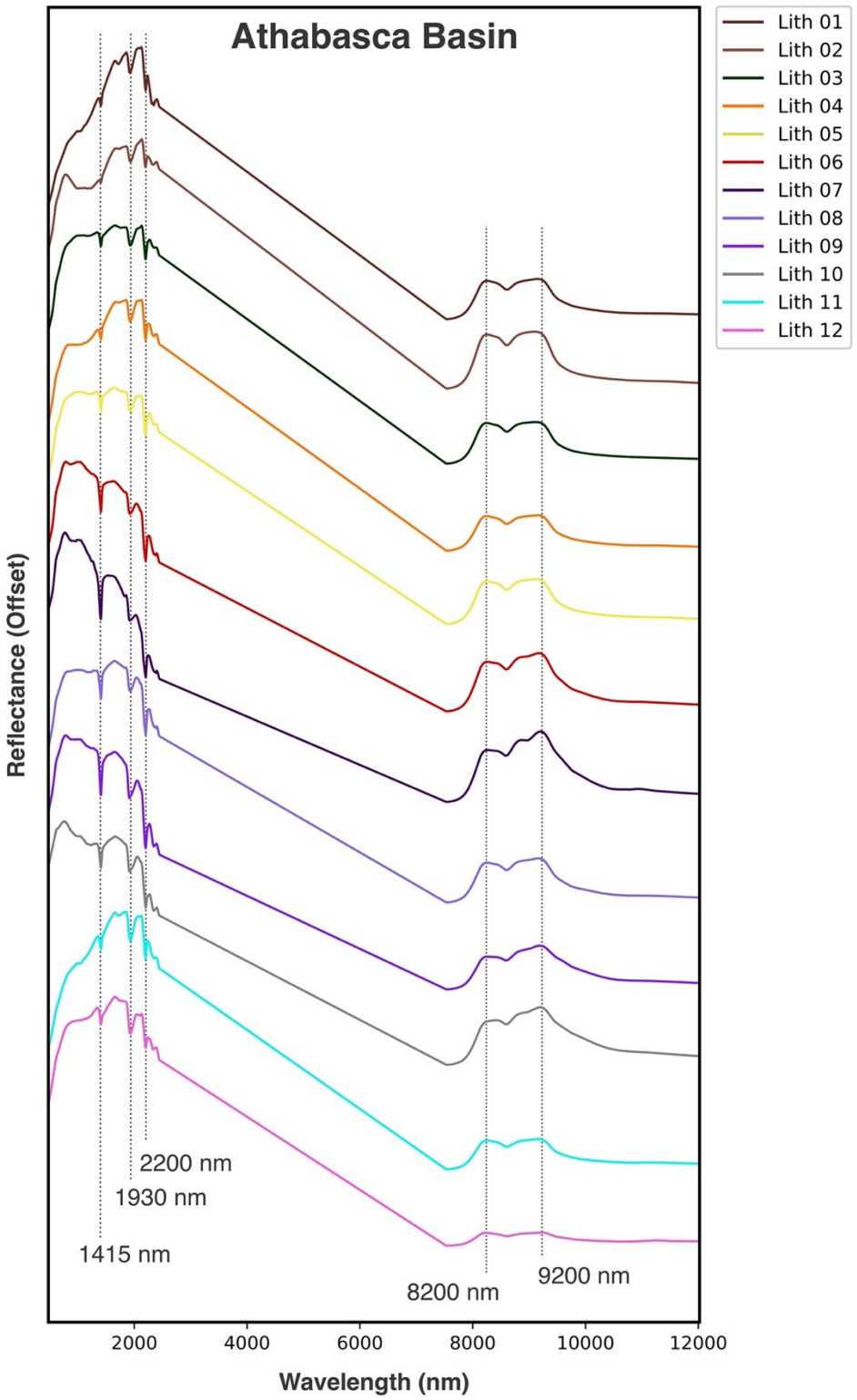

Figure 2-1. Representative lithotype spectra for the 12 lithotypes identified in the Athabasca Basin. Each spectrum is a composite of data collected from three different wavelength ranges (VNIR, SWIR, and LWIR), and the straight line between 2450 and 7500 nm is due to a gap in sensor coverage. Vertical lines at 1415, 1930, 2200, 8200, and 9200 nm show locations of important spectral features.

Class	Primary SWIR-Active Minerals	Secondary SWIR-Active Mineral	LWIR-Active Minerals
Lith 01	Muscovitic Illite		Quartz
Lith 02	Muscovitic Illite	Fe2+ Bearing	Quartz
Lith 03	Muscovitic Illite		Quartz
Lith 04	Muscovitic Illite	Fe2+ Bearing	Quartz
Lith 05	Muscovitic Illite		Quartz
Lith 06	Muscovitic Illite		Phyllosilicates + Quartz
Lith 07	Muscovitic Illite		Phyllosilicates + Quartz
Lith 08	Muscovitic Illite		Phyllosilicates + Quartz
Lith 09	Muscovitic Illite		Phyllosilicates + Quartz
Lith 10	Muscovitic Illite		Phyllosilicates + Quartz
Lith 11	Muscovitic Illite		Phyllosilicates + Quartz
Lith 12	Muscovitic Illite + Carbonate		Phyllosilicates + Quartz + Carbonate

Figure 2-2. Legend for the 12 lithotypes identified in drill cores from the Athabasca Basin. The lithotypes are described in terms of their short- and long-wave infrared-active minerals.

Zone 2: Paleoproterozoic sediments that are primarily from the Fair Point Formation (or lower units) that show evidence of alteration. This zone also consists of basement rocks that have been altered and fragmented. Consequently, this zone has the highest likelihood of containing uranium mineralization. Rocks in this zone may also have been affected by paleo-weathering. This zone is dominated by Lithotypes 5 through 9.

Zone 3: Basement rocks that do not show evidence of alteration or fragmentation. This zone does not have a high potential for uranium mineralization and is dominated by Lithotype 10.

These three zones are consistent with results from the literature that states that the Fair Point Formation is a unique stratigraphic target for uranium mineralization in the western Athabasca Basin (Kupsch and Catuneanu, 2002, and references therein). An example of a high-grade uraniferous zone at the base of the Fair Point Formation, near the unconformity, was intersected in drill hole MR-39 (5 m-averaged U_3O_8 content of 21%, see Orr,1989a).

Overall, in the Maybelle River area, uranium appears to be concentrated in the permeable units that are below the Manitou Falls Formation, such as in the Fair Point Formation, and also in the permeable units of the altered basement. This observation is in contrast to what is observed in the central and eastern Athabasca Basin, where Kupsch and Catuneanu (2002) noted that the uranium mineralization is located at or near the unconformity between the permeable units of the basal Manitou Falls Formation and the underlying Paleoproterozoic basement gneisses and schists.

Although the relationship between uranium mineralization and stratigraphy has been recognized in the western Athabascan Basin, some critical questions remain: How is the base of the Manitou Falls Formation being identified, how are the sediments below the base of the Manitou Falls Formation being logged, and how deep can the basement rocks be considered permeable and altered?

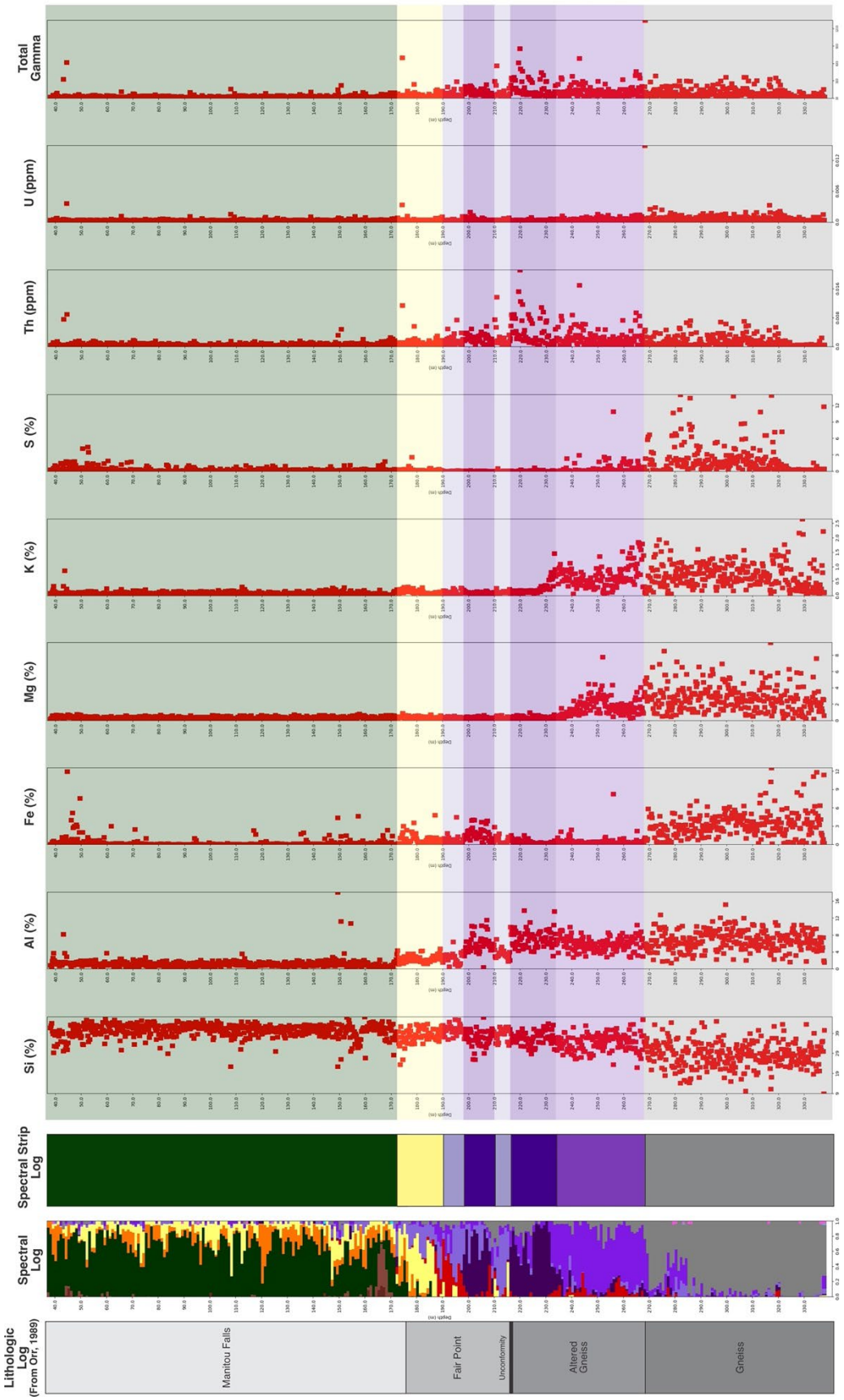

Figure 2-3. Spectral logs for MR-54 at one-meter depth binning intervals plotted along elemental concentrations (from handheld XRF) for Si, Al, Fe, Mg, K, S, Th, and U. The lithotype legend is provided in Figure 2-2. Lithologic log for MR-54 was published in Orr (1989).

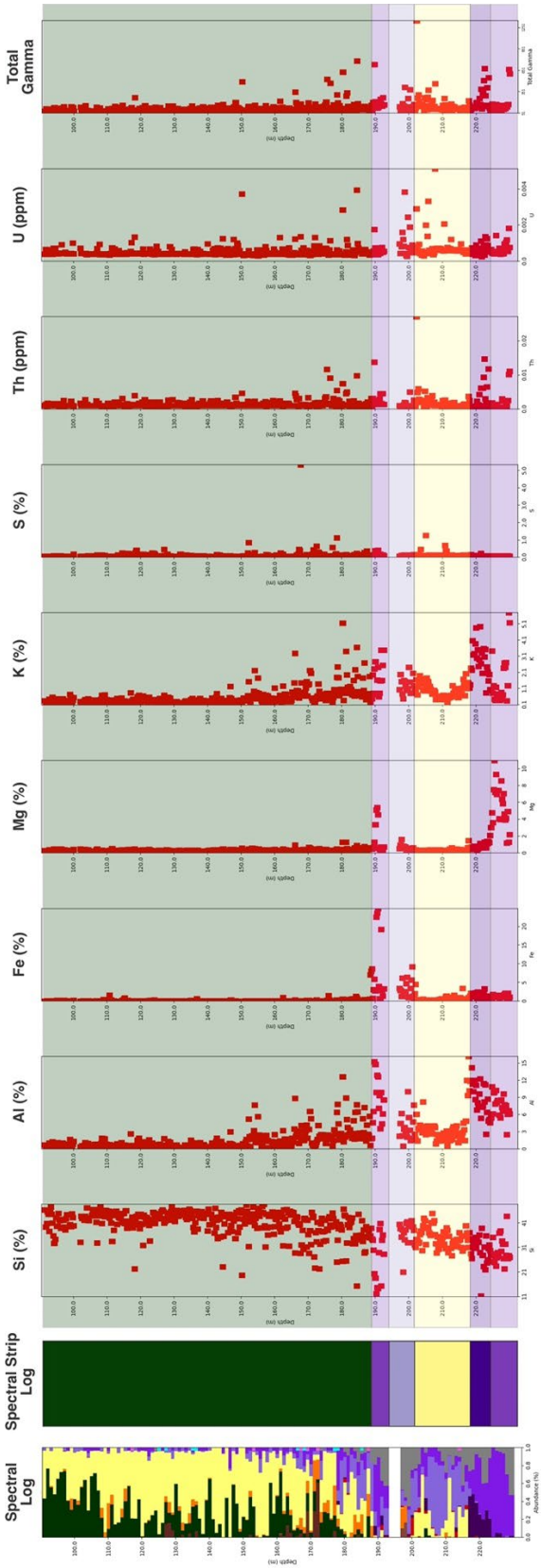

Figure 2-4. Spectral logs for MR102-C at one-meter depth binning intervals plotted along elemental concentrations (from handheld XRF) for Si, Al, Fe, Mg, K, S, Th, and U.

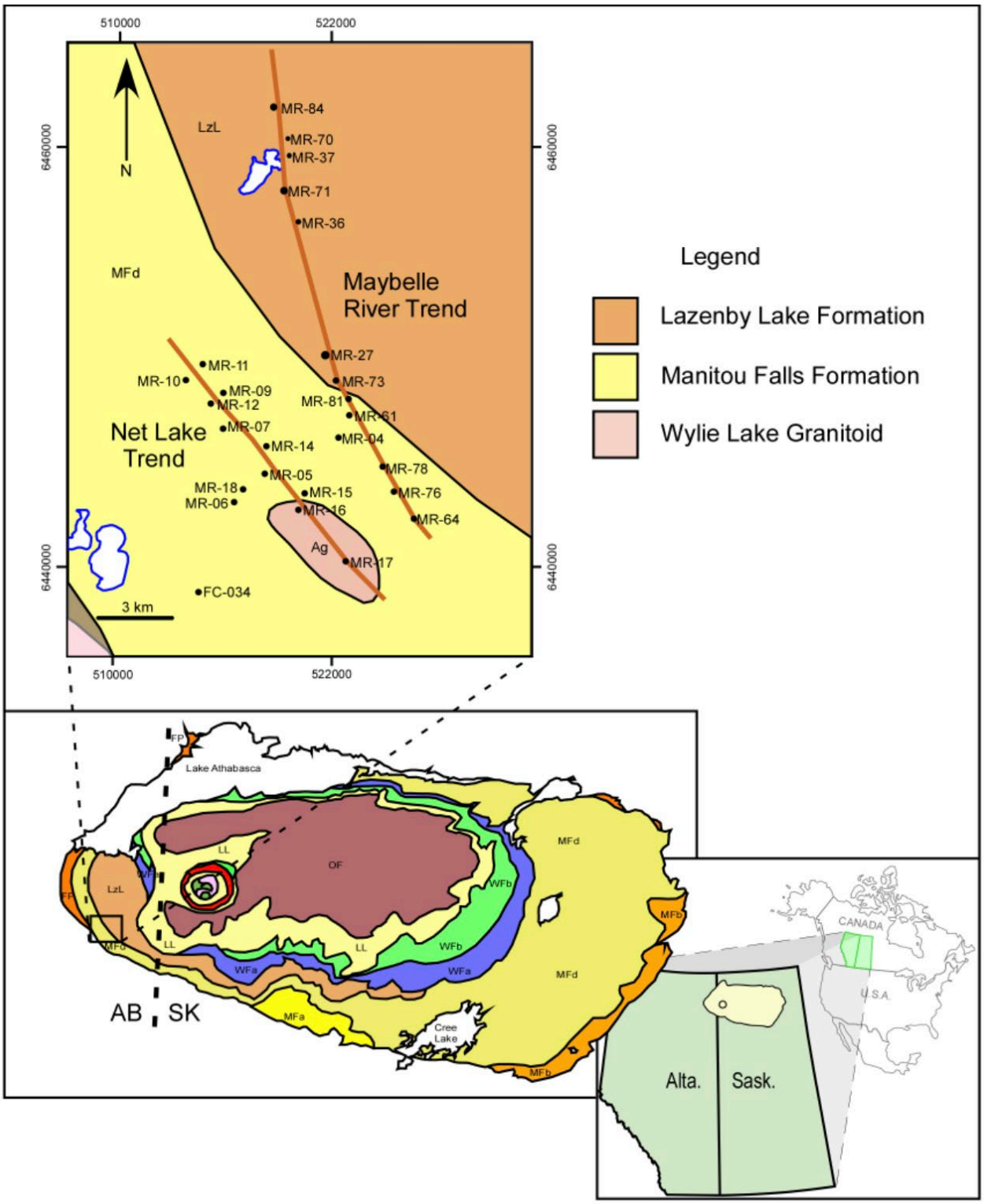

Figure 2-4. Location of the cross-section shown in Figures 2-5 and 2-6 in relation to the Maybelle River and Net Lake trends (taken from Post, 2004, which contains content modified from Ramaekers et al., 2001).

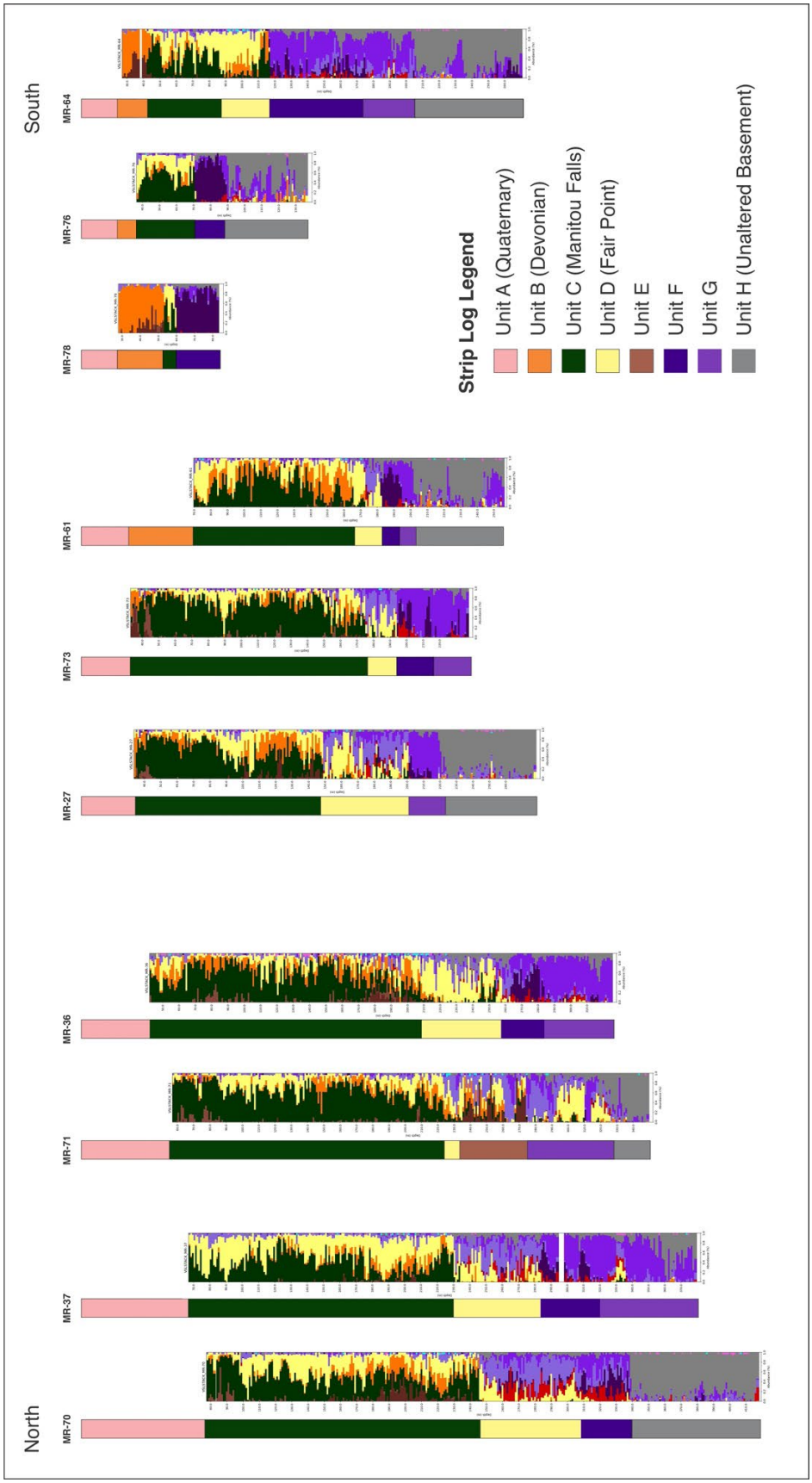

Figure 2-5. Cross-section through the Maybelle River trend showing spectral logs and spectral strip logs. The strip logs were created visually using the spectral logs to provide an example of how this type of work can be done. The portions of the strip logs that extend above the spectral logs were generated using lithologic logs from Orr (1989a, and 1989b). The strip log legend is generic to avoid introducing bias or unintentional errors because Units E, F, and G are logged differently in different publications.

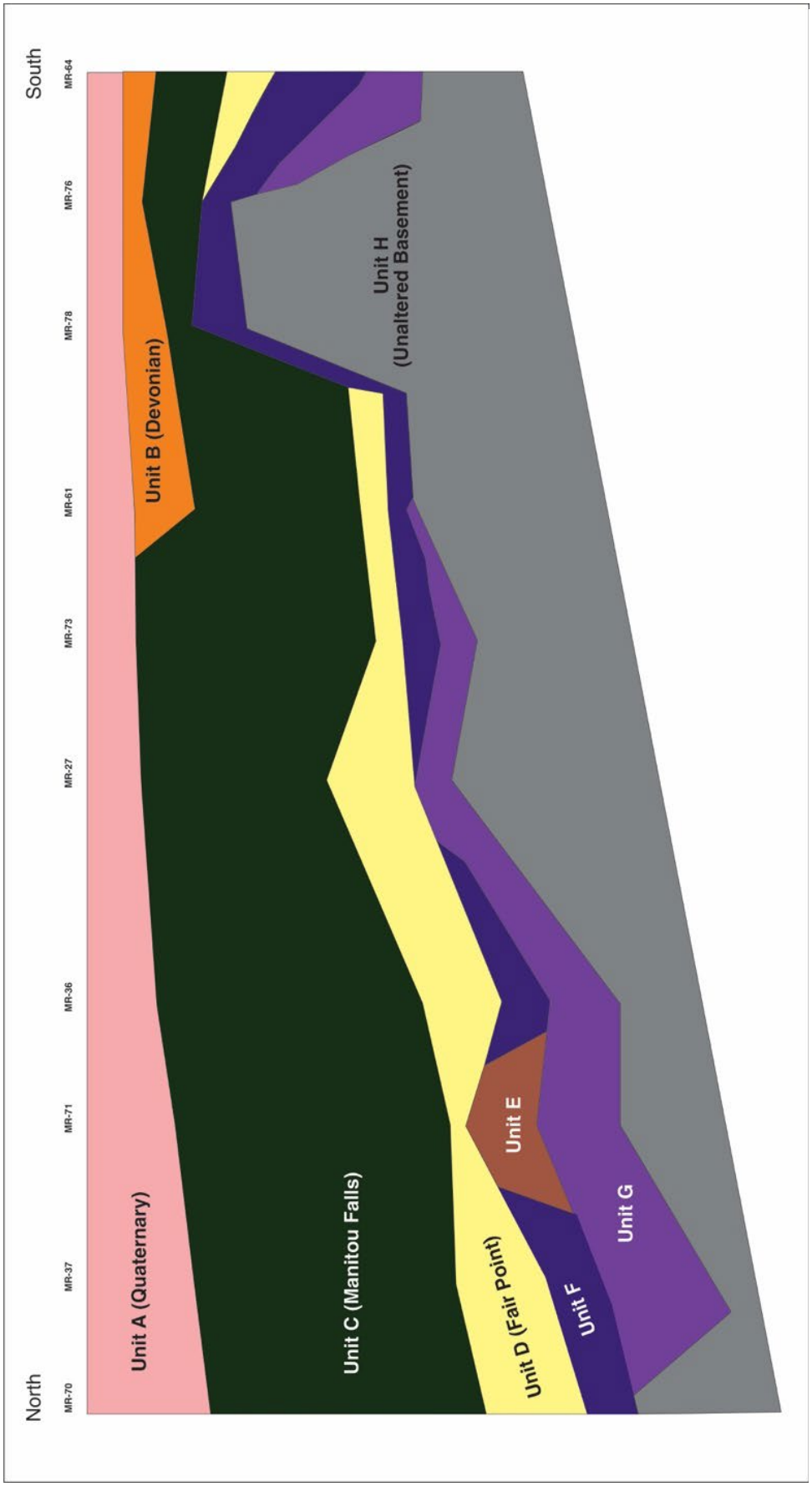

Figure 2-6. Cross-section through the Maybelle River trend showing one possible subsurface interpretation of the visually derived spectral strip logs created using spectral logs. The datum is the top of each drill core.

Due to the subjective nature of human observation, most lithologic logs created visually are not reproducible, and they contain errors and unintentional omissions. While it can be straightforward to generate accurate lithologic logs from drill cores dominated by flat-lying sediments, it is much more challenging for the human eye to identify evidence of alteration and mineralization, especially in rocks that have been folded or faulted. Therefore, it is vital to have objective and continuous compositional information that can be used to consistently identify alteration and mineralization, and that information is best provided using hyperspectral rock scanning techniques.

To optimize the drill core logging process so that compositional units are identified in a reproducible manner, the information from spectral logs can be used to generate spectral strip logs or be combined with textural and structural information and published data to generate lithologic logs. These informed strip logs and/or lithologic logs can then be validated using other analytical datasets (e.g., XRF, Gamma Ray, etc.) to ensure that the results are accurate.

To demonstrate how spectral strip logs generated using spectral logs and published information can be used as a tool for advancing the understanding of a region, a cross-section through the Maybelle River trend, originally published by Post et al. (2003, Figure 5), was re-generated using the spectral logs and spectral strip logs produced using the Lithotype™ Method. In total, eight different compositional units were labelled in the strip logs, which are referred to as Units A through H (Figure 2-5).

Where it was possible to unambiguously label the units using lithologic logs and published literature, the unit has been provided with a formation name. For Units E, F, and G, however, the literature was less straightforward, as three of these compositional units were not logged consistently. Most likely, these units relate to permeable basement rocks that have been significantly altered and fragmented. However, in some locations, they may also relate to rocks of the Fair Point Formation and its underlying sediments.

Based on published data, it appears challenging to identify the location of the unconformity between the Proterozoic sediments and the basement rocks in the Maybelle River area consistently and reproducibly. The likely reason is that sedimentary rocks of the Fair Point Formation have been extensively altered and fragmented in some locations, making them difficult to differentiate from the underlying basement rocks, which have also been extensively altered and fragmented. Rocks belonging to compositional Units E, F, and G can therefore be viewed as parts of a transition zone (e.g., Zone 2) that typically starts within the Fair Point Formation and extends into the basement. Within this transition zone, Lithotypes 6, 7, 8, and 9 are dominant, and they likely relate to paleo-weathering and/or alteration of the sedimentary and basement rocks above and below the unconformity, which in some places can host uranium mineralization.

The spectral logs can be used to identify unit boundaries, as shown in Figure 2-5, which in turn allows for the creation of strip logs that can be used to connect unit boundaries consistently across other drillholes from the area. When these strip logs are used to generate a possible representation of the subsurface, several observations can be made (Figure 2-6). First, the sedimentary rock package generally thickens and deepens towards the north, which is consistent with regional trends. Second, the extent of alteration within the transition zone appears to be linked to the paleo-topography, as marked by variations in the depth of the unaltered basement rocks. Relatively lower-lying parts of the basement (paleo-valleys) tend to be more altered than other parts. In general, units F and G in the strip logs should be considered to have a higher potential for uranium mineralization because they contain a high abundance of phyllosilicates (e.g., Lithotypes 6, 7, 8, and 9), which most likely formed during the alteration process.

3. Archean and Paleoproterozoic – Canadian Shield

3.1 Overview

The Archean and Paleoproterozoic crystalline basement rocks of the Canadian Shield are known to host various minerals and metals throughout Canada, including gold, silver, zinc, copper, and diamonds (see GSC Current Research 1996-C, https://publications.gc.ca/collections/collection_2017/rncan-nrcan/M44-1996-3.pdf). Although the surface exposure of the Canadian Shield in Alberta is minimal, Archean and Paleoproterozoic rocks form the basement of the Western Canada Sedimentary Basin, and they may be an exploration interest. Due to the structure of the basin and its tectonic history, the depth to basement rocks varies significantly across Alberta—ranging from just a few meters in the northeastern part of the province (e.g., Peace River Arch; O'Connell et al., 1990) to over 5,000 meters in the southwest (Burwash, et al., 1990). The depth of the basement is of significant interest because it influences the potential for discovering mineral deposits, with shallower deposits being easier to discover and mine (Nguyen and Pham, 2019). The average depth of an underground mine can vary depending on the type of mining operation and the resources being extracted. However, most mineral exploration projects are drilled to depths of 300 meters, with brownfields exploration occasionally extending to 1000 meters.

3.2 Results

In total, 27 drill cores, totalling 970 meters, that intersected Archean and Paleoproterozoic basement rocks were analyzed using the Lithotype™ Method (Table 3-1), and 12 lithotypes were identified.

A representative spectrum for each lithotype is provided in Figure 3-1. Each spectrum is a composite of data collected from three different hyperspectral imaging cameras (VNIR, SWIR, and LWIR).

Table 3-1. Drill cores of Archean and Paleoproterozoic rocks from the Canadian Shield analyzed in this study.

Drill Core ID	Number of Boxes	Start Depth (m)	End Depth (m)	Total Length (m)
100013206403W400	31	1273	1336.2	63.2
100083607419W500	11	2480	2491.5	11.5
100131808811W500	7	1588	1605.4	17.4
100162208314W500	5	1798.4	1803.6	5.2
FC-013	4	63.4	102.7	39.3
FC-018	8	58.5	79.5	21
FC-019	40	12.3	99.6	87.3
FC-020	20	28.6	72.2	43.6
FC-021	6	23.7	35.6	11.9
FC-023	32	28.6	97.7	69.1
FC-025	18	67.8	111.6	43.8
FC-034	37	36.9	118	81.1
FC-036	10	53.3	72.5	19.2
FC-038	41	26.5	112.7	86.2
FC-040	58	32.6	153.3	120.7
FC-047	6	64.3	102	37.7
FC-074	26	39.4	102.7	63.3
FC-077	12	15.6	41	25.4
FC-078	20	16	60	44
FC-079	10	12.9	60	47.1
FC-080	4	9.7	17	7.3
FC-087	7	9.75	25	15.25
FC-089	5	16.5	29.5	13
FC-090	3	13.4	19	5.6
FC-091	1	38	40	2
FC-092	10	24	60.2	36.2
K-00-01	41	83.82	189.2808	105.46

The straight line between 2450 and 7500 nm is due to a gap in sensor coverage. Vertical lines at 1415, 1930, 2200, 2330, 8200, 9200, and 11,200 nm show the locations of important spectral features (e.g., troughs or peaks).

Although there are numerous features observed in these spectra, there are seven spectral regions of interest that provide important compositional information: 400-1000, 1415, 1930, 2200, 2330, 8200, and 9200 nm:

- 400-1000 nm: Referred to as the visible and near-infrared (VNIR), troughs and peaks observed in this range relate primarily to the electronic processes of transition elements, such as iron. Spectral variability in this wavelength region typically correlates with changes in colour.
- 1415 nm: Troughs observed in this wavelength region are produced by the overtones of the -OH stretch of hydroxyl and indicate the presence of the hydroxyl anion.
- 1930 nm: Troughs observed in this wavelength region are produced by the overtones of the -OH stretch and HOH bend of water and indicate the presence of molecular water.
- 2200 nm: Troughs observed near 2200 nm are produced by the combination band involving the -OH fundamental stretch of hydroxyl bound to aluminum and indicate the presence of white micas such as muscovite and phengite, and clays such as montmorillonite.
- 2330 nm: Troughs observed near 2330 nm are often produced by the carbonate anion (CO_3^{2-}) bound to cations, such as magnesium and/or iron, indicating the presence of various carbonate minerals. The detailed position and shape of trough in this wavelength region help identify the minerals present.
- 8200 nm: Peaks observed near 8200 nm are produced by the fundamental vibration modes of the Si-O asymmetrical stretch. The wavelength position of these peaks indicates the presence of minerals like quartz.
- 9200 nm: Peaks observed near 9200 nm are produced by the fundamental vibration modes of the Si-O asymmetrical stretch. The wavelength position of these peaks indicates the presence of white micas and chlorites, for example.
- 11,200 nm: Peaks observed around 11,200 nm are produced by the vibration of the carbonate anion (CO_3^{2-}) in carbonate minerals.

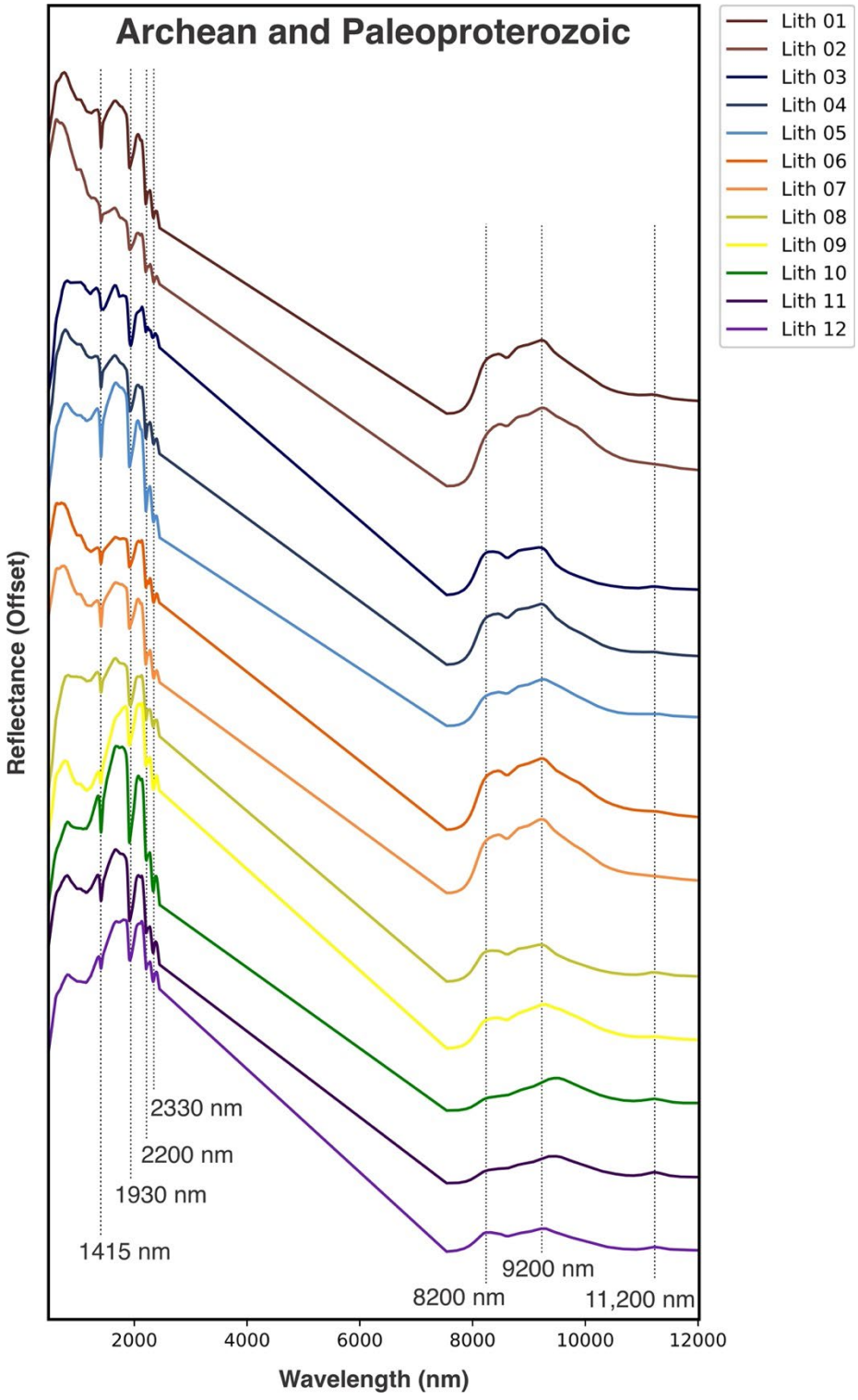

Figure 3-1. Representative spectra for the 12 lithotypes identified in drill core that primarily intersect Archean and Paleoproterozoic basement rocks. Each spectrum is a composite of data collected from three different wavelength ranges (VNIR, SWIR, and LWIR), and the straight line between 2450 and 7500 nm is due to a gap in sensor coverage. Vertical lines at 1415, 1930, 2200, 2330, 8200, 9200, and 11,200 nm show the locations of important spectral features.

Class	Primary SWIR-Active Minerals	Secondary SWIR-Active Mineral	LWIR-Active Minerals
Lith 01	Muscovitic Illite		Quartz + Phyllosilicates
Lith 02	Muscovitic Illite		Phyllosilicates + Quartz
Lith 03	Muscovitic Illite + Chlorite	Fe2+ bearing	Phyllosilicates + Quartz
Lith 04	Phengitic Illite + Carbonate		Phyllosilicates + Quartz + Carbonate
Lith 05	Phengitic Illite + Carbonate		Phyllosilicates + Quartz + Carbonate
Lith 06	Muscovitic Illite + Chlorite	Fe2+ bearing	Phyllosilicates + Quartz
Lith 07	Chlorite + Muscovitic Illite	Fe2+ bearing	Phyllosilicates + Quartz
Lith 08	Chlorite + Muscovitic Illite	Fe2+ bearing	Chlorite + Phyllosilicates
Lith 09	Muscovitic Illite + Chlorite	Carbonate	Phyllosilicates + Quartz + Carbonate
Lith 10	Muscovitic Illite + Chlorite		Phyllosilicates + Quartz
Lith 11	Muscovitic Illite + Chlorite	Carbonate	Phyllosilicates + Quartz + Carbonate
Lith 12	Muscovitic Illite + Chlorite	Carbonate	Phyllosilicates + Quartz + Carbonate

Figure 3-2. Legend describing the 12 lithotypes identified in drill cores that primarily intersect the Archean and Paleoproterozoic basement. The lithotypes are described in terms of their short- and long-wave infrared-active minerals

A spectral log was produced for each drill core showing the frequency and distribution of the 12 different lithotypes at one-meter depth intervals. These spectral logs allow for the visualization of compositional change along the surface of the drill core. For this chronostratigraphic interval, spectral logs are presented for FC-019, FC-023, FC-034, FC-038, FC-040, and FC-074 (Figure 3-3). These drill cores were selected because they are the longest continuous drill cores in this chronostratigraphic interval.

3.3 Discussion

As observed in the reflectance spectra, the rocks from this interval are dominated by felsic, silicic minerals, such as illite and quartz, with additional intermediate-to-mafic compositions as indicated by the higher prevalence of chlorite (Figures 3-1 and 3-2). In comparison to the lithotypes extracted from the Athabasca Basin, the lithotypes from this interval are more intermediate and/or mafic in composition, which is likely due to the fact that these rocks represent a wider assortment of intrusive and extrusive rocks, whereas the rocks of the Athabasca Basin are comprised mainly of sediments dominated by felsic minerals.

Several lithotypes contain evidence of the presence of carbonate, which is identified primarily by a peak at 11,200 nm, and a trough at 2330 nm. This is due to the fact that several drill cores also intersect rocks from other chronostratigraphic units, such as the Devonian, in addition to the Archean and Paleoproterozoic rocks.

To show how spectral logs can be used to assist with the correlation of compositional units, strip logs were visually generated for drill cores FC-019 and FC-023 (Figure 3-4). These strip logs show similar spatial lithotype distributions, particularly between 50 and 60 meters. In that depth range, Lithotype 9 is dominant, which likely correlates to the presence of a more intermediate/mafic rock compared to Lithotypes 6 and 7.

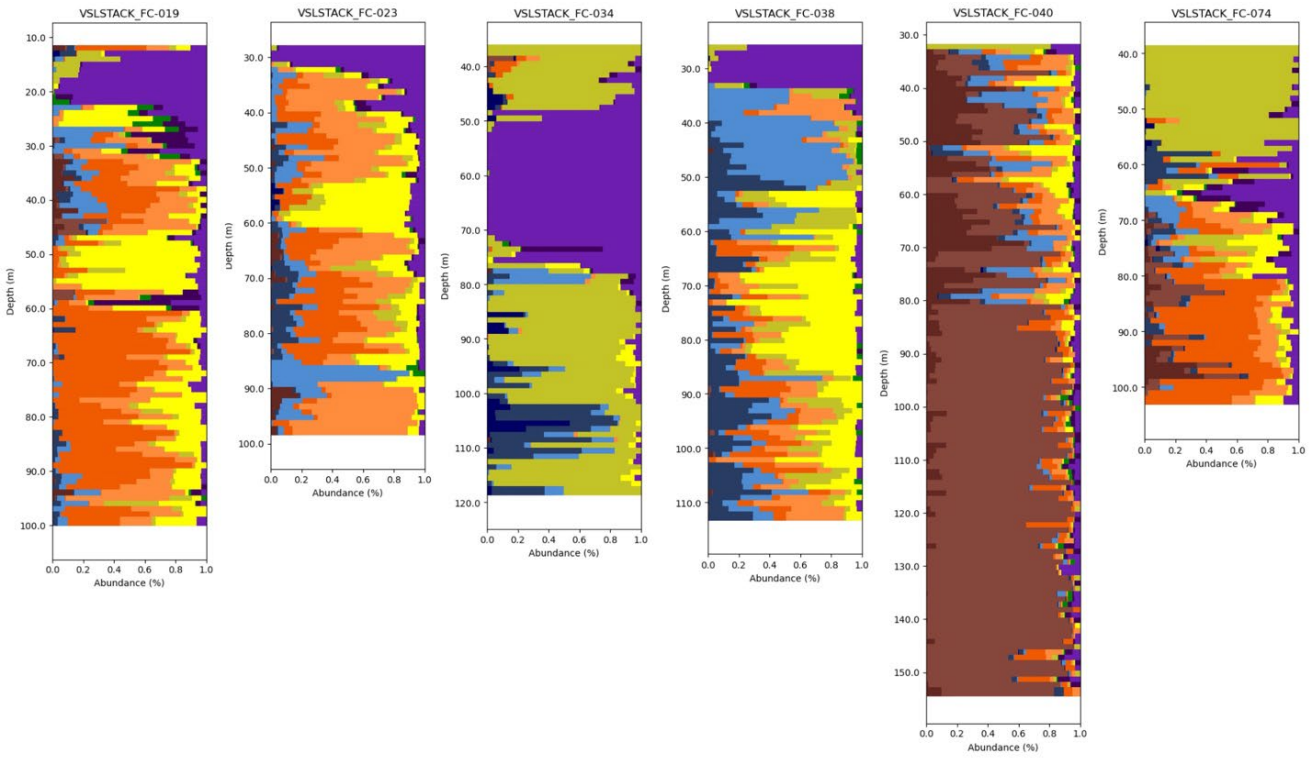

Figure 3-3. Spectral logs for FC-019, FC-023, FC-034, FC-038, FC-040, and FC-074, which intersect Archean and Paleoproterozoic basement at one-meter depth binning intervals. The lithotype legend is provided in Figure 3-2.

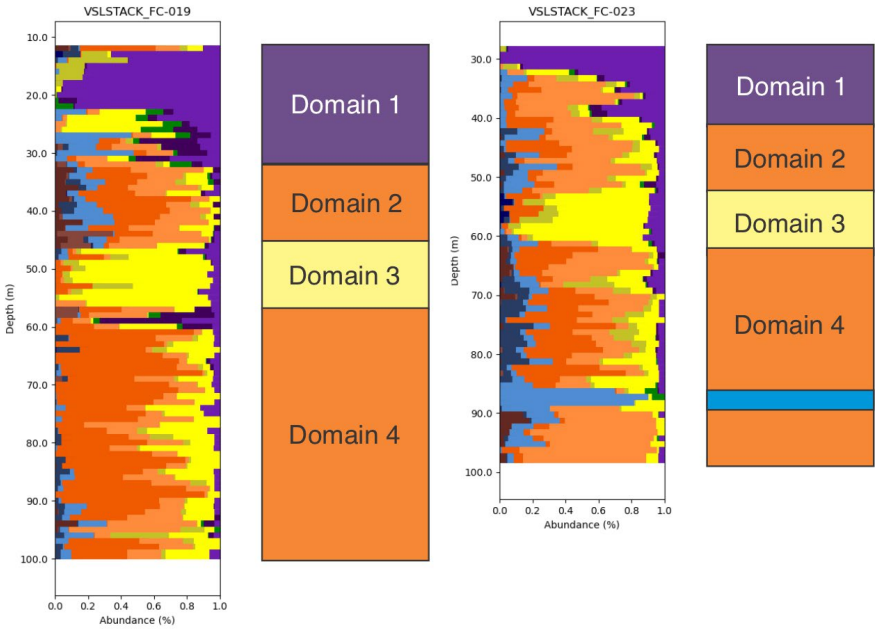

Figure 3-4. Spectral logs for FC-019 and FC-023 at one-meter depth binning intervals with visually derived strip logs showing how spectral logs can be used to generate correlations. The lithotype legend is provided in Figure 3-2.

4. Cambrian, Lower Ordovician, Silurian

4.1 Overview

During the Cambrian, Ordovician, and Silurian periods, the geology of Alberta was defined by the presence of both siliciclastic and carbonate sequences that formed on the passive margin of the western side of the North American protocontinent (Kent, 1994, and references therein). Overlying Precambrian basement rocks and an extensive unconformity, the rocks deposited during the Cambrian to Late Ordovician include the Gog quartzite (Aitken, 1989), sedimentary rocks characteristic of shallow marine sediments (Hein, 1987), and silicic-carbonate sequences (Slind et al., 1994).

During the Middle Ordovician to Silurian, the geological record of Alberta represents shallow-water carbonates with minor clastic rocks and evaporites on the craton, bordered to the west by shales and limestones (Norford et al., 1994, and references therein). This period is noted for the development of more complex ecosystems, including the rise of the first coral reefs (Layer, 1949).

4.2 Results

Altogether 18 drill cores totalling 990 meters were analyzed for this chronostratigraphic interval using the Lithotype™ Method (Table 4-1), and ten lithotypes were identified.

The representative spectra for each lithotype are provided in Figure 4-1. Each spectrum is a composite of data collected from three different hyperspectral imaging cameras (VNIR, SWIR, and LWIR), and the straight line between 2450 and 7500 nm is due to a gap in sensor coverage. Vertical lines at 1415, 1930, 2200, 2300, 8200, 9200, and 11,200 nm show the locations of important spectral features (Figure 4-1).

Although there are numerous features observed in these spectra, there are eight spectral regions of interest that provide important compositional information: 400-1000, 1415, 1930, 2200, 2330, 8200, 9200, and 11,200 nm.

- 400-1000 nm: Referred to as the visible and near-infrared (VNIR), troughs and peaks observed in this range relate primarily to the electronic processes of transition elements, such as iron. Spectral variability in this wavelength region typically correlates with changes in colour.
- 1415 nm: Troughs observed in this spectral range are produced by the overtones of the -OH stretch of hydroxyl and indicate the presence of the hydroxyl anion.
- 1930 nm: Troughs observed in this spectral range are produced by the overtones of the -OH stretch and HOH bend of water and indicate the presence of molecular water.
- 2200 nm: Troughs observed near 2200 nm are produced by the combination band involving the -OH fundamental stretch of hydroxyl bound to aluminum and indicate the presence of white micas such as muscovite and phengite, and clays such as montmorillonite.
- 2330 nm: Troughs observed near 2330 nm are often produced by the carbonate anion (CO_3^{2-}) bound to cations, such as magnesium and/or iron, indicating the presence of various carbonate minerals. The detailed position and shape of troughs in this wavelength region help identify the minerals present.

Table 4-1. Drill cores of Cambrian, Ordovician, and Silurian rocks analyzed in this study.

Drill Core ID	Number of Boxes	Start Depth (m)	End Depth (m)	Total Length (m)
100012706026W400	9	2249.1	2271.5	22.4
100013303703W400	3	1618.5	1852.4	233.9
100041201527W400	29	3408.9	3573.2	164.3
100053506218W500	37	3202.8	3422.9	220.1
100063601901W400	7	2169	2187	18
100063606312W500	8	3050.1	3264.4	214.3
100071405706W400	7	1344.2	1363.4	19.2
100081905920W400	66	1947	2085.1	138.1
100082605805W400	30	1537.8	1618.8	81
100090602306W500	41	1018.9	1133.6	114.6
100091603212W500	7	1765.4	2155.9	390.5
100101603820W400	5	2702.4	2728.6	26.2
100112206403W400	34	1214.4	1277	62.6
102011406308W400	11	1386	1401.8	15.8
102020306503W400	34	1259	1312.8	53.8
103030405720W400	155	1885.1	2118	232.9
103071105920W400	50	2009	2063.5	54.5
103113205521W400	87	1953	2202.5	249.5

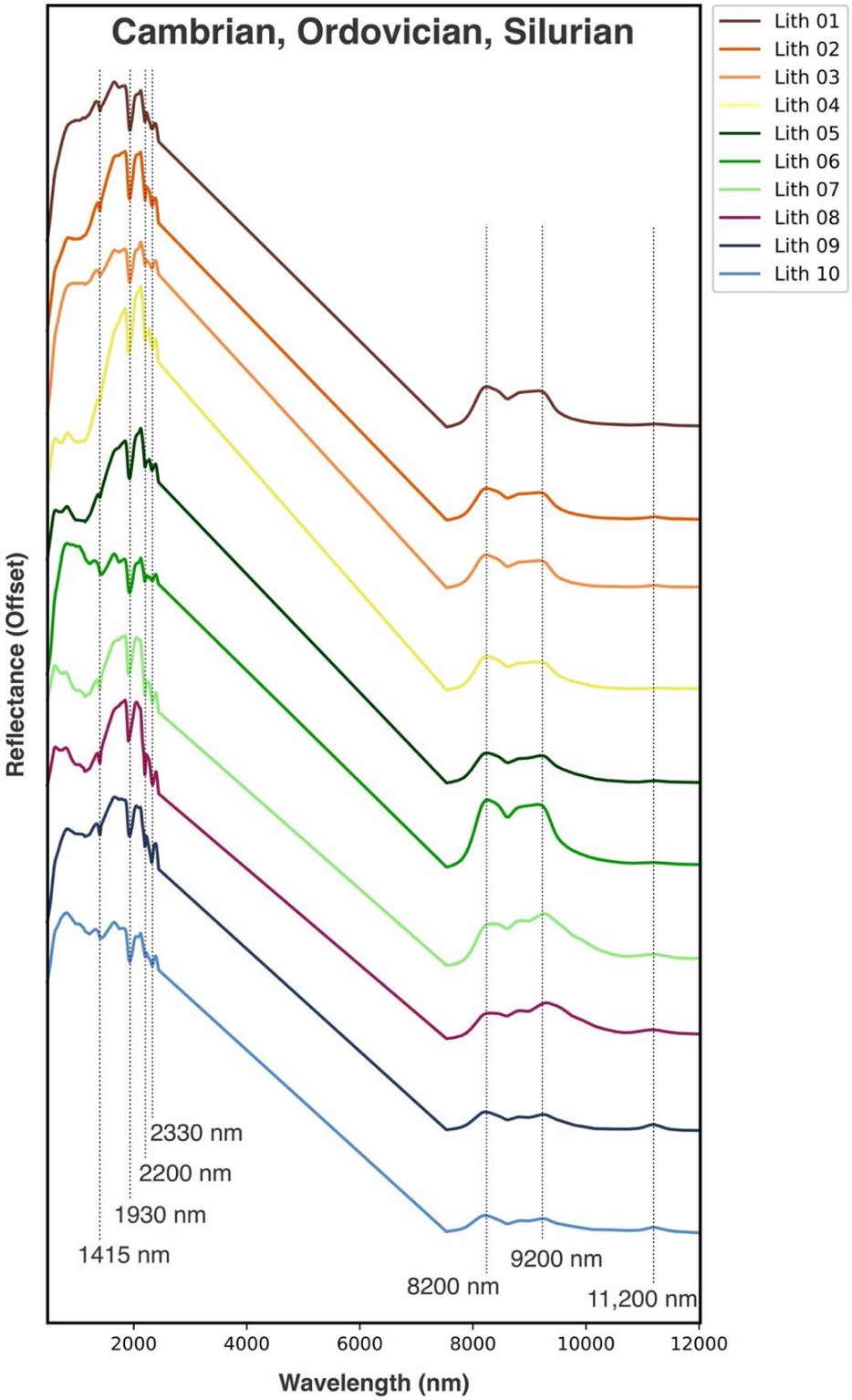

Figure 4-1. Representative spectra for the ten lithotypes identified in the drill cores that primarily intersect Cambrian, Lower Ordovician, and Silurian rocks. Each spectrum is a composite of data collected from three different wavelength ranges (VNIR, SWIR, and LWIR), and the straight line between 2450 and 7500 nm is due to a gap in sensor coverage. Vertical lines at 1415, 1930, 2200, 2330, 8200, 9200, and 11,200 nm show locations of important spectral features.

- 8200 nm: Peaks observed near 8200 nm are produced by the fundamental vibration modes of the Si-O asymmetrical stretch. The wavelength position of these peaks indicates the presence of minerals like quartz.
- 9200 nm: Peaks observed near 9200 nm are produced by the fundamental vibration modes of the Si-O asymmetrical stretch. The wavelength position of these peaks indicates the presence of white micas and chlorites, for example.
- 11,200 nm: Peaks observed around 11,200 nm are produced by the vibration of the carbonate anion (CO_3^{2-}) in carbonate minerals.

The infrared-active minerals identified in this dataset are included in the lithotype legend (Figure 4-2). It is critical to note that spectroscopy of this type is not a quantitative mineralogical technique, and other non-infrared-active minerals can be present in these rocks. Many minerals do not produce intense infrared spectral features that can be easily detected. Therefore, the legend provided for the lithotypes describes only those minerals that produce obvious diagnostic spectral absorption features. For a comprehensive mineralogical assessment of the different lithotypes, other analytical techniques, such as microscopy, X-Ray Diffractometry (XRD), Scanning Electron Microscopy (SEM), and/or Wavelength- or Energy-Dispersive X-Ray Spectroscopy (WDS/EDS), should be employed.

A spectral log was produced for each drill core showing the frequency and distribution of the ten different lithotypes at one-meter depth intervals. Spectral logs are presented in Figure 4-3 for a selection of drill cores, which were selected because of their drill core length.

Class	Primary SWIR-Active Minerals	Secondary SWIR-Active Mineral	LWIR-Active Minerals
Lith 01	Muscovitic Illite		Quartz + Phyllosilicates + Carbonate
Lith 02	Muscovitic Illite		Quartz + Phyllosilicates + Carbonate
Lith 03	Muscovitic Illite		Quartz + Phyllosilicates + Carbonate
Lith 04	Muscovitic Illite	Fe2+ Bearing	Quartz + Phyllosilicates + Carbonate
Lith 05	Muscovitic Illite	Fe2+ Bearing	Quartz + Phyllosilicates + Carbonate
Lith 06	Muscovitic Illite		Quartz + Phyllosilicates + Carbonate
Lith 07	Muscovitic Illite + Carbonate	Fe2+ Bearing	Phyllosilicates + Carbonate + Phyllosilicates
Lith 08	Muscovitic Illite + Carbonate	Fe2+ Bearing	Phyllosilicates + Carbonate + Phyllosilicates
Lith 09	Carbonate + Muscovitic Illite		Carbonate + Quartz + Phyllosilicates
Lith 10	Carbonate + Muscovitic Illite		Carbonate + Quartz + Phyllosilicates

Figure 4-2. Representative spectra for the ten lithotypes identified in the drill cores that primarily intersect Cambrian, Lower Ordovician, and Silurian rocks. Each spectrum is a composite of data collected from three different wavelength ranges (VNIR, SWIR, and LWIR), and the straight line between 2450 and 7500 nm is due to a gap in sensor coverage. Vertical lines at 1415, 1930, 2200, 2330, 8200, 9200, and 11,200 nm show locations of important spectral features.

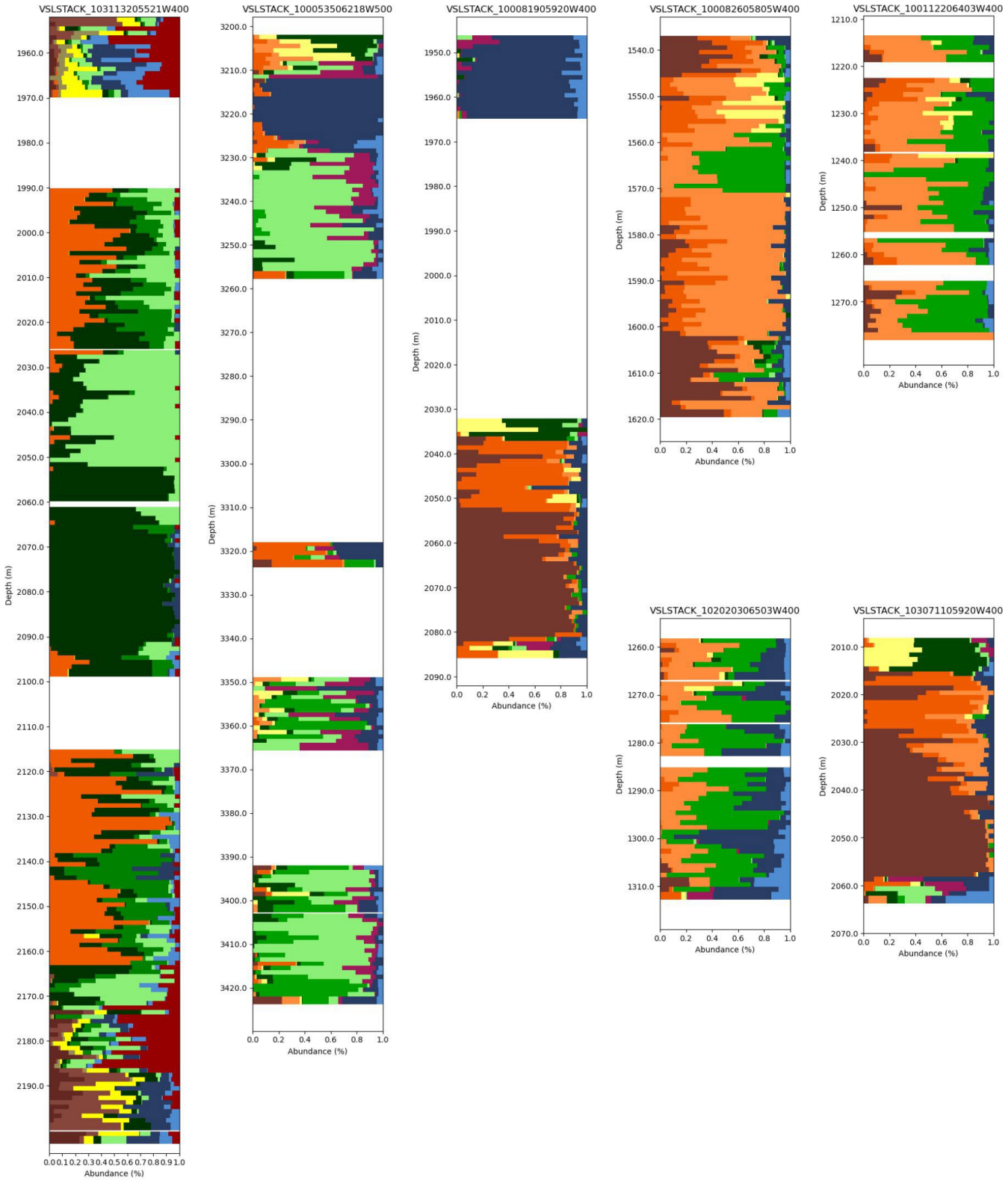

Figure 4-3. Spectral logs for seven drill cores that primarily intersect Cambrian, Lower Ordovician, and Silurian rocks at one-meter depth binning intervals. The lithotype legend is provided in Figure 4-2.

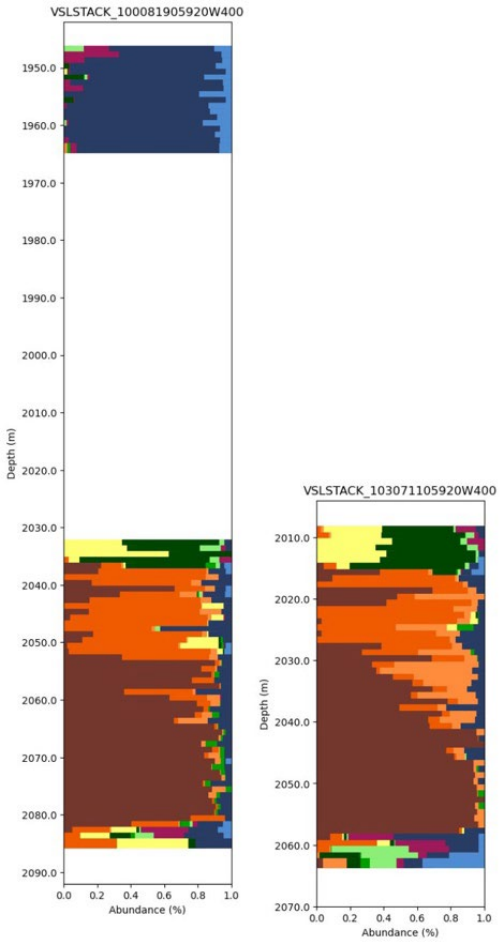

Figure 4-4. Spectral logs for 100081905920W400 and 103071105920W400 at one-meter depth binning intervals showing how spectral logs can be used to correlate similar compositions across different drill cores. The lithotype legend is provided in Figure 4-2.

4.3 Discussion

As observed in the reflectance spectra, the rocks from this interval are dominated by felsic minerals and carbonates (Figures 4-1 and 4-2). For example, felsic minerals are primarily observed in Lithotypes 1 to 6, which show a high abundance of quartz and illite with minor carbonate, Lithotypes 7 and 8 show illite and quartz with higher carbonate abundances, and Lithotypes 9 and 10 show some quartz and illite but are mainly dominated by carbonate.

In comparison to the lithotypes extracted from the Archean and Proterozoic rocks, this chronostratigraphic interval shows a much higher presence of carbonate, which correlates with the development of carbonate-based ecosystems, including the rise of the first coral reefs (Layer, 1949).

For the Cambrian, Lower Ordovician, and Silurian chronostratigraphic interval, only 18 drill cores were scanned. Many of these drill cores were short in length or contained large gaps, and this can make it difficult to generate plots that show large-scale correlations. However, using the spectral logs produced using the Lithotype™ Method, it was possible to correlate compositional units between two drill cores, as observed for drill cores 100081905920W400 and 103071105920W400, which show similar spatial lithotype distributions (Figure 4-4).

5. Devonian

5.1 Overview

During the Devonian, Alberta was situated near the equator and was mainly covered by a warm, inland sea. This facilitated the deposition of a wide range of sedimentary rocks, including limestones, dolomites, shales, and evaporites (Meijer Drees et al., 1994). In Alberta, Devonian rocks are amongst the most studied due to their association with oil and gas reserves. Yet, Lower to Middle Devonian rocks are also associated with ore mineralization, particularly in the District of Mackenzie, Northwest Territories, where the Pine Point lead-zinc deposits are located (Krebs and Macqueen, 1984), and in northeastern British Columbia where other lead-zinc deposits are found (Taylor et al., 1975). Overall, the Devonian can be subdivided into three major sequences: (1) Lower Devonian, which is

characterized by the deposition of thick carbonate formations, indicative of warm, shallow marine environments, (2) Middle Devonian, which is defined by the development of extensive reef complexes, some of which represent some of the largest hydrocarbon reservoirs in Alberta, and the evaporites of the Elk Point Group, and (3) Upper Devonian, which is marked by a transition to more varied depositional environments, including deeper basin settings, which include the deposition of black shales (Halbertsma et al., 1994; Meijer Drees et al., 1994; Oldale et al., 1994).

5.2 Results

Altogether 145 drill cores totalling 5201 meters from this chronostratigraphic interval were analyzed using the Lithotype™ Method (Table 5-1), and eight lithotypes were identified.

The representative spectra for each lithotype are provided in Figure 5-1. Each spectrum is a composite of data collected from three different hyperspectral imaging cameras (VNIR, SWIR, and LWIR), and the straight line between 2450 and 7500 nm is due to a gap in sensor coverage. Vertical lines at 1415, 1930, 2200, 2300, 8200, 9200, and 11,200 nm show the locations of important spectral features (Figure 5-1).

Table 5-1. Drill cores of Devonian rocks analyzed in this study.

Drill Core ID	Number of Boxes	Start Depth (m)	End Depth (m)	Total Length (m)
100010105822W400	14	950.4	990.0	39.6
100010309606W500	35	1224.0	1260.0	36.0
100010605821W400	24	960.7	1013.2	52.4
100010803620W400	6	1700.8	1717.2	16.5
100011806018W500	5	3195.5	3201.3	5.8
100013503804W500	7	2980.0	2986.8	6.8
100020106514W500	19	2818.0	2840.1	22.1
100020407001W600	4	3330.2	3339.7	9.5
100021009506W500	11	1253.0	1280.0	27.0
100021211107W600	42	1639.8	1868.3	228.5
100021707118W500	11	2587.8	2614.1	26.4
100022308414W500	5	1666.0	1672.0	6.0
100023007118W500	16	2571.6	2617.3	45.7
100023612123W500	16	1123.0	1140.7	17.7
100030801114W400	7	1328.4	1346.3	17.9
100031212123W500	16	1042.5	1060.3	17.8
100031703620W400	5	1691.6	1702.6	11.0
100032705621W400	2	979.3	984.5	5.2
100032904301W500	3	2434.7	2441.1	6.4
100033204301W500	12	2400.6	2415.2	14.6
100040310007W500	6	246.3	271.3	25.0
100041003820W400	13	1583.1	1641.2	58.1
100041005624W400	25	1160.4	1193.3	32.9
100041009205W500	7	1275.0	1293.7	18.7
100041407808W500	14	1737.4	1752.6	15.2
100041410810W600	54	1816.3	1951.6	135.3
100042108708W500	6	1457.6	1465.2	7.6
100042308912W500	19	1600.5	1646.2	45.7
100042706903W500	4	1674.2	1683.3	9.1
100043309604W500	7	891.0	1135.4	244.4
100051605621W400	7	980.2	994.0	13.7
100052305918W500	24	3245.5	3272.9	27.4
100053006802W500	7	1679.0	1697.3	18.3
100053605621W400	13	926.9	964.1	37.2
100061008509W500	6	1543.0	1559.7	16.7
100061107304W500	3	1599.0	1601.9	2.9
100061204906W400	36	1102.2	1192.1	89.9
100061902919W400	3	1652.0	1660.9	8.8

Table 5-1 continued.

Drill Core ID	Number of Boxes	Start Depth (m)	End Depth (m)	Total Length (m)
100062208314W500	10	1794.0	1804.8	10.8
100062308414W500	2	1662.8	1667.7	4.9
100062308611W500	5	1528.4	1539.7	11.3
100062508611W500	5	1512.0	1523.9	11.9
100063311307W600	15	1522.8	1563.3	40.5
100063401306W400	10	1210.0	1235.0	25.0
100070205822W400	4	990.0	997.0	7.0
100070803620W400	11	1704.1	1719.0	14.9
100072204912W500	41	2983.5	3080.0	96.5
100072606923W500	3	2667.8	2673.8	6.0
100073002919W400	15	1632.0	1647.6	15.6
100073008610W500	3	1501.0	1508.6	7.6
100073210908W600	21	1762.4	1790.7	28.4
100080403820W400	15	1586.5	1642.3	55.8
100081008903W500	7	1448.0	1466.0	18.0
100081308708W500	13	1474.6	1488.8	14.2
100081408109W500	10	1729.0	1739.3	10.3
100082609204W500	14	1239.0	1275.0	36.0
100083101215W400	30	1353.0	1385.3	32.3
100090511408W600	7	1680.4	1698.7	18.3
100090608811W500	11	1562.5	1574.8	12.3
100090908314W500	7	1801.0	1819.3	18.3
100092509006W500	7	1485.0	1503.0	18.0
100092605010W502	7	2579.0	2599.0	20.0
100092705918W500	16	3207.7	3226.0	18.3
100093007418W500	14	2344.0	2359.7	15.7
100100506802W500	20	1681.9	1799.8	118.0
100100708714W500	15	1601.7	1617.9	16.2
100101505918W500	4	3359.2	3369.9	10.7
100102105918W500	14	3250.1	3265.3	15.2
100102505621W400	8	957.7	1000.0	42.4
100102803202W500	22	2723.7	2750.5	26.8
100103204501W400	57	1030.2	1094.2	64.0
100103305621W400	7	987.9	1004.6	16.8
100110209606W500	26	1234.0	1261.3	27.3
100110808306W600	5	2220.5	2227.2	6.7
100111208708W500	16	1344.0	1468.3	124.3
100111305027W400	9	1577.9	1601.5	23.6
100111404202W500	5	2378.7	2386.4	7.8
100111911008W600	8	1938.5	1947.1	8.5
100112505010W500	39	2527.0	2624.8	97.8
100112505621W400	25	945.5	1004.6	59.1
100112605621W400	18	957.1	1005.5	48.5
100112611203W600	18	225.0	260.0	35.0
100112904301W500	2	2290.0	2292.7	2.7
100113500605W400	7	1643.5	1661.7	18.2
100120204501W500	85	2044.6	2329.9	285.3
100120303820W400	17	1577.3	1642.3	64.9
100120808707W500	6	1502.7	1516.7	14.0
100121109402W500	7	1286.0	1303.0	17.0
100121311405W600	12	269.9	286.4	16.5
100121703620W400	9	1690.1	1714.2	24.1
100122003820W400	11	1570.0	1619.4	49.4
100122102926W400	16	2153.0	2171.0	18.0
100122705621W400	6	966.2	980.5	14.3
100130303820W400	15	1576.4	1636.2	59.7
100130708707W500	16	1466.0	1484.3	18.3
100131605724W400	10	1201.2	1224.1	22.9
100131704521W400	11	1468.8	1485.9	17.1
100132010709W600	20	1889.8	1941.9	52.1

Table 5-1 continued.

Drill Core ID	Number of Boxes	Start Depth (m)	End Depth (m)	Total Length (m)
100140708714W500	9	1612.4	1623.1	10.7
100142209606W500	16	945.0	963.3	18.3
100142407418W500	3	2323.0	2330.0	7.0
100142904521W400	58	1342.3	1482.9	140.5
100143108903W500	7	1442.8	1460.3	17.5
100143502921W400	8	1672.4	1691.6	19.1
100143602001W400	51	1640.0	1694.0	54.0
100143603520W400	16	1570.3	1610.0	39.6
100150209606W500	17	1212.0	1229.8	17.8
100150908314W500	3	1806.4	1813.4	7.0
100150908509W500	17	1533.0	1551.5	18.5
100152208611W500	3	1527.2	1535.5	8.3
100152507708W500	4	1771.4	1782.7	11.3
100152710907W500	18	760.8	809.9	49.1
100160503620W400	17	1711.2	1729.4	18.2
100160507108W500	8	2082.0	2175.4	93.4
100161308110W500	3	1732.0	1745.8	13.8
100163411821W500	43	1204.0	1311.9	107.9
100163505722W400	7	992.1	1004.6	12.5
100163605722W400	14	952.5	992.1	39.6
102040103021W400	10	1700.5	1730.7	30.2
102053508214W500	16	1767.0	1812.7	45.7
102062502920W400	2	1635.0	1639.9	4.9
102101208708W500	12	1457.9	1490.5	32.6
102102803820W400	8	1640.0	1647.5	7.5
102163503520W400	36	1594.5	1646.0	51.5
103022603520W400	33	1590.0	1638.8	48.8
103102212221W500	7	916.0	922.6	6.6
BM-96-2	50	22.0	161.6	139.6
BM-96-4	57	13.7	147.5	133.8
BM-96-7	44	70.0	183.5	113.5
BM96-03	33	4.7	160.0	155.3
BM96-05	49	32.0	178.3	146.3
BM96-06	2	69.8	74.7	4.9
BM96-08	51	51.7	180.8	129.1
BM96-09	52	48.0	182.7	134.7
CP-01	44	180.1	253.5	73.4
CP-02	38	170.9	298.9	128.0
DDH86-R1	153	5.2	328.9	323.7
FC-010	4	43.6	86.9	43.3
FC-012	4	28.0	61.5	33.5
FC-073	9	50.0	75.3	25.3
FC-076	54	112.7	226.6	113.9
L06-01	42	27.4	172.2	144.8
Synenco-01-02-FB-NLP	40	34.3	85.6	51.3
Synenco-20-12-Firebag	13	12.2	45.8	33.6
Synenco-20-52B-Firebag	8	9.5	53.9	44.4

Although there are numerous features observed in these spectra, there are eight spectral regions of interest that provide important compositional information: 400-1000, 1415, 1930, 2200, 2330, 8200, 9200, and 11,200 nm.

- 400-1000 nm: Referred to as the visible and near-infrared (VNIR), troughs and peaks observed in this range relate primarily to the electronic processes of transition elements, such as iron. Spectral variability in this wavelength region typically correlates with changes in colour.
- 1415 nm: Troughs observed in this wavelength region are produced by the overtones of the -OH stretch of hydroxyl and indicate the presence of the hydroxyl anion.
- 1930 nm: Troughs observed in this wavelength region are produced by the overtones of the -OH stretch and

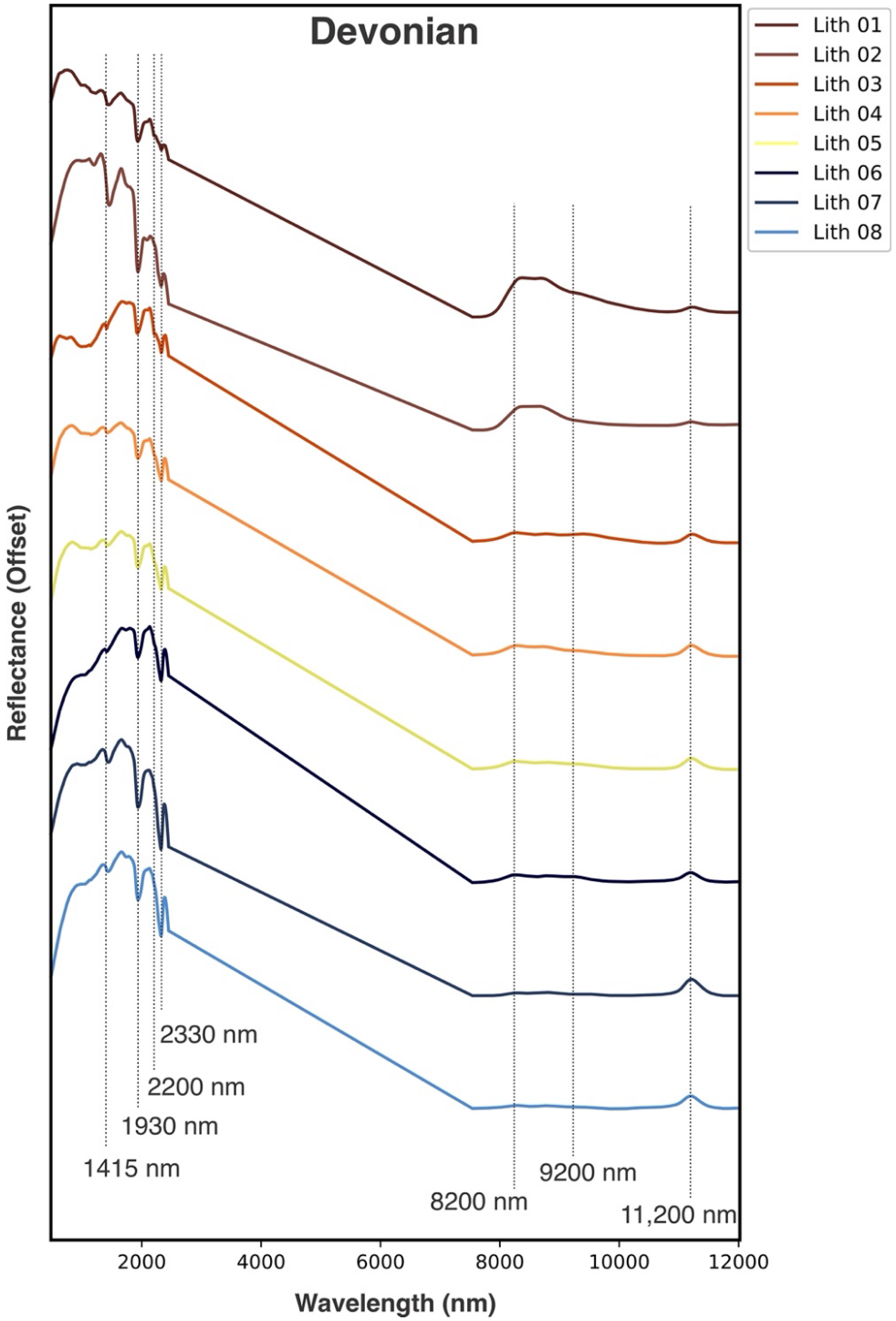

Figure 5-1. Representative spectra for the eight lithotypes identified in drill cores that primarily intersect Devonian rocks. Each spectrum is a composite of data collected from three different wavelength ranges (VNIR, SWIR, and LWIR), and the straight line between 2450 and 7500 nm is due to a gap in sensor coverage. Vertical lines at 1415, 1930, 2200, 2300, 8200, 9200, and 11,200 nm show locations of important diagnostic spectral features.

HOH bend of water and indicate the presence of molecular water.

- 2200 nm: Troughs observed near 2200 nm are produced by the combination band involving the -OH fundamental stretch of hydroxyl bound to aluminum and indicate the presence of white micas such as muscovite and phengite, and clays such as montmorillonite.
- 2330 nm: Troughs observed near 2330 nm are often produced by the carbonate anion (CO_3^{2-}) bound to cations, such as magnesium and/or iron, indicating the presence of various carbonate minerals. The detailed position and shape of troughs in this wavelength region help identify the minerals present.
- 8200 nm: Peaks observed near 8200 nm are produced by the fundamental vibration modes of the Si-O asymmetrical stretch. The wavelength position of these peaks indicates the presence of minerals like quartz.
- 9200 nm: Peaks observed near 9200 nm are produced by the fundamental vibration modes of the Si-O asymmetrical stretch. The wavelength position of these peaks indicates the presence of white micas and chlorites, for example.
- 11,200 nm: Peaks observed around 11,200 nm are produced by the vibration of the carbonate anion (CO_3^{2-}) in carbonate minerals.

The infrared-active minerals identified in this dataset are included in the lithotype legend (Figure 5-2). It is critical to note that spectroscopy of this type is not a quantitative mineralogical technique, and other non-infrared-active minerals can be present in these rocks. Many minerals do not produce intense infrared spectral features that can be easily detected. Therefore, the legend provided for the lithotypes describes only those minerals that produce obvious diagnostic spectral absorption features. For a comprehensive mineralogical assessment of the different lithotypes, other analytical techniques, such as microscopy, X-Ray Diffractometry (XRD), Scanning Electron Microscopy (SEM), and/or Wavelength- or Energy-Dispersive X-Ray Spectroscopy (WDS/EDS), should be employed.

Class	Primary SWIR-Active Minerals	Secondary SWIR-Active Mineral	LWIR-Active Minerals
Lith 01	Muscovitic Illite	Carbonate	Quartz + Phyllosilicates + Carbonate
Lith 02	Muscovitic Illite	Carbonate	Quartz + Phyllosilicates + Carbonate
Lith 03	Carbonate + Muscovitic Illite	Fe2+ Bearing	Quartz + Carbonate + Phyllosilicates
Lith 04	Carbonate	Muscovitic Illite	Carbonate + Quartz + Phyllosilicates
Lith 05	Carbonate	Muscovitic Illite	Carbonate + Quartz + Phyllosilicates
Lith 06	Carbonate	Muscovitic Illite	Carbonate + Quartz + Phyllosilicates
Lith 07	Carbonate		Carbonate
Lith 08	Carbonate		Carbonate

Figure 5-2. Legend describing the eight lithotypes identified in drill cores that intersect Devonian rocks. The lithotypes are described in terms of their short- and long-wave infrared-active minerals.

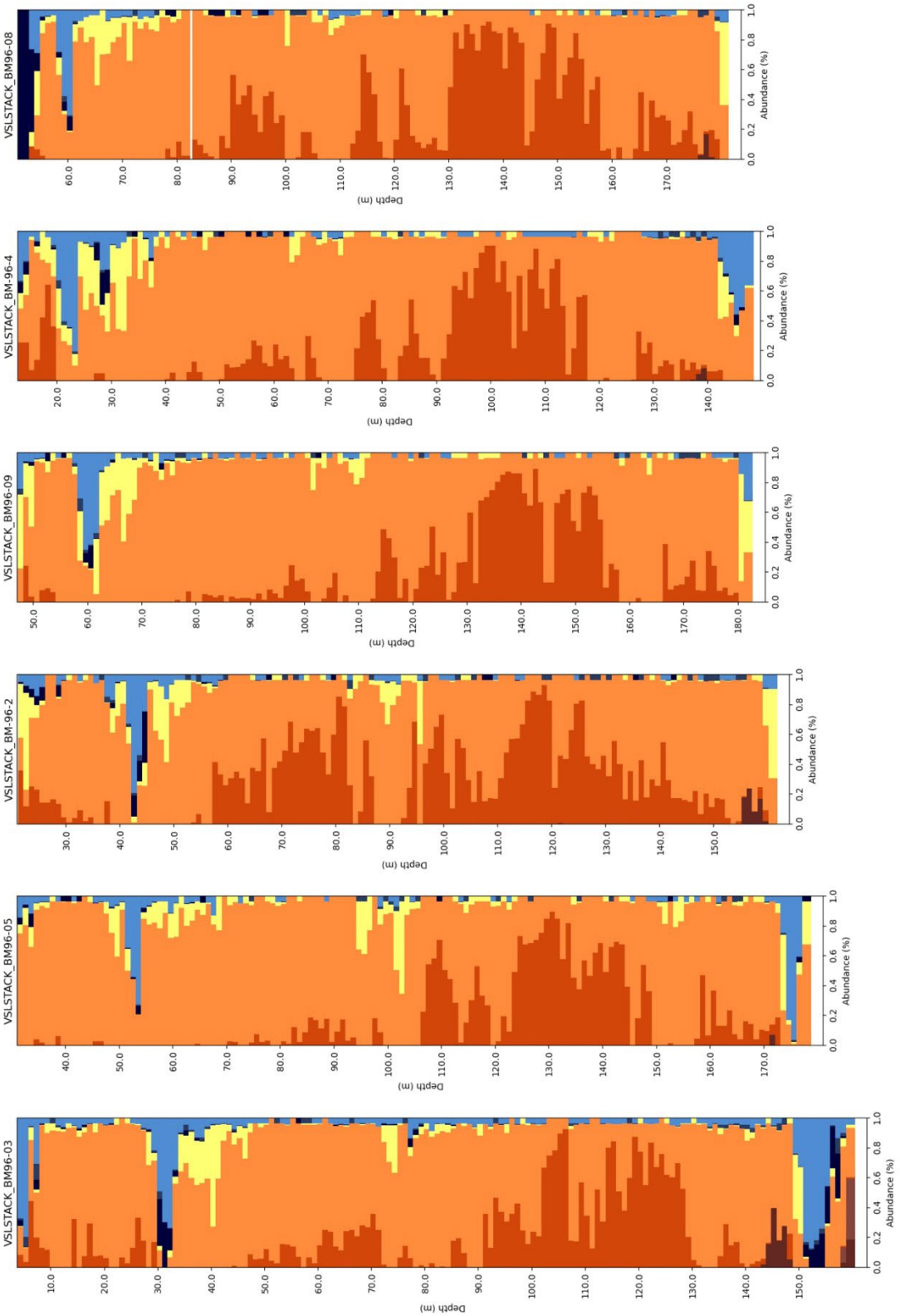

Figure 5-3. Spectral logs for drill cores that intersect Devonian rocks shown at one-meter depth binning intervals. The lithotype legend is provided in Figure 5-2.

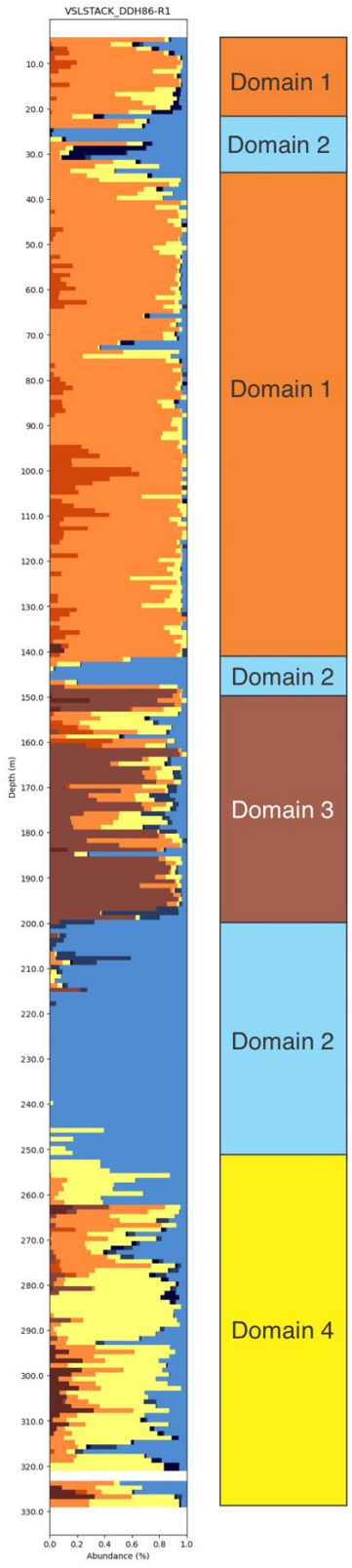

Figure 5-4. Spectral log for DDH86-R1 plotted next to the visually generated strip log. The lithotype legend is provided in Figure 5-2.

A spectral log was produced for each drill core showing the frequency and distribution of the eight different lithotypes at one-meter depth intervals. The spectral logs presented were chosen because they show similar lithotype patterns that likely represent compositional change that can be useful for unit or facies correlation.

5.3 Discussion

As observed in the reflectance spectra, the rocks from the Devonian are dominated by carbonates (Figures 5-1 and 5-2), which are inferred by the presence of intense troughs at 2330 nm, and a peak near 11,200 nm. Lithotypes 1, 2, and 3 show a lower abundance of carbonate, with more carbonate observed in Lithotypes 4, 5, and 6, and even more carbonate observed in Lithotypes 7 and 8 (Figure 5-2).

In the six spectral logs shown in Figure 5-3, similar spatial lithotype distributions are observed. Although these drill cores have different starting depths (e.g., 0 to 70 meters), they all show very similar lithotype patterns. Overall, these drill cores are dominated by Lithotype 4, which is mainly comprised of carbonate, but the presence and distribution of Lithotype 3—which contains more muscovitic illite—is similar between the different drill cores. This lithotype pattern may indicate a higher influence of siliciclastic sediments at certain times during the Devonian.

Furthermore, using spectral logs, it is possible to observe compositional change as a function of depth (Figure 5-4). For example, in DDH86-R1—which is over 300 meters long—several different carbonate compositions are observed. A visually generated strip log is plotted alongside the spectral log to show the compositional change between siliciclastic and carbonate sedimentary influences, with each compositional change represented by a different domain.

6. Carboniferous to Jurassic

6.1 Overview

In Alberta, the Carboniferous to Jurassic periods included significant geological change. During the Carboniferous, Alberta was situated near the equator, where limestones and dolomites were deposited in shallow, warm, marine environments, along with significant coal beds in terrestrial areas (Richards et al., 1990). During the transition to the Permian, the climate became drier, depositing predominantly siliciclastic sandstones and siltstones (Henderson et al., 1990). During the Triassic, siliciclastic rocks were common, primarily representing fluvial and deltaic environments (Edwards et al., 1990). In the Jurassic, the effects of the western Cordilleran mountain-building event led to the deposition of thick sedimentary sequences, including marine shales and volcanic ash layers, reflecting the active tectonic and volcanic activity that existed during the formation of the Rocky Mountains (Poulton et al., 1994).

6.2 Results

Altogether 32 drill cores totalling 616 meters from this chronostratigraphic interval were analyzed using the Lithotype™ Method (Table 6-1), and 17 lithotypes were identified. Although this particular interval covers a relatively long period of geologic time, it comprises the lowest amount of scanned rock within this project. Despite that, it produced the second-largest set of extracted lithotypes.

The representative spectra for each lithotype are provided in Figure 6-1. Each spectrum is a composite of data collected from three different hyperspectral imaging cameras (VNIR, SWIR, and LWIR), and the straight line between 2450 and 7500 nm is due to a gap in sensor coverage. Vertical lines at 1415, 1930, 2200, 2300, 8200, 9200, and 11,200 nm show the locations of important spectral features (Figure 6-1).

Although there are numerous features observed in these spectra, there are eight spectral regions of interest that provide important compositional information: 400-1000, 1415, 1930, 2200, 2330, 8200, 9200, and 11,200 nm.

- 400-1000 nm: Referred to as the visible and near-infrared (VNIR), troughs and peaks observed in this range relate primarily to the electronic processes of transition elements, such as iron. Spectral variability in this wavelength region typically correlates with changes in colour.
- 1415 nm: Troughs observed in this wavelength region are produced by the overtones of the -OH stretch of hydroxyl and indicate the presence of the hydroxyl anion.
- 1930 nm: Troughs observed in this wavelength region are produced by the overtones of the -OH stretch and HOH bend of water and indicate the presence of molecular water.
- 2200 nm: Troughs observed near 2200 nm are produced by the combination band involving the -OH fundamental stretch of hydroxyl bound to aluminum and indicate the presence of white micas such as muscovite and phengite, and clays such as montmorillonite.
- 2330 nm: Troughs observed near 2330 nm are often produced by the carbonate anion (CO_3^{2-}) bound to cations, such as magnesium and/or iron, indicating the presence of various carbonate minerals. The detailed position and shape of troughs in this wavelength region help identify the minerals present.
- 8200 nm: Peaks observed near 8200 nm are produced by the fundamental vibration modes of the Si-O asymmetrical stretch. The wavelength position of these peaks indicates the presence of minerals like quartz.

Table 6-1. Drill cores of Carboniferous to Jurassic rocks analyzed in this study.

Drill Core ID	Number of Boxes	Start Depth (m)	End Depth (m)	Total Length (m)
100020208807W600	6	1151.0	1167.6	16.6
100021401114W400	3	900.8	908.8	8.0
100021906724W500	10	1907.0	1934.1	27.1
100023303703W500	8	2220.5	2241.5	21.0
100060807705W600	7	1385.0	1403.2	18.2
100062300703W400	14	1417.3	1432.6	15.2
100071606925W500	17	1773.0	1791.0	18.0
100072906925W500	16	1783.0	1801.2	18.2
100073200804W400	3	1327.4	1329.4	2.0
100081606925W500	17	1765.0	1783.6	18.6
100082101114W400	6	934.0	949.5	15.5
100082907705W600	28	1350.0	1390.4	40.4
100083507506W600	14	1759.0	1795.3	36.3
100091701114W400	4	898.0	908.8	10.8
100110101114W400	7	915.5	933.5	18.0
100110108513W600	5	1321.3	1334.1	12.8
100120508605W600	32	999.0	1035.6	36.6
100121006925W500	17	1724.0	1742.8	18.8
100130108411W600	4	1210.0	1219.0	9.0
100133006418W500	17	1779.0	1797.6	18.6
100140106725W500	6	2149.0	2161.7	12.7
100142605812W500	3	1791.0	1799.3	8.3
100151607509W600	18	2271.0	2289.7	18.7
100151800804W400	18	1278.6	1323.4	44.8
100161006925W500	16	1727.0	1745.0	18.0
100162006925W500	16	2070.5	2088.5	18.0
100162605812W500	5	1896.0	1908.8	12.8
102051507509W600	12	2289.0	2321.1	32.1
102062911211W600	13	315.0	333.0	18.0
102063608313W600	6	1308.0	1323.4	15.4
102101706424W500	35	2262.5	3595.5	1333.0
102160907205W600	7	1893.0	1910.9	17.9

- 9200 nm: Peaks observed near 9200 nm are produced by the fundamental vibration modes of the Si-O asymmetrical stretch. The wavelength position of these peaks indicates the presence of white micas and chlorites, for example.
- 11,200 nm: Peaks observed around 11,200 nm are produced by the vibration of the carbonate anion (CO_3^{2-}) in carbonate minerals.

The infrared-active minerals identified in this dataset are included in the lithotype legend (Figure 6-2). It is critical to note that spectroscopy of this type is not a quantitative mineralogical technique, and other non-infrared-active minerals can be present in these rocks. Many minerals do not produce intense infrared spectral features that can be easily detected. Therefore, the legend provided for the lithotypes describes only those minerals that produce obvious diagnostic spectral absorption features. For a comprehensive mineralogical assessment of the different lithotypes, other analytical techniques, such as microscopy, X-Ray Diffractometry (XRD), Scanning Electron Microscopy (SEM), and/or Wavelength- or Energy-Dispersive X-Ray Spectroscopy (WDS/EDS), should be employed.

A spectral log was produced for each drill core showing the frequency and distribution of the 17 different lithotypes at one-meter depth intervals. The spectral logs from 15 drill cores from this interval are presented in Figure 6-3. These drill cores were selected because they are the longest drill cores in this interval, and they show the full range of compositional heterogeneity. The drill cores from this interval are quite short. Most are <20 meters in length, with the longest being ~50 meters.

6.3 Discussion

This chronostratigraphic interval is the smallest interval in this dataset with respect to drill core meterage, with 32 drill cores totalling just over 600 meters. However, in this limited dataset, extensive compositional heterogeneity was observed as indicated by the extraction of 17 lithotypes. The identification of such a large number of lithotypes indicates that the rocks from the Carboniferous to Jurassic encompass a very wide range of rock compositions. This observation is consistent with the fact that this interval represents a time of terrestrial and marine deposition, including several transgression and regression events (e.g., Edwards et al., 1990; Henderson et al.,

1990; Poulton et al., 1994; Richards et al., 1990, and references therein), leading to extensive diversity in Carboniferous to Jurassic rock compositions in Alberta.

As observed in the reflectance spectra, the rocks from this interval are dominated by silicate minerals, such as illite and quartz, which produce troughs near 2200 nm and peaks near 8200 and 9200 nm, and carbonates, which produce troughs near 2330 nm and peaks near 11,200 nm (Figure 6-1). Overall, compared to the Devonian, there is a much higher abundance of silicic compositions. Six drill cores that represent a single, distinct compositional zone are plotted in Figure 6-4. With one exception, these drill cores are found at similar depths (e.g., 1,700 meters vs 2,000 meters).

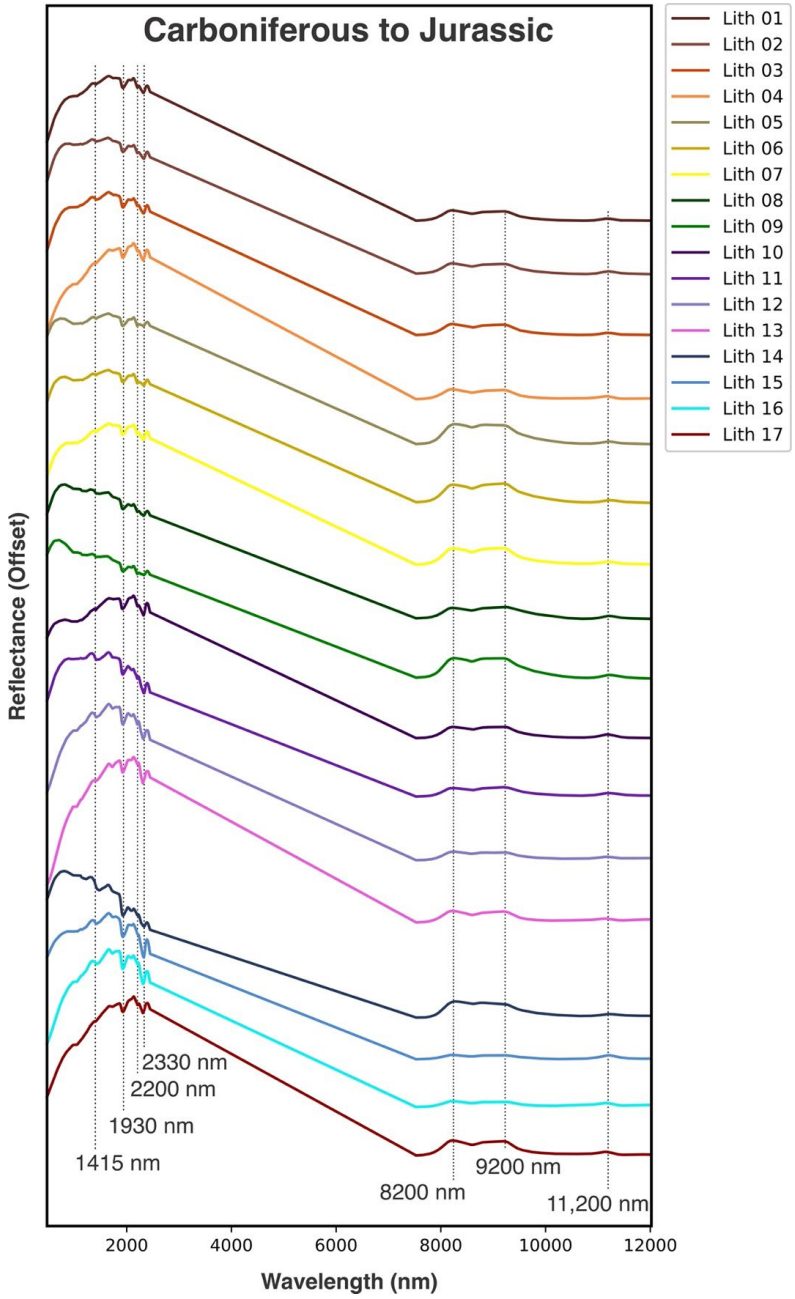

Figure 6-1. Representative spectra for the 17 lithotypes identified in drill cores that intersect Carboniferous to Jurassic rocks. Each spectrum is a composite of data collected from three different wavelength ranges (VNIR, SWIR, and LWIR), and the straight line between 2450 and 7500 nm is due to a gap in sensor coverage. Vertical lines at 1415, 1930, 2200, 2300, 8200, 9200, and 11,200 nm show locations of important diagnostic spectral features.

Class	Primary SWIR-Active Minerals	Secondary SWIR-Active Mineral	LWIR-Active Minerals
Lith 01	Carbonate + Muscovitic Illite		Quartz + Phyllosilicates + Carbonate
Lith 02	Carbonate + Muscovitic Illite		Quartz + Phyllosilicates + Carbonate
Lith 03	Carbonate + Muscovitic Illite		Quartz + Phyllosilicates + Carbonate
Lith 04	Carbonate + Muscovitic Illite	Chlorite	Quartz + Carbonate + Phyllosilicates
Lith 05	Carbonate + Muscovitic Illite	Fe2+ bearing	Quartz + Phyllosilicates + Carbonate
Lith 06	Carbonate + Muscovitic Illite	Fe2+ bearing	Phyllosilicates + Quartz + Carbonate
Lith 07	Carbonate + Muscovitic Illite		Phyllosilicates + Quartz + Carbonate
Lith 08	Carbonate + Muscovitic Illite		Phyllosilicates + Quartz + Carbonate
Lith 09	Carbonate + Muscovitic Illite		Quartz + Phyllosilicates + Carbonate
Lith 10	Carbonate + Muscovitic Illite	Fe2+ bearing	Phyllosilicates + Carbonate + Quartz
Lith 11	Carbonate + Muscovitic Illite		Phyllosilicates + Carbonate + Quartz
Lith 12	Carbonate + Muscovitic Illite		Quartz + Carbonate + Phyllosilicates
Lith 13	Carbonate + Muscovitic Illite		Quartz + Phyllosilicates + Carbonate
Lith 14	Carbonate + Muscovitic Illite		Quartz + Phyllosilicates + Carbonate
Lith 15	Carbonate		Carbonate + Quartz + Phyllosilicates
Lith 16	Carbonate	Illite	Carbonate + Quartz + Phyllosilicates
Lith 17	Carbonate + Muscovitic Illite		Quartz + Phyllosilicates + Carbonate

Figure 6-2. Legend describing the 17 lithotypes identified in drill cores that intersect Carboniferous to Jurassic rocks. The lithotypes are described in terms of their short- and long-wave infrared-active minerals.

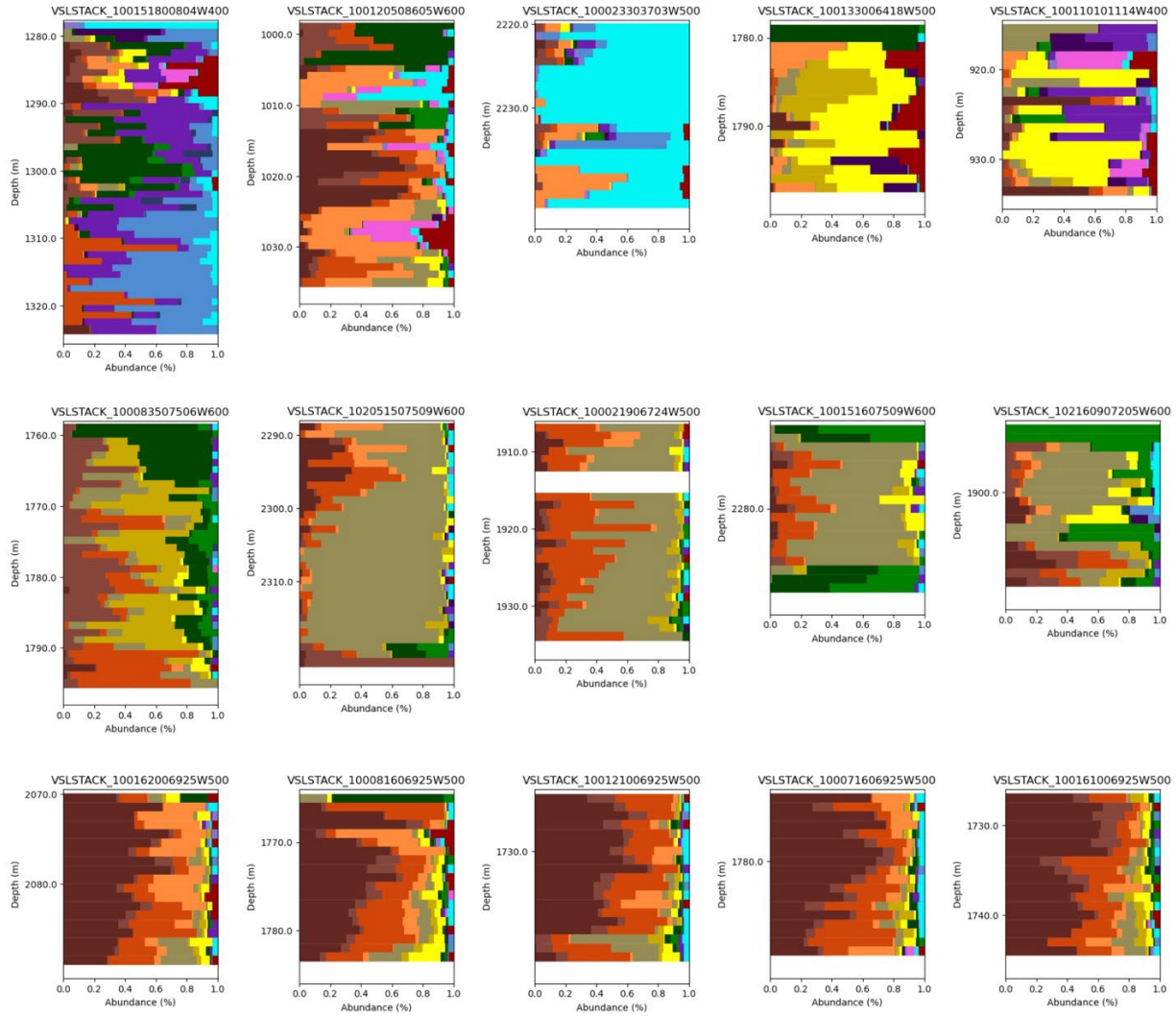

Figure 6-3. Spectral logs for 15 drill cores that intersect Carboniferous to Jurassic rocks, at one-meter depth binning intervals. The lithotype legend is provided in Figure 6-2

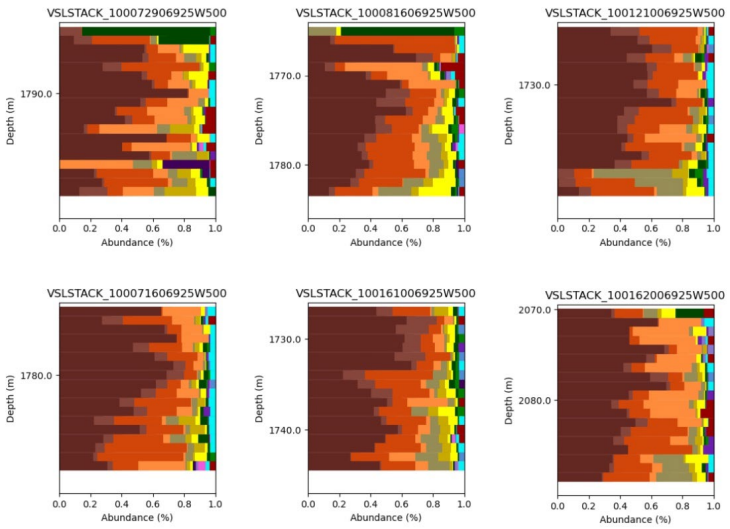

Figure 6-4. Spectral logs at one-meter depth binning intervals showing how spectral logs can be used to correlate similar compositions. The lithotype legend is provided in Figure 6-2.

7. Cretaceous

7.1 Overview

During the Cretaceous, Alberta's landscape was strongly influenced by an inland sea (Williams and Stelck, 1975; Caldwell, 1984). As a result, this period is characterized by the deposition of a wide array of sandstones, shales, and limestones in marine environments, and coal in terrestrial areas (Stott, 1982; Reinson, et al., 1994). In the Early Cretaceous, Alberta was largely covered by shallows seas that stretched from the Arctic Ocean to the Gulf of Mexico (Hayes et al., 1994). By the Late Cretaceous, the seas began to retreat, and large parts of Alberta became dominated by coastal and continental environments, resulting in the deposition of clastic sedimentary rocks, (Bhattacharya et al., 1994, and references therein).

Table 7-1. Drill cores of Cretaceous rocks analyzed in this study.

Drill Core ID	Number of Boxes	Start Depth (m)	End Depth (m)	Total Length (m)
00DH-02	4	3.0	19.8	16.8
00DH-03	5	2.3	22.9	20.6
00DH-04	6	2.9	25.9	23.1
00DH-05	4	4.3	19.8	15.5
00DH-06	6	2.0	29.0	27.0
00DH-07	7	1.5	29.0	27.5
00DH-08	3	1.5	13.7	12.2
00DH-09	18	3.9	77.7	73.8
00DH-10	6	0.7	25.9	25.2
00DH-11	5	2.8	25.9	23.2
00DH-12	4	2.0	22.9	20.9
00DH-13	5	3.9	22.8	18.9
00DH-14	5	3.7	22.8	19.1
00DH-15	5	2.5	22.9	20.3
08-014	8	0.3	31.7	31.4
100011802324W400	26	209.0	403.8	194.8
100012401427W400	17	681.2	724.6	43.4
100013302326W400	7	735.0	744.0	9.0
100013602422W400	11	220.0	234.3	14.3
100020103408W500	7	2085.4	2103.7	18.3
100021301114W400	4	908.9	919.0	10.1
100021605617W500	17	1199.0	1218.0	19.0
100022204008W400	6	880.0	893.4	13.4
100022704008W400	6	887.0	900.9	13.9
100023003519W400	1	1174.2	1175.3	1.1
100040501323W400	87	140.0	568.4	428.4
100041002426W400	40	335.0	535.9	200.9
100042001728W400	41	889.5	989.9	100.4
100042103407W502	4	2480.0	2489.8	9.8
100050200408W400	12	339.0	356.7	17.7
100050507421W500	19	221.3	247.0	25.7
100051501913W400	48	145.0	274.2	129.2
100052601908W400	6	142.0	150.7	8.7
100060103408W500	7	1022.0	1027.3	5.3
100060405608W400	11	292.6	308.9	16.3
100060503406W500	16	3003.0	3021.0	18.0
100060602422W400	14	229.0	247.2	18.2
100060802619W400	28	469.1	511.0	41.9
100061001008W400	5	321.0	328.5	7.5
100061001307W400	18	368.5	391.3	22.8
100061501114W400	4	880.0	890.0	10.0
100062201204W400	5	377.6	391.4	13.7
100062501205W400	6	360.9	370.0	9.1
100062900806W400	33	250.0	294.6	44.6
100062903307W500	2	2957.5	2960.8	3.3
100063102721W400	7	503.0	512.0	9.0

Table 7-1 continued.

Drill Core ID	Number of Boxes	Start Depth (m)	End Depth (m)	Total Length (m)
100063606413W500	17	1688.0	1706.3	18.3
100070101514W400	12	176.0	194.0	18.0
100070400904W400	2	1194.0	1199.0	5.0
100070503407W500	3	2609.8	2613.0	3.2
100071001406W400	7	376.4	388.3	11.9
100071101726W400	41	804.0	857.0	53.0
100071102526W400	44	198.8	502.0	303.2
100071202525W400	6	194.8	203.9	9.1
100071700307W400	6	316.1	325.2	9.1
100071703407W500	38	2550.9	2592.3	41.5
100072001106W400	5	324.6	333.7	9.1
100072004605W400	12	363.0	378.3	15.3
100072100525W400	39	506.7	562.1	55.4
100072502227W400	44	329.0	577.7	248.7
100080201724W400	46	248.1	314.5	66.4
100081003407W500	12	2411.0	2424.0	13.0
100081105009W400	63	310.0	392.9	82.9
100081302015W400	5	164.5	171.9	7.4
100081702512W400	5	200.0	207.5	7.5
100081801926W400	16	875.0	897.3	22.3
100081804904W400	6	351.0	360.1	9.1
100081901927W400	14	643.0	697.6	54.6
100082403407W500	26	3044.0	3111.6	67.6
100082605812W500	3	552.9	554.9	2.0
100083501025W400	19	359.3	407.3	48.0
100083603408W500	16	2473.0	2490.3	17.3
100090202323W400	14	160.0	598.5	438.5
100090203408W500	7	2334.0	2351.7	17.7
100090703406W500	10	2974.0	2987.0	13.0
100092000325W400	55	614.0	697.0	83.0
100092102303W500	11	1131.0	1186.1	55.1
100092700209W400	14	301.6	319.8	18.2
100092705504W500	1	1330.0	1330.6	0.6
100092801823W400	45	144.4	315.9	171.5
100093001404W400	14	375.0	392.8	17.8
100100906210W500	3	1473.5	1480.4	6.9
100101101204W400	8	365.8	378.0	12.2
100101303408W500	9	2567.0	2576.2	9.2
100101502425W400	11	680.3	695.6	15.2
100101701114W400	4	907.0	916.5	9.5
100101702217W400	49	122.0	319.5	197.5
100102001405W400	5	357.2	364.8	7.6
100102400804W400	6	996.0	1003.7	7.7
100102503307W500	9	2448.0	2457.0	9.0
100102802427W400	60	334.0	759.6	425.6
100102901105W400	3	360.9	368.4	7.5
100110803406W500	3	2945.0	2951.6	6.6
100110903407W500	7	2465.0	2483.0	18.0
100111104109W500	4	2681.0	2692.6	11.6
100111501205W400	12	326.1	344.4	18.3
100112301505W400	7	367.3	379.2	11.9
100112307609W600	12	805.9	1177.7	371.9
100112606414W400	6	282.3	290.2	7.9
100113105624W400	2	1066.5	1070.5	4.1
100113507806W500	13	190.0	207.9	17.9
100113604806W400	22	362.0	398.0	36.0
100120800625W400	37	525.0	579.5	54.5

Table 7-1 continued.

Drill Core ID	Number of Boxes	Start Depth (m)	End Depth (m)	Total Length (m)
100123003307W500	14	2089.8	2104.0	14.2
100123103307W500	4	2443.0	2446.3	3.3
100131101511W400	5	930.0	942.4	12.4
100141201826W400	12	253.6	453.5	199.9
100141202202W500	12	1286.0	1303.0	17.0
100141601014W400	15	930.0	946.5	16.5
100141701726W400	53	575.0	650.2	75.2
100141803407W500	1	2555.0	2557.4	2.4
100142102323W400	66	230.0	420.8	190.8
100142903418W400	7	1196.0	1214.0	18.0
100143102521W400	100	181.0	327.4	146.4
100143202027W400	16	590.0	689.9	99.9
100143601629W400	10	950.8	985.5	34.7
100151005006W400	74	280.0	397.0	117.0
100160101623W400	11	160.0	200.8	40.8
100160903407W500	4	2535.0	2545.7	10.7
100161401114W400	7	861.1	879.3	18.3
100161502820W400	5	446.0	453.5	7.5
100161900408W400	8	344.0	359.7	15.7
100162903418W400	7	1203.0	1221.7	18.7
102012900904W400	13	638.0	656.0	18.0
102021202328W400	5	655.0	664.9	9.9
102031302520W400	34	83.0	191.3	108.3
102041302523W400	52	237.2	362.5	125.3
102060606605W400	9	237.0	254.0	17.0
102061100903W400	3	352.0	357.8	5.8
102061502026W400	7	549.5	606.3	56.8
102062001727W400	14	770.0	799.0	29.0
102062501525W400	21	480.0	532.4	52.4
102070104501W400	6	285.0	294.1	9.1
102070500904W400	8	678.0	690.9	12.9
102071301008W400	8	313.0	325.0	12.0
102072206703W400	39	252.8	327.7	74.9
102101201706W400	34	353.1	401.8	48.8
102102106704W400	64	204.7	286.8	82.1
102111206218W400	19	360.0	396.5	36.5
102112801428W400	49	1007.0	1078.9	71.9
102120205209W400	42	340.0	395.4	55.4
102132201811W400	5	117.0	124.5	7.5
102141707003W400	8	229.6	241.6	12.0
103032306703W400	12	272.4	290.1	17.7
103082400906W400	33	243.0	283.2	40.2
10LD-06	45	0.0	99.7	99.7
110140306503W400	13	261.0	279.0	18.0
1AA103206604W400	7	250.0	259.2	9.2
1AA123106503W400	8	211.4	225.0	13.6
1AA123406604W400	7	260.8	271.5	10.7
1AA151206703W400	9	277.5	289.0	11.6
1AN070806503W400	110	148.0	272.8	124.8
1F1043606603W400	127	179.9	376.7	196.8
1F1052908219W400	2	346.0	348.7	2.7
1F1060911112W600	9	336.0	348.0	12.0
8CH-01	10	0.9	16.2	15.2
8CH-02	16	0.9	26.8	25.9
8CH-04	12	0.6	21.9	21.3
8CH-06	5	0.8	25.5	24.7
8CH-07	5	0.8	22.1	21.3

Table 7-1 continued.

Drill Core ID	Number of Boxes	Start Depth (m)	End Depth (m)	Total Length (m)
8CH-08	19	0.9	40.5	39.6
8CH-09	6	0.9	10.1	9.1
8VIP001	94	21.6	178.9	157.6
98-DH-LE-01	77	17.2	228.6	211.4
98-DH-PH-02	45	108.0	201.2	93.2
98-DH-PH01	74	97.5	225.9	128.4
98-DH-RO-1	32	85.7	177.5	91.8
98-DH-VA-01	15	98.2	131.6	33.4
98-DH-VA-02	38	119.8	200.3	80.5
9BAH-52	23	9.1	81.7	72.5
9MMU001	22	37.8	100.6	62.8
9MMU002	16	10.4	43.9	33.5
9MMU003	39	21.9	105.2	83.2
9MMU004	38	7.3	101.8	94.5
9MMU006	64	4.0	150.9	146.9
BHH04-KHR-1	28	18.6	99.1	80.5
BHH04-KHR-2	41	9.1	105.2	96.0
BP-Athabasca-4C	37	11.9	59.7	47.9
CC98-2	18	42.0	387.0	345.0
CC98-8	18	50.3	151.5	101.2
CH16-79	86	26.0	213.8	187.8
CLK-002	12	37.5	86.3	48.8
CLK-003	37	29.0	107.6	78.6
CLK-004	5	97.5	109.7	12.2
CLK-005	29	28.3	106.7	78.3
CLK-006	17	28.3	98.5	70.1
CLK-007	24	23.5	140.2	116.7
CLK-008	12	35.7	103.3	67.7
CLK-009	43	40.2	100.6	60.4
COX-99-1	37	0.0	120.5	120.5
COX-99-2	51	0.0	166.7	166.7
COX-99-3	19	6.1	63.1	57.0
DDH-8VIP002	109	0.0	173.7	173.7
DDH-A3-01	69	26.8	164.0	137.2
DDH-SR-01	128	9.1	266.1	257.0
DDH97-14-1	1	92.8	95.8	3.0
DDH97-14-6	20	69.2	114.9	45.7
DDH97-14-7	26	5.2	247.3	242.1
DDH97-14B-1	4	7.5	89.0	81.5
DDH97-14B-2	17	74.2	137.8	63.6
DDH97-14B-3	11	23.5	92.8	69.3
DDH97-14C-1	14	11.9	81.8	69.9
DDH97-14C-3	9	64.6	84.9	20.3
DDH97-14C-4	2	66.9	69.2	2.3
DDH97-14C-6	4	61.6	69.2	7.6
DDH97-14C-7	9	24.6	79.0	54.4
DDH97-19-1	1	130.2	133.2	3.0
DDH97-1A-1	21	109.0	160.2	51.2
DDH97-1A-3	13	43.0	78.3	35.4
DDH97-1B-1	8	138.0	155.5	17.5
DDH97-1B-2	4	73.4	153.4	80.0
DDH97-5A-10	5	141.9	154.5	12.6
DDH97-5A-1	3	129.2	213.5	84.3
DDH97-5A-5	2	114.0	120.0	6.1
DDH97-5A-6	4	96.5	223.0	126.5
DDH97-5A-7	2	120.1	126.3	6.2
DDH97-5A-8	2	123.2	127.1	4.0

Table 7-1 continued.

Drill Core ID	Number of Boxes	Start Depth (m)	End Depth (m)	Total Length (m)
DDH97-5B-1	1	194.6	197.5	3.0
DDH97-6-4	2	107.4	111.9	4.5
DDH97-6-8	3	229.6	237.5	7.9
DDH97-6-9	13	61.0	197.2	136.3
DDH97-6D-1	32	35.7	108.8	73.1
DDH97-91-1	1	128.6	133.2	4.6
DDH97-91-3	4	128.6	145.4	16.7
DDH97-91-B1	28	30.7	93.5	62.8
ECC2008-01	59	0.0	150.0	150.0
GCA08-01	10	78.2	106.2	28.0
GCA08-02	36	51.8	160.3	108.5
GCA08-03	48	74.8	188.1	113.2
ITS98-E4	30	11.0	106.7	95.7
ITS98-M	14	15.2	88.4	73.2
ITS98-M2a	18	18.3	97.5	79.3
ITS98-M2b	3	6.1	27.4	21.3
ITS98-N4	14	15.2	51.2	36.0
ITS98-W3	9	12.2	76.4	64.2
J42-01	19	93.5	150.5	57.0
J6-01	9	87.5	121.0	33.5
JZ08-01	6	121.0	130.0	9.0
JZ24-01	6	109.0	118.0	9.0
L06-02	39	40.0	167.0	127.0
L07-03	60	29.0	111.3	82.3
L07-06	4	104.7	112.8	8.1
L07-07	15	131.6	161.9	30.2
L07-08	12	139.2	163.1	23.9
L07-10	1	47.8	50.5	2.8
L07-12	16	33.8	73.0	39.2
ML-95-1	42	5.8	123.9	118.1
ML-01-91	6	5.0	21.5	16.5
ML-03-91	18	246.1	290.0	43.9
ML-04-91	22	172.0	220.0	48.0
ML-05-91	18	10.0	125.0	115.0
ML-06-91	9	76.3	113.0	36.7
ML-07-91	21	43.0	261.0	218.0
ML-08-91	16	16.6	206.0	189.4
ML-09-91	35	12.0	155.0	143.0
Mobil-Ov-37-98-12-Kearl	43	118.0	182.6	64.6
NWG-05-03	49	0.0	147.0	147.0
PM-00-04	7	4.6	24.4	19.8
PM99-01	41	6.7	87.8	81.1
PM99-02	23	2.4	48.2	45.7
PM99-03	14	4.3	48.2	43.9
PR24-1-PR24-1a	17	18.9	79.2	60.3
PR98-08	16	103.9	134.4	30.5
PR98-11	36	30.5	127.1	96.6
PR98-12	21	17.1	60.7	43.6
PR98-13	14	12.2	47.9	35.7
PR99-02	12	112.8	166.7	54.0
PR99-03	30	126.5	174.7	48.2
SID01	33	1.8	40.9	39.1
SL98-1	30	50.9	145.4	94.5
SMB08-01	9	101.9	147.0	45.1
SMB08-02	3	157.8	170.1	12.3
SMB08-03	12	139.6	178.6	39.0
SMB08-04	38	109.7	182.0	72.2

Table 7-1 continued.

Drill Core ID	Number of Boxes	Start Depth (m)	End Depth (m)	Total Length (m)
SMB08-05	4	89.1	199.5	110.4
SMB08-06	8	168.1	190.0	21.9
SMB08-07	13	91.5	186.0	94.5
SMB08-08	11	158.5	189.5	31.0
ST00-1	190	9.1	389.0	379.9
ST00-2	113	15.2	252.1	236.8
ST00-3	124	18.3	377.0	358.7
Synenco-01-86-NLP	50	9.1	84.1	75.0
Synenco-01-92-NLP	22	5.0	48.8	43.8
Synenco-01-95-NLP	26	19.1	58.1	39.0
Synenco-20-79-Firebag	63	4.8	92.0	87.2

7.2 Results

Altogether 285 drill cores totalling 11,972 meters from this chronostratigraphic interval were analyzed using the Lithotype™ Method (Table 7-1), and 18 lithotypes were identified. With 18 lithotypes, this interval produced the largest number of lithotypes and had the second-largest amount of scanned rock in this project.

The representative spectra for each lithotype are provided in Figure 7-1. Each spectrum is a composite of data collected from three different hyperspectral imaging cameras (VNIR, SWIR, and LWIR), and the straight line between 2450 and 7500 nm is due to a gap in sensor coverage. Vertical lines at 1415, 1930, 2200, 2300, 8200, 9200, and 11,200 nm show the locations of important spectral features (Figure 7-1).

Although there are numerous features observed in these spectra, there are seven spectral regions of interest that provide important compositional information: 400-1000, 1415, 1930, 2200, 2330, 8200, and 9200 nm.

- 400-1000 nm: Referred to as the visible and near-infrared (VNIR), troughs and peaks observed in this range relate primarily to the electronic processes of transition elements, such as iron. Spectral variability in this wavelength region typically correlates with changes in colour.
- 1415 nm: Troughs observed in this wavelength region are produced by the overtones of the -OH stretch of hydroxyl and indicate the presence of the hydroxyl anion.
- 1930 nm: Troughs observed in this wavelength region are produced by the overtones of the -OH stretch and HOH bend of water and indicate the presence of molecular water.
- 2200 nm: Troughs observed near 2200 nm are produced by the combination band involving the -OH fundamental stretch of hydroxyl bound to aluminum and indicate the presence of white micas such as muscovite and phengite, and clays such as montmorillonite.
- 2330 nm: Troughs observed near 2330 nm can be produced by the Mg-OH bond. The detailed position and shape of troughs in this wavelength region help identify the minerals present.
- 8200 nm: Peaks observed near 8200 nm are produced by the fundamental vibration modes of the Si-O asymmetrical stretch. The wavelength position of these peaks indicates the presence of minerals like quartz.
- 9200 nm: Peaks observed near 9200 nm are produced by the fundamental vibration modes of the Si-O asymmetrical stretch. The wavelength position of these peaks indicates the presence of white micas and chlorites, for example.

The infrared-active minerals identified in this dataset are included in the lithotype legend (Figure 7-2). It is critical to note that spectroscopy of this type is not a quantitative mineralogical technique, and other non-infrared-active minerals can be present in these rocks. Many minerals do not produce intense infrared spectral features that can be easily detected. Therefore, the legend provided for the lithotypes describes only those minerals that produce obvious diagnostic spectral absorption features. For a comprehensive mineralogical assessment of the different lithotypes, other analytical techniques, such as microscopy, X-Ray Diffractometry (XRD), Scanning Electron Microscopy (SEM), and/or Wavelength- or Energy-Dispersive X-Ray Spectroscopy (WDS/EDS), should be employed.

A spectral log was produced for each drill core showing the frequency and distribution of the 18 different lithotypes at one-meter depth intervals. The spectral logs from a series of drill cores selected from this interval are presented in Figures 7-3, 7-4, and 7-5. These drill cores were selected because they are the longest drill cores in this chronostratigraphic interval, and they show the full range of compositional heterogeneity that is observed in these Cretaceous rocks.

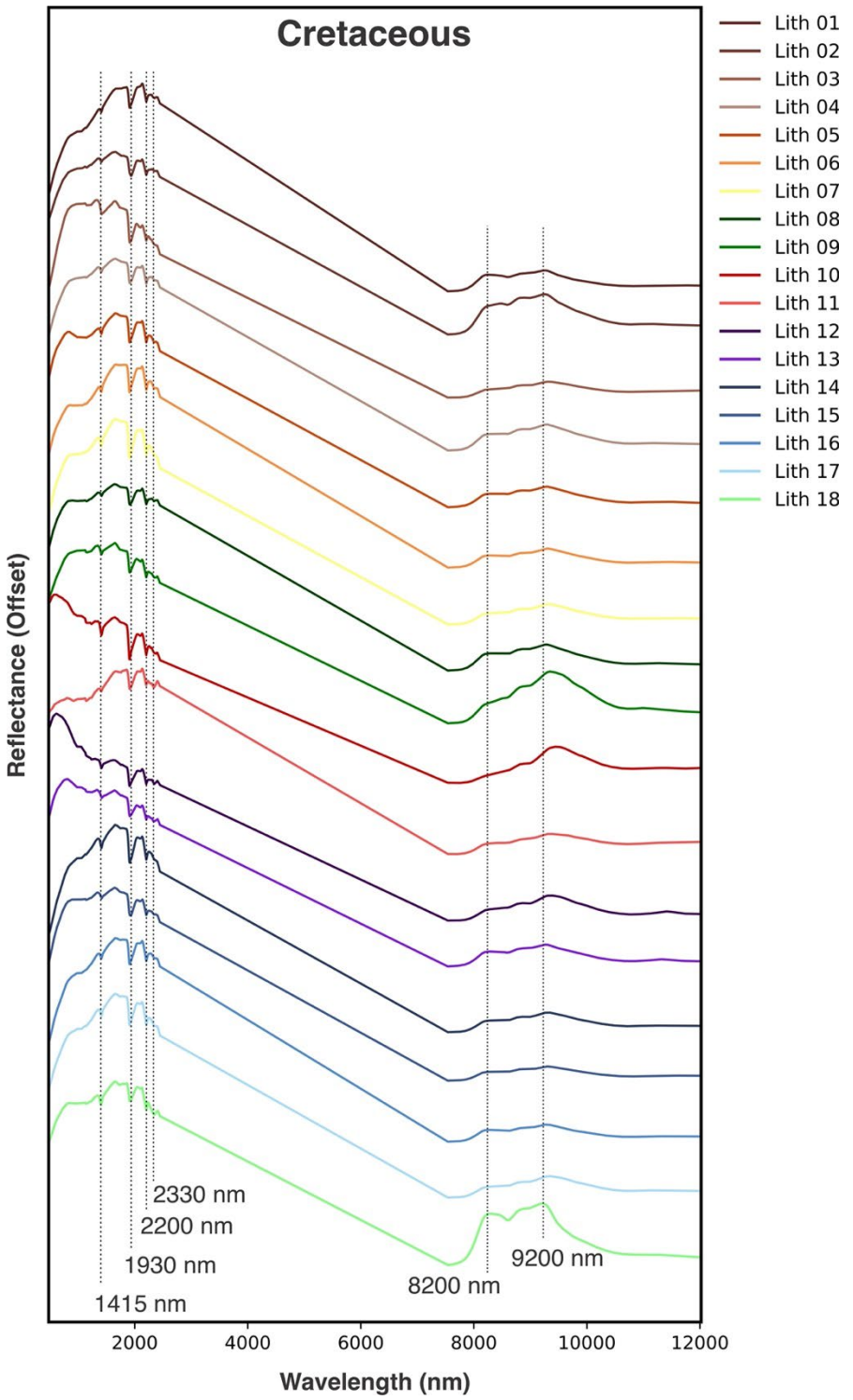

Figure 7-1. Representative spectra for the 18 lithotypes identified in drill cores that primarily intersect Cretaceous rocks. Each spectrum is a composite of data collected from three different wavelength ranges (VNIR, SWIR, and LWIR), and the straight line between 2450 and 7500 nm is due to a gap in sensor coverage. Vertical lines at 1415, 1930, 2200, 2300, 8200, and 9200 nm show locations of important diagnostic spectral features.

Class	Primary SWIR-Active Minerals	Secondary SWIR-Active Mineral	LWIR-Active Minerals
Lith 01	Muscovitic Illite		Phyllosilicates + Quartz
Lith 02	Muscovitic Illite		Phyllosilicates + Quartz
Lith 03	Muscovitic Illite		Phyllosilicates + Quartz
Lith 04	Muscovitic Illite		Phyllosilicates + Quartz
Lith 05	Muscovitic Illite	Fe2+ Bearing	Phyllosilicates + Quartz
Lith 06	Muscovitic Illite	Fe2+ Bearing	Phyllosilicates + Quartz
Lith 07	Muscovitic Illite	Fe2+ Bearing	Phyllosilicates + Quartz
Lith 08	Muscovitic Illite	Fe2+ Bearing	Phyllosilicates + Quartz
Lith 09	Amphibole		Chlorite + Serpentine
Lith 10	Amphibole		Chlorite + Serpentine
Lith 11	Amphibole		Chlorite + Serpentine
Lith 12	Amphibole		Chlorite + Serpentine
Lith 13	Muscovitic Illite		Phyllosilicates + Quartz
Lith 14	Muscovitic Illite		Phyllosilicates + Quartz
Lith 15	Muscovitic Illite		Phyllosilicates + Quartz
Lith 16	Muscovitic Illite		Phyllosilicates + Quartz
Lith 17	Muscovitic Illite		Phyllosilicates + Quartz
Lith 18	Muscovitic Illite		Phyllosilicates + Quartz

Figure 7-2. Legend describing the 18 lithotypes identified in drill cores that intersect Cretaceous rocks. The lithotypes are described in terms of their short- and long-wave infrared-active minerals.

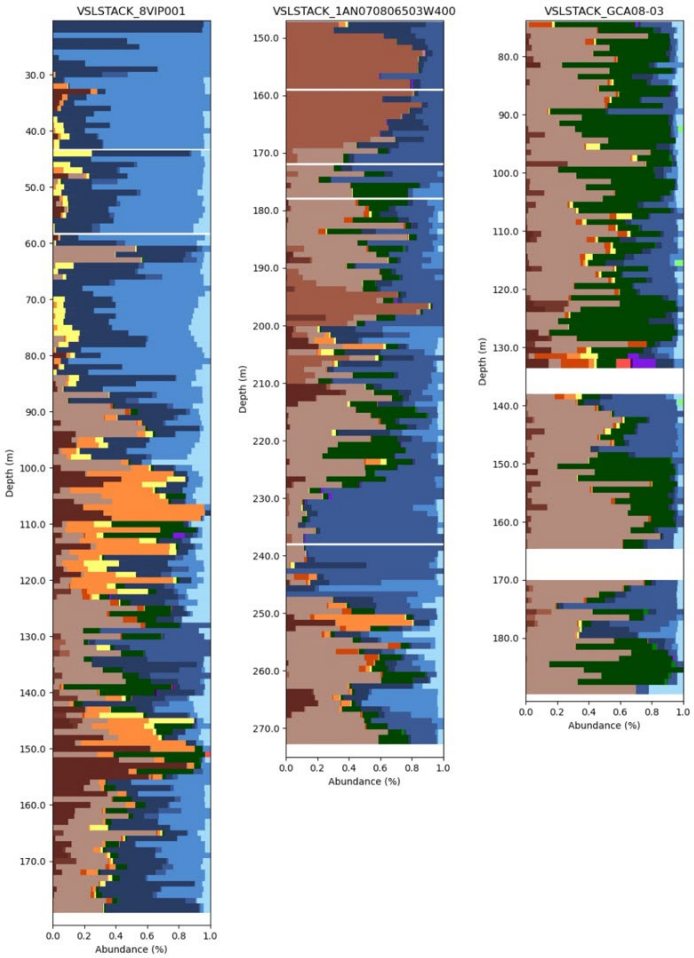

Figure 7-3. Spectral logs for a selection of drill cores that intersect Cretaceous rocks, at one-meter depth binning intervals. The lithotype legend is provided in Figure 7-2.

7.3 Discussion

The Cretaceous is the second-largest interval by meterage in this dataset, with 285 drill cores totalling 11,972 meters, and 18 lithotypes were identified. The identification of such a large number of lithotypes indicates that the Cretaceous encompasses a very wide range of rock compositions, which is consistent with the fact that this interval represents a time of extensive terrestrial and marine deposition in Alberta (Stott, 1982; Bhattacharya et al., 1994; Reinson et al., 1994).

In addition to being a marker of compositional diversity, the lithotypes can also be used as a tool for tracking and tracing sediment sources. For example, lithotype abundances could be used over an extensive areal extent to trace the depositional path or origin of a particular sediment, providing valuable information about the sediment source and depositional conditions.

Overall, the lithotypes identified in this chronostratigraphic interval are overwhelmingly influenced by silicic compositions. For example, illite and quartz are dominant in most spectra, as indicated by the presence of troughs near 2200 nm and peaks at 8200 and 9200 nm (Figure 7-1). In addition, four lithotypes (e.g., Lithotypes 10, 11, 12, and 13) contain spectral features consistent with the presence of mafic minerals (e.g., amphibole and/or pyroxene), which are indicated by troughs near 2330 nm and peaks at 9500 nm. Furthermore, the lithotypes extracted from this interval show little or no evidence of carbonate.

For the Cretaceous, two spectral logs were selected to show how they can be used to build robust compositional correlations between drill cores. The spectral logs for ST00-1 and ST00-2 show that the lithotypes have similar spatial distributions, and strip logs generated visually for these two drill cores show that similar compositional patterns are observed in both drill cores (Figure 7-4). By examining the spatial distribution of the different lithotypes, it is possible to identify distinct compositional zones in multiple drill cores, making the task of correlating compositional units between drill cores more straightforward and reproducible.

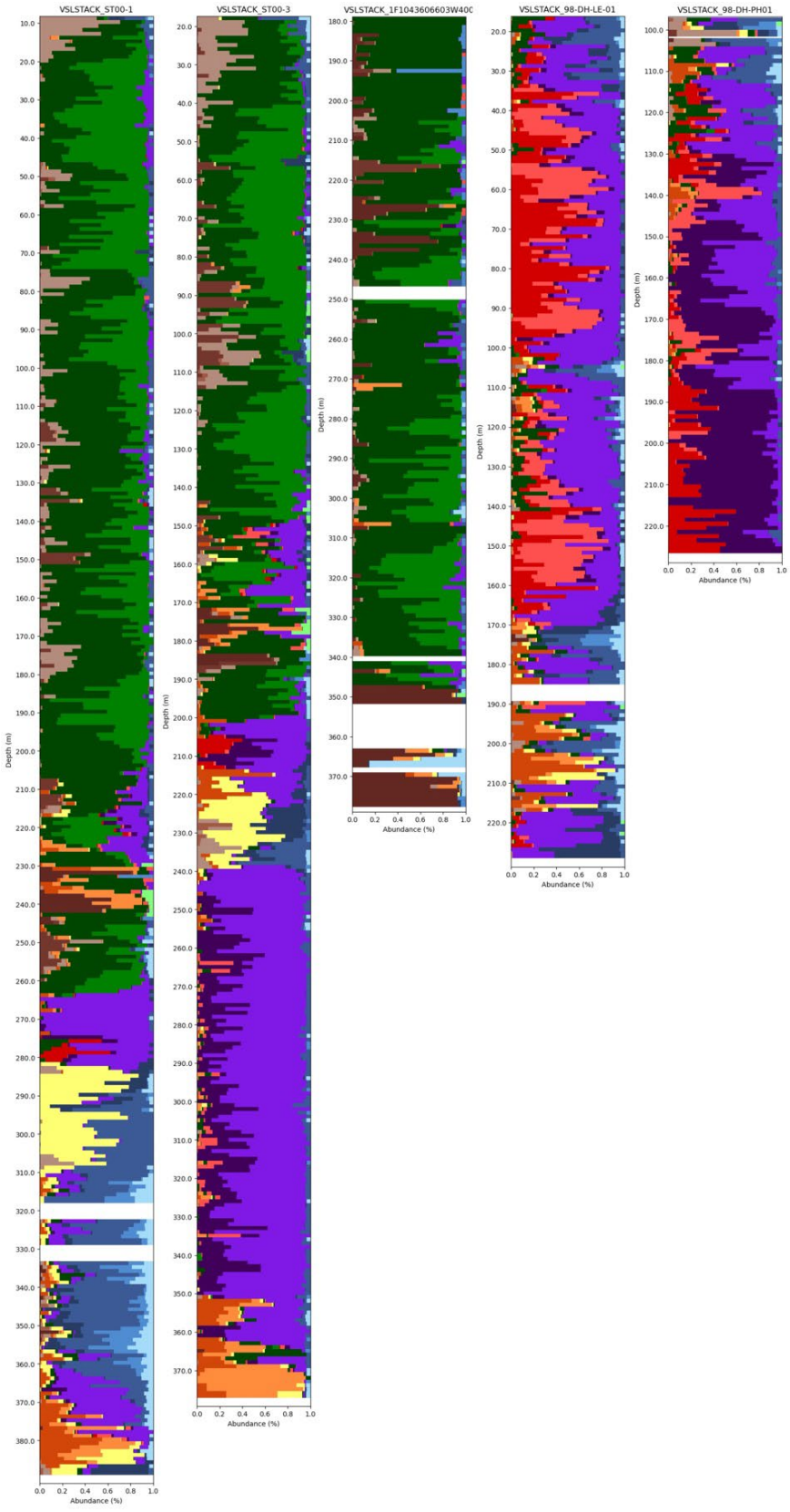

Figure 7-4. Spectral logs for a selection of drill cores that intersect Cretaceous rocks, at one-meter depth binning intervals. The lithotype legend is provided in Figure 7-2.

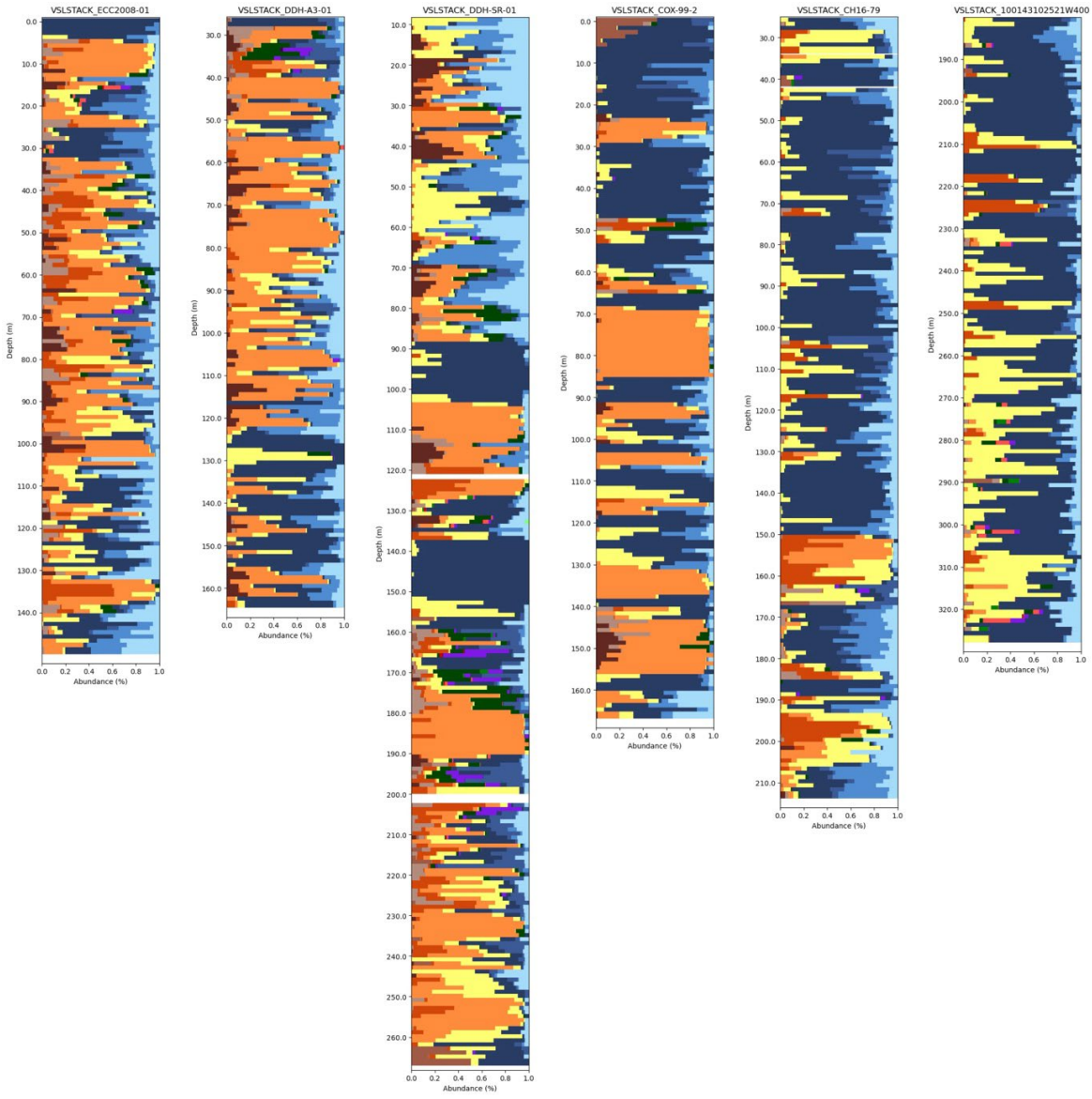

Figure 7-5. Spectral logs for a selection of drill cores that intersect Cretaceous rocks, at one-meter depth binning intervals. The lithotype legend is provided in Figure 7-2.

8. Paleogene-Quaternary

8.1 Overview

A large extinction event at the end of the Cretaceous marked the start of the Paleogene. During the early Paleogene, the inland sea that covered much of Alberta started to recede, leading to the deposition of sandstones, shales, and limestones in marine environments, and coal formations in terrestrial settings (Dawson et al., 1990, and references therein). In the late Paleogene, global temperatures began to fall, and depositional environments shifted to more fluvial and lacustrine settings during a period of mountain uplift (Smith et al., 1990; Leckie, 2006). In the Quaternary, pre-glacial basal gravels were deposited throughout the plains of Alberta during a period of fluvial incision, planation, and deposition (Hardman, et al., 2023). The subsequent advanced and retreat of ice sheets transformed the landscape, while depositing a variety of sediments, including till containing clasts of Precambrian and Paleozoic bedrock (Fenton, et al., 1990). Non-glacial sediments deposited during the Quaternary include stratified material of lacustrine and fluvial origin, ranging from gravel to clay (Teller and Clayton, 1983).

8.2 Results

Altogether 153 drill cores totalling 6,770 meters from this chronostratigraphic interval were analyzed using the Lithotype™ Method (see Section 8.5 for drill core list), and 11 lithotypes were identified.

Table 8-1. Drill cores of Carboniferous to Jurassic rocks analyzed in this study.

Drill Core ID	Number of Boxes	Start Depth (m)	End Depth (m)	Total Length (m)
00DH-16	1	2.6	4.6	2.0
08-002	6	0.3	22.9	22.6
08-003	6	0.4	21.0	20.6
08-004	6	5.3	25.7	20.4
08-005	4	0.6	16.5	15.9
08-006	9	0.6	31.7	31.1
08-007	9	0.4	31.6	31.2
08-008	9	0.6	31.7	31.1
08-009	5	0.4	16.4	16.0
08-010	9	0.6	31.7	31.1
08-011	9	0.3	31.7	31.4
08-012	8	0.7	31.8	31.1
08-013	9	0.6	31.7	31.1
08-015	8	0.5	30.3	29.7
08-016	8	0.5	27.1	26.7
100102706120W500	20	254.5	282.9	28.4
102071307606W400	69	15.0	161.4	146.4
102113304606W500	4	275.6	280.7	5.1
10LD-10A	6	0.0	21.6	21.6
10LD-10B	7	0.0	21.0	21.0
1AB103109405W400	160	3.7	202.7	199.1
8CH-03	14	0.8	23.6	22.9
8CH-05	18	0.8	28.2	27.4
8CH-10	6	0.9	10.1	9.1
8CH-11	8	0.9	13.1	12.2
97DDH-MT19-2	113	6.1	224.6	218.5
97DDH-MT28-1	49	14.3	113.3	99.0
97DDH-MT28-2	78	12.2	175.9	163.7
97DDH-NC05-1	100	20.4	221.6	201.2
97DDH-NC19-1	86	12.2	188.0	175.8
97DDH-NC19-2	73	30.5	178.9	148.4
97DDH-NC20-2	94	9.1	194.2	185.0
97DDH-NC44-1	62	12.8	136.2	123.4
97DDH-NC45-1	62	9.1	139.2	130.1
97DDH-NC5-2	52	24.4	188.1	163.7
97MT-19-1	52	15.0	167.0	152.0
97NC20-1	89	9.1	182.0	172.8
9BAH-001	11	0.0	15.7	15.7
9BAH-002	1	16.5	18.8	2.4
9BAH-003	4	0.0	5.7	5.7
9BAH-004	1	3.8	5.0	1.2
9BAH-005	17	0.8	36.0	35.2
9BAH-006	21	1.7	37.5	35.8
9BAH-007	6	2.4	17.7	15.2
9BAH-008	16	19.2	46.6	27.4
9BAH-009	12	2.4	36.0	33.5
9BAH-010	3	0.9	5.5	4.6
9BAH-011	3	20.7	34.4	13.7
9BAH-012	15	0.9	25.6	24.7
9BAH-013	4	25.6	37.5	11.9
9BAH-014	14	0.9	39.0	38.1
9BAH-015	12	2.9	30.5	27.6
9BAH-016	18	0.9	37.5	36.6
9BAH-017	13	1.7	31.4	29.7
9BAH-018	20	0.9	32.9	32.0
9BAH-019	14	5.5	31.4	25.9
9BAH-020	17	2.4	40.5	38.1

Table 8-1 continued.

Drill Core ID	Number of Boxes	Start Depth (m)	End Depth (m)	Total Length (m)
9BAH-021	14	0.9	22.3	21.3
9BAH-022	12	2.4	20.7	18.3
9BAH-023	10	2.4	17.7	15.2
9BAH-024	9	0.9	16.2	15.2
9BAH-025	23	0.9	39.0	38.1
9BAH-026	12	2.4	29.0	26.5
9BAH-027	21	2.4	37.5	35.1
9BAH-028	18	2.4	45.1	42.7
9BAH-029	10	2.4	26.8	24.4
9BAH-030	19	4.0	45.1	41.2
9BAH-031	14	0.9	34.4	33.5
9BAH-032	12	2.4	45.1	42.7
9BAH-033	9	0.9	14.6	13.7
9BAH-034	9	2.4	17.7	15.2
9BAH-035	21	0.9	39.0	38.1
9BAH-036	21	4.0	36.0	32.0
9BAH-037	17	0.9	31.4	30.5
9BAH-038	12	2.4	25.3	22.9
9BAH-039	17	2.4	28.3	25.9
9BAH-040	25	0.9	42.1	41.2
9BAH-041	23	0.9	42.1	41.2
9BAH-042	5	0.9	8.5	7.6
9BAH-043	17	8.5	43.6	35.1
9BAH-044	20	8.5	42.1	33.5
9BAH-045	27	0.9	45.1	44.2
9BAH-046	25	0.9	40.5	39.6
9BAH-047	28	0.9	43.6	42.7
9BAH-048	20	0.9	37.5	36.6
9BAH-049	19	0.9	29.9	29.0
9BAH-050	29	0.9	45.1	44.2
9BAH-051	29	0.9	45.1	44.2
9BAH-053	12	0.9	42.1	41.2
9BAH-054	12	0.9	39.0	38.1
9BAH-055	18	0.9	42.1	41.2
9BAH-056	22	2.4	39.0	36.6
9BAH-57	21	28.3	63.9	35.5
9BSH-001	12	0.0	23.8	23.8
9BSH-002	3	4.6	9.0	4.4
9BSH-002A	6	3.0	13.4	10.4
9BSH-003	10	0.0	14.5	14.5
9BSH-004	5	0.9	11.6	10.7
9BSH-005	4	0.0	7.6	7.6
9BSH-006	5	0.0	12.8	12.8
9BSH-007	8	0.9	13.1	12.2
9BSH-008	4	2.1	13.1	11.0
9BSH-009	6	0.0	11.3	11.3
9BSH-010	3	0.0	4.0	4.0
9BSH-011	2	0.0	3.5	3.5
9BSH-012	3	0.0	5.3	5.3
9BSH-013	6	0.0	19.2	19.2
9BSH-014	8	0.0	14.3	14.3
BA00-01	6	9.1	65.5	56.4
BA00-02	4	30.5	38.1	7.6
BHH02-10	10	0.0	23.8	23.8
BHH02-11	13	0.0	42.6	42.6
BHH02-8	11	0.0	35.5	35.5
BHH02-9	6	0.0	16.2	16.2

Table 8-1 continued.

Drill Core ID	Number of Boxes	Start Depth (m)	End Depth (m)	Total Length (m)
BU00-02	5	27.4	45.1	17.7
CC-98-20	37	9.1	121.5	112.3
CC-98-21	22	57.9	132.3	74.4
CC98-16	6	61.0	93.6	32.6
CC98-19	8	22.6	67.7	45.1
CC98-22	15	56.4	97.5	41.2
CLK-001	45	20.3	89.3	69.0
CNRL-1-22WOBS-1WN	94	6.3	120.4	114.1
CNRL-10-01-WOBS-1WT	83	0.0	110.9	110.9
CNRL-15-15-WOBS-1WE	96	0.0	114.3	114.2
DDH97-14C-5	10	6.7	58.5	51.8
DDH97-4A-3	4	18.9	27.5	8.6
DDH97-5A-9	3	5.7	72.2	66.6
DDH97-6-7	16	5.2	160.3	155.1
DDH97-612	29	52.5	96.6	44.1
DDH97-6E-01	50	5.8	99.5	93.7
DDH97-MT24-2	91	16.8	189.3	172.5
DDH97-NC44-2	58	15.2	184.9	169.7
DDH97-NC45-2	55	15.2	178.9	163.7
ECC2008-10	78	0.0	149.5	149.5
FC-011	4	33.6	56.4	22.8
JZ02-01	1	82.0	85.0	3.0
L06-03	6	37.1	56.3	19.2
PM-00-06	7	3.7	25.9	22.3
PM-00-07	7	3.7	25.9	22.3
PR17-1	7	7.6	43.3	35.7
PR3-1	10	27.4	68.6	41.2
PR98-07	20	41.1	84.4	43.3

The representative spectra for each lithotype are provided in Figure 8-1. Each spectrum is a composite of data collected from three different hyperspectral imaging cameras (VNIR, SWIR, and LWIR), and the straight line between 2450 and 7500 nm is due to a gap in sensor coverage. Vertical lines at 1415, 1930, 2200, 2300, 8200, and 9200 nm show the locations of important spectral features (Figure 8-1).

Although there are numerous features observed in these spectra, there are seven spectral regions of interest that provide important compositional information: 400-1000, 1415, 1930, 2200, 2330, 8200, and 9200 nm.

- 400-1000 nm: Referred to as the visible and near-infrared (VNIR), troughs and peaks observed in this range relate primarily to the electronic processes of transition elements, such as iron. Spectral variability in this wavelength region typically correlates with changes in colour.
- 1415 nm: Troughs observed in this wavelength region are produced by the overtones of the -OH stretch of hydroxyl and indicate the presence of the hydroxyl anion.
- 1930 nm: Troughs observed in this wavelength region are produced by the overtones of the -OH stretch and HOH bend of water and indicate the presence of molecular water.
- 2200 nm: Troughs observed near 2200 nm are produced by the combination band involving the -OH fundamental stretch of hydroxyl bound to aluminum and indicate the presence of white micas such as muscovite and phengite, and clays such as montmorillonite.
- 2330 nm: Troughs observed near 2330 nm can be produced by the Mg-OH bond. The detailed position and shape of troughs in this wavelength region help identify the minerals present.
- 8200 nm: Peaks observed near 8200 nm are produced by the fundamental vibration modes of the Si-O asymmetrical stretch. The wavelength position of these peaks indicates the presence of minerals like quartz.
- 9200 nm: Peaks observed near 9200 nm are produced by the fundamental vibration modes of the Si-O asymmetrical stretch. The wavelength position of these peaks indicates the presence of white micas and other phyllosilicates, for example.

The infrared-active minerals identified in this dataset are included in the lithotype legend (Figure 8-2). It is critical to note that spectroscopy of this type is not quantitative, and there can be many other minerals in these rocks that are not infrared active. Many minerals do not produce intense infrared spectral

features that can be easily detected. Therefore, the legend provided for the lithotypes describes only those minerals that produce obvious diagnostic spectral absorption features. For a comprehensive mineralogical assessment of the different lithotypes, other analytical techniques, such as microscopy, X-Ray Diffractometry (XRD), Scanning Electron Microscopy (SEM), and/or Wavelength- or Energy-Dispersive X-Ray Spectroscopy (WDS/EDS), should be employed.

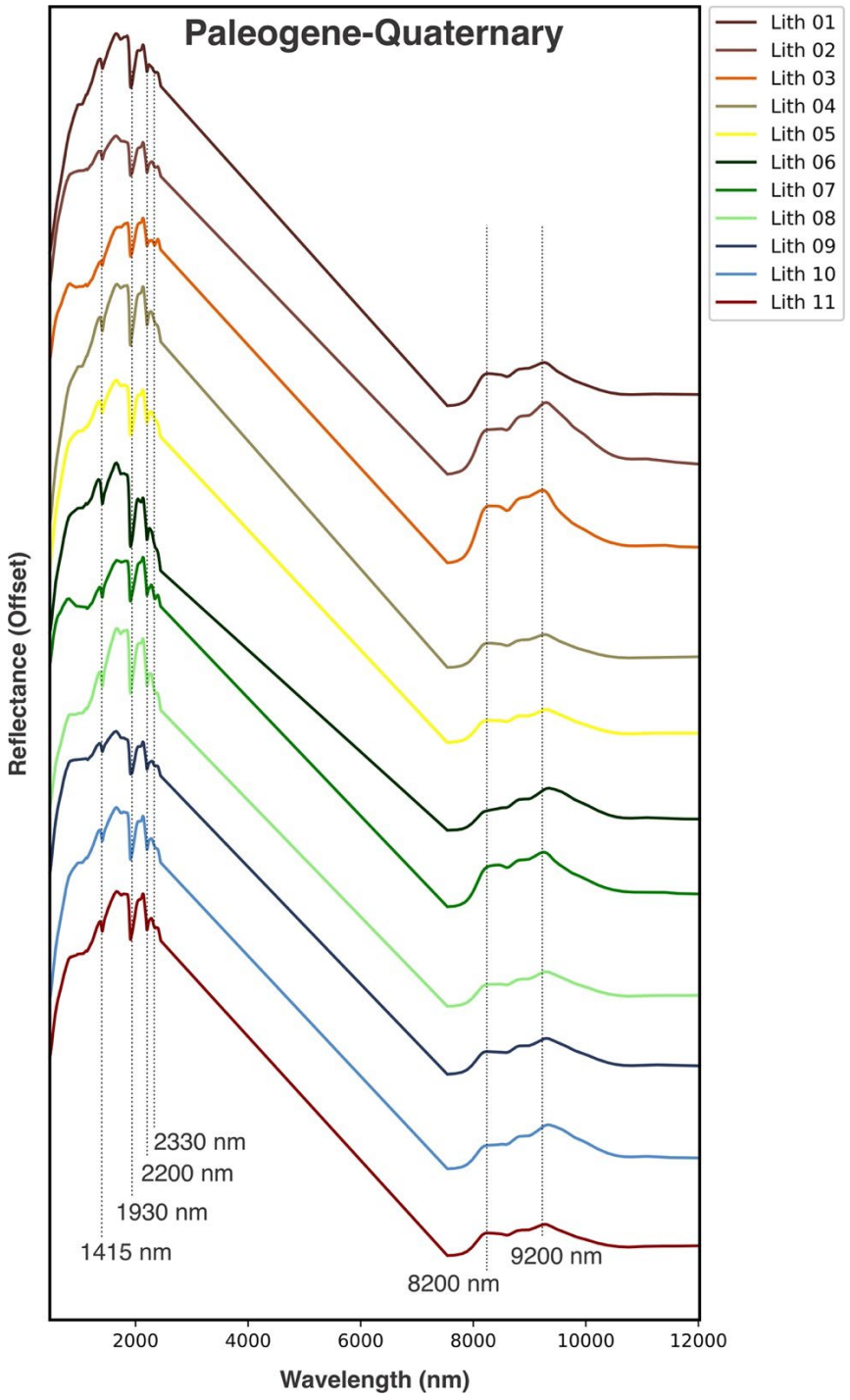

Figure 8-1. Representative spectra for the 11 lithotypes identified in drill cores that intersect Paleogene to Quaternary rocks. Each spectrum is a composite of data collected from three different wavelength ranges (VNIR, SWIR, and LWIR), and the straight line between 2450 and 7500 nm is due to a gap in sensor coverage. Vertical lines at 1415, 1930, 2200, 2300, 8200, and 9200 nm show locations of important diagnostic spectral features.

Class	Primary SWIR-Active Minerals	Secondary SWIR-Active Mineral	LWIR-Active Minerals
Lith 01	Muscovitic Illite		Phyllosilicates + Quartz
Lith 02	Muscovitic Illite		Phyllosilicates + Quartz
Lith 03	Muscovitic Illite	Fe2+ Bearing	Phyllosilicates + Quartz
Lith 04	Muscovitic Illite		Phyllosilicates + Quartz
Lith 05	Muscovitic Illite		Phyllosilicates + Quartz
Lith 06	Muscovitic Illite	Fe2+ Bearing	Phyllosilicates + Quartz
Lith 07	Muscovitic Illite	Fe2+ Bearing	Phyllosilicates + Quartz
Lith 08	Muscovitic Illite	Fe2+ Bearing	Phyllosilicates + Quartz
Lith 09	Muscovitic Illite		Phyllosilicates + Quartz
Lith 10	Muscovitic Illite		Phyllosilicates + Quartz
Lith 11	Muscovitic Illite		Phyllosilicates + Quartz

Figure 8-2. Legend describing the 11 lithotypes identified in drill cores that intersect Paleogene and Quaternary rocks. The lithotypes are described in terms of their short- and long-wave infrared-active minerals.

8.3 Discussion

As observed in the reflectance spectra, the rocks from this chronostratigraphic interval are dominated by silicate minerals, such as illite and quartz, which are inferred by the presence of troughs near 2200 nm and 2300 nm, and peaks at 8200 and 9200 nm (Figures 8-1 and 8-2). No carbonate spectral features were identified in this interval. Altogether 11 lithotypes were identified from 153 drill cores totalling 6,770 meters. The presence of 11 lithotypes is typical for a dataset of this size, and shows that while there is some compositional variability, these rocks are not overly diverse.

The spectral logs shown in Figures 8-3 and 8-4 show distinct lithotype distribution trends, which is important because these two drill core collections originate from different locations.

For example, Figure 8-3 shows drill core from the Paskapoo Formation, which contains an important aquifer system (Grasby et al., 2014; Hughes et al., 2017). In these drill cores, a Paleogene fluvial deposit is dominated by siltstone and mudstone and is interbedded with highly permeability coarse-grained channel sands (Grasby et al., 2008). It is possible to use the different lithotypes as indicators of distinct compositional units. For example, in drill cores 97DDK-NC05-1, 97DDK-NC05-2, and 97DDK-NC019-1, Lithotype 6 forms distinct compositional layers that may have an effect on the permeability of these rocks.

In Figure 8-4, drill cores from locations overlying the Wiau Valley are presented, which are linked with Early Pleistocene glaciation in north-central Alberta (Andriashek and Barendregt, 2017), with Lithotype 4 correlating with more oxidized layers in these sediments.

The abundance and distribution of different lithotypes in the spectral logs can be used as a tool for correlation and also tracking and tracing different sediment sources. Mapping lithotype abundances over wider areas could be used to trace the depositional path or origin of a particular sediment source, which would provide important information about fluid flow and depositional environments in a particular area.

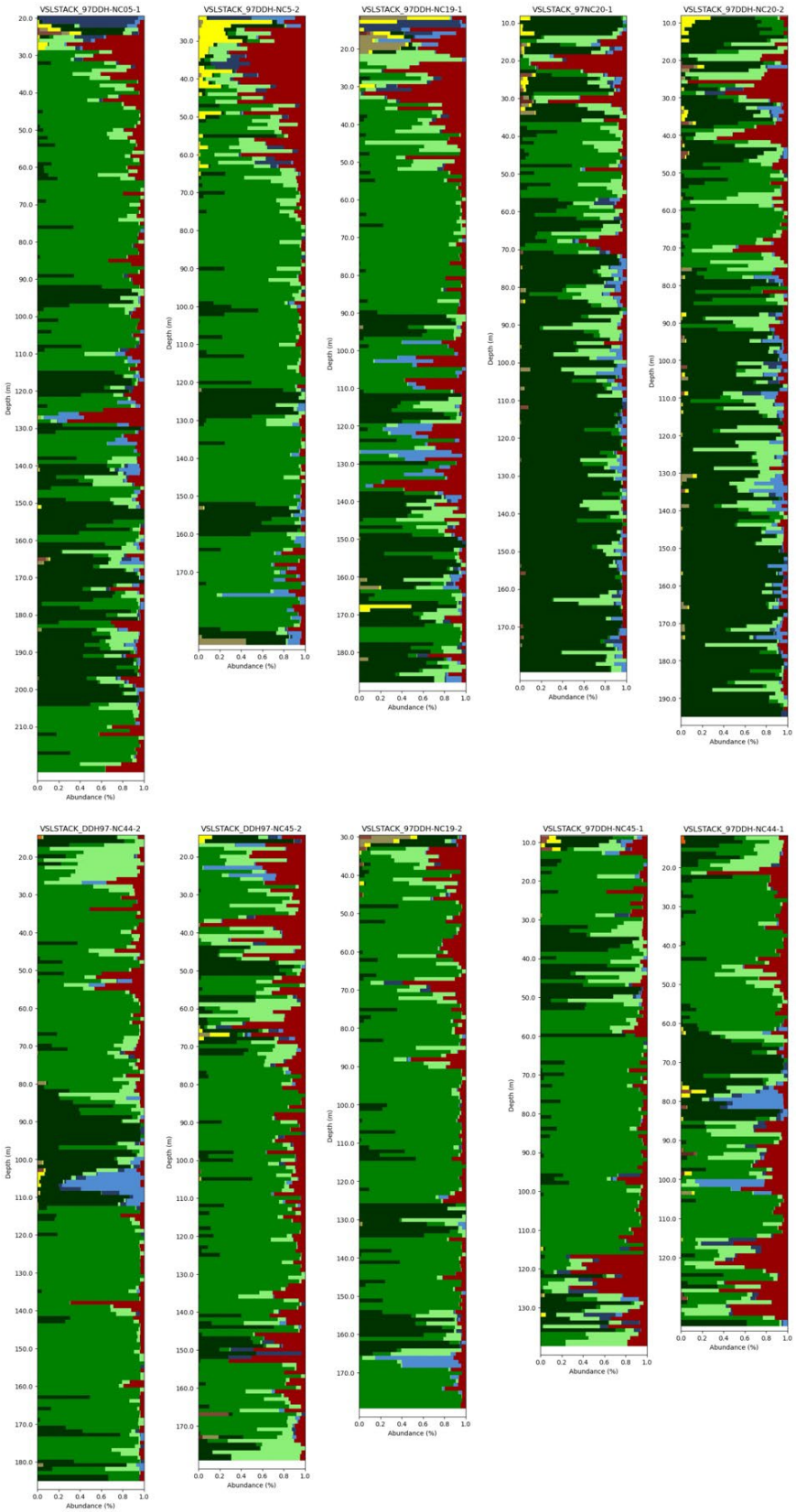

Figure 8-3. Spectral logs for a selection of drill cores from the Paskapoo formation that intersect Paleogene to Quaternary rocks, at one-meter depth binning intervals. The lithotype legend is provided in Figure 8-2.

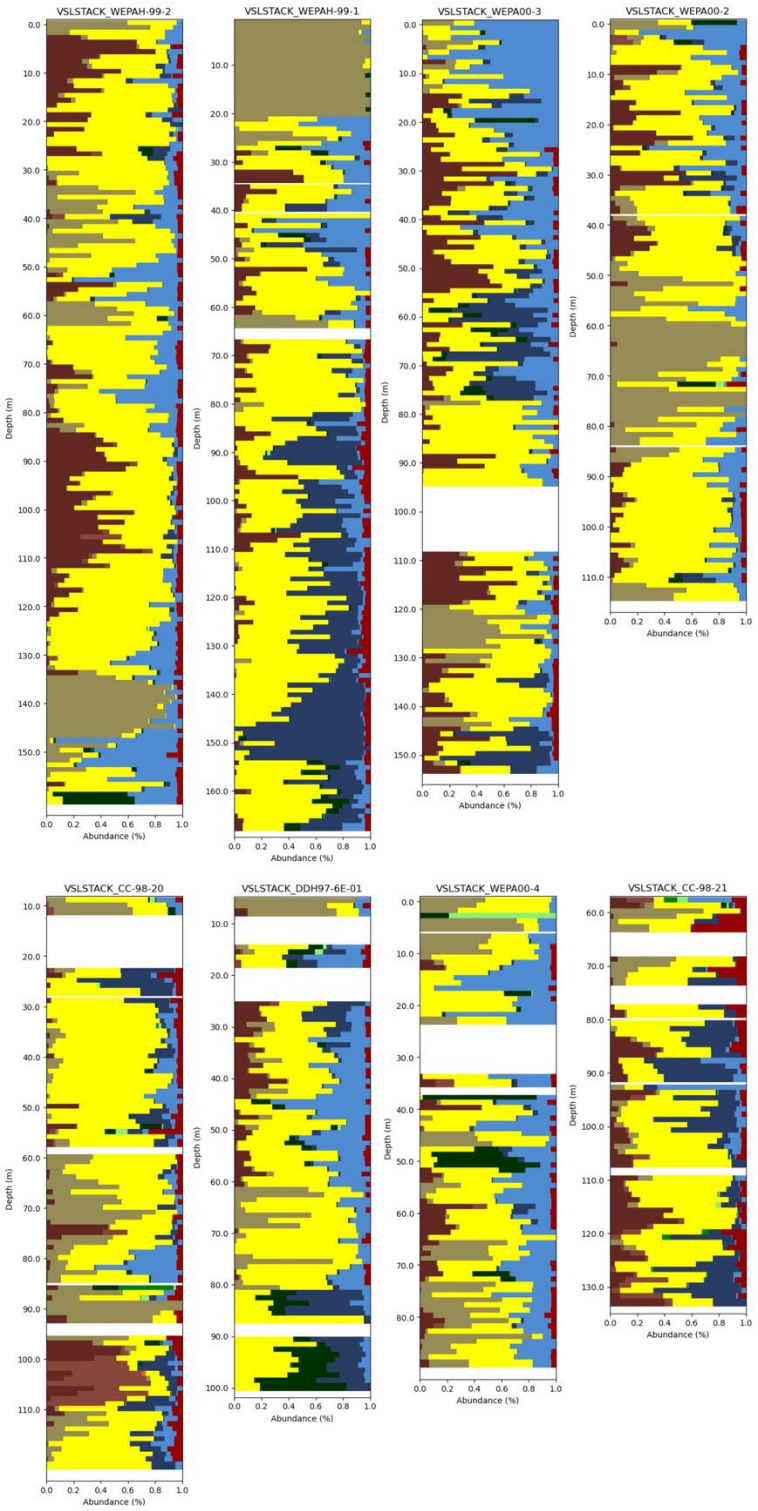

Figure 8-4. Spectral logs for a selection of drill cores from above the buried Wiau Valley that intersect Paleogene to Quaternary rocks, showing a record of Early Pleistocene glaciation, at one-meter depth binning intervals. The lithotype legend is provided in Figure 8-2.

9. Conclusions

9.1 Overview

Due to the subjective nature of human observation, most lithologic logs created visually are not reproducible, and they can contain errors and unintentional omissions. While it can be more straightforward to generate accurate lithologic logs from drill cores dominated by flat-lying sediments, such as those that are found throughout Alberta, it is still very difficult for the human eye to differentiate between subtle changes in composition that may affect correlation relationships. As a result, it is vital to have objective and continuous compositional information. Continuous compositional information is best provided using hyperspectral rock scanning instruments. However, some systems can be very expensive to operate, produce very large volumes of data, and generate outputs that can be difficult to integrate into existing workflows.

HII has developed a novel method of data processing for hyperspectral imagery that reduces data volumes by >97%. Furthermore, through the use of its Lithotype -Method, HII is able to identify distinct compositional groups in hyperspectral data to produce spectral logs, which should then be combined with textural and structural information to generate lithologic logs.

Although the spectral logs produced using the Lithotype™ Method are reproducible and can be validated using auxiliary data (e.g., XRF, Gamma Ray, XRD, etc.), it is the responsibility of the qualified geologist working on a project to ensure that the results of all data sources have been reviewed and considered. It is therefore strongly suggested that the spectral logs generated using the Lithotype™ Method be used in combination with other data sources to validate and critique the spectral logs, with the goal of ensuring that all outputs are robust and reproducible.

Spectral logs can be used to better understand the Western Canadian Sedimentary Basin and its underlying Archean and Proterozoic rocks. In particular, spectral logs can be used to identify units of identical composition, which allow accurate correlations between different drill cores. This could be particularly useful in locations where multiple episodes of transgression and regression have produced a complex assemblage of repeating sediments, and where fossils that can help with correlation are absent. Without continuous compositional information, it would be difficult to map the different stratigraphic layers accurately. Plus, the spectral logs can be used to trace the source, movement, and distribution of compositionally distinct sedimentary packages.

9.2 Lithotype Extraction and Mineralogy Assignment

Overall, the goal of this project is to provide additional insights into the compositional characteristics of the rocks in Alberta. To accomplish this, a series of lithotypes were extracted for each chronostratigraphic interval of interest (Table 1-1).

To identify lithotypes, reflectance spectra were organized into groups based on spectral similarity and spatial proximity. A lithotype is a compositional group that represents a distinct mineral assemblage that produces a distinct set of spectra. It is a very sensitive method for extracting compositional information from a hyperspectral dataset. However, it is critical to note that hyperspectral data collected from rocks cannot be used to generate quantitative mineralogical results because the rocks can contain many rock-forming minerals that are not strongly infrared active.

Therefore, the lithotype legend provided for the different chronostratigraphic intervals describes only those minerals that produce intense and obvious spectral absorption features. Although some mineral assemblages are repeated within the legends (e.g., the lithotype legend for the Carboniferous to Jurassic interval contains “Carbonate + Illite” as the primary SWIR-active minerals for 15 of the 17 identified lithotypes; Figure 6-1), subtle differences between the lithotypes exist. Spectral differences of this type are due to minor changes in mineral chemistry, mineral abundance, and/or the presence of other minerals that are not highly infrared active. Overall, the spectral logs produced by the Lithotype™ Method do not typically provide direct evidence for the deposition of economically important minerals or metals. Instead, the spectral logs provide a measure of subtle compositional change that can be used as a tool to identify zones of exploration interest.

For a comprehensive mineralogical assessment of the different lithotypes, other analytical techniques, such as microscopy, X-Ray Diffractometry (XRD), Scanning Electron Microscopy (SEM), and/or Wavelength- or Energy-Dispersive X-Ray Spectroscopy (WDS/EDS), should be employed.

9.3 Compositional Trends

In total, there were 87 lithotypes extracted from all seven chronostratigraphic intervals (Table 1-1). To illustrate existing compositional trends, these lithotypes were divided into two groups: (1) carbonate-bearing lithotypes, and (2) silicic-dominated lithotypes, using a band ratio that calculates the intensity of the carbonate peak at 11,200 nm and divides it by the absolute intensity of the spectrum at 10,700 nm (Figure 9-1).

These results show the presence of a carbonate field and a silicic field. During the Archean to Proterozoic, the lithotypes are dominated by silicic compositions. In the Cambrian to the Lower Ordovician, there is a mix of silicic and carbonate compositions. The lithotypes in the Devonian are overwhelmingly dominated by carbonates, with carbonates persisting until the end of the Jurassic.

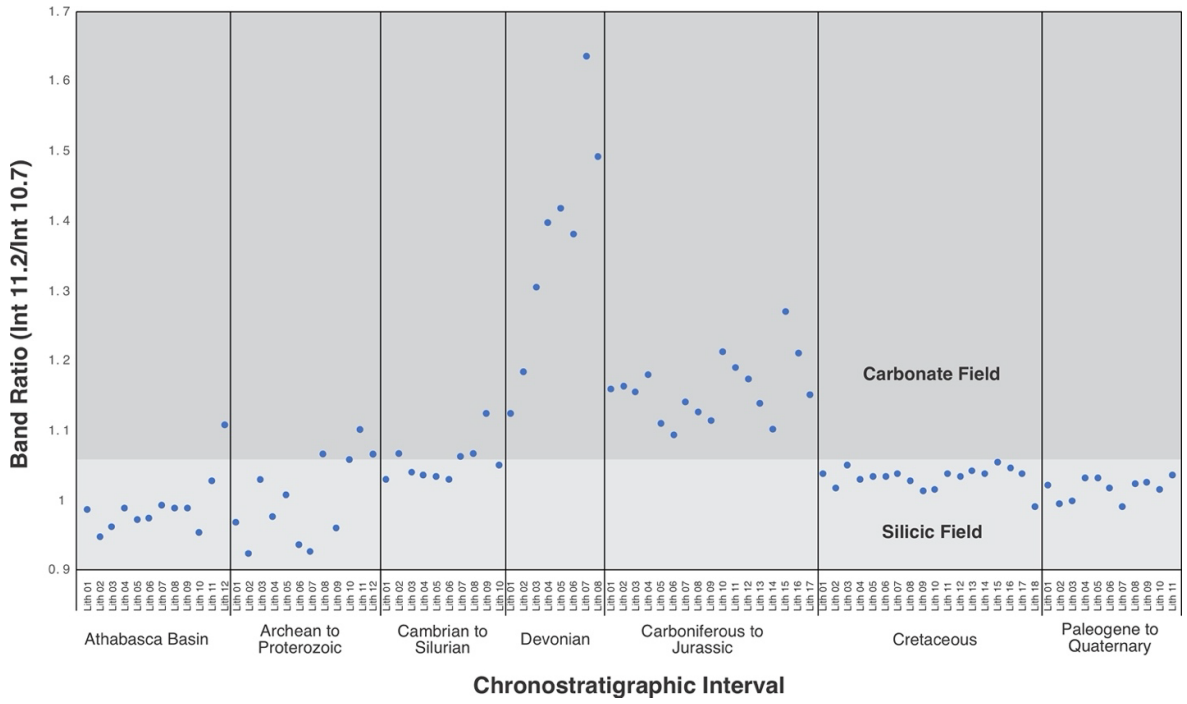

Figure 9-1. Band ratio calculation showing whether individual lithotypes plot in the carbonate or silicic field.

From the Cretaceous to the Quaternary, the lithotypes are dominated by silicic compositions. Overall, this lithotype plot shows how the rock compositions of Alberta transitioned from silicic to carbonate to silicic again through time.

References

Aitken, J. D. (1989). The Sauk sequence—Cambrian to Lower Ordovician miogeocline and platform.

Andriashek, L. D., and Barendregt, R. W. (2017). Evidence for Early Pleistocene glaciation from borecore stratigraphy in north-central Alberta, Canada. *Canadian Journal of Earth Sciences*, *54*(4), 445-460.

Bhattacharya, J. P., Mossop, G. D. and Shetsen, I. (1994). Cretaceous Dunvegan Formation of the Western Canada Sedimentary Basin. In: *Geological atlas of the Western Canada Sedimentary Basin*. G. D. Mossop and I. Shetsen (comp.), Canadian Society of Petroleum Geologists and Alberta Research Council, pp. 365-373.

Burwash, R. A., McGregor, C. R., and Wilson, J. A. (1990). Precambrian basement beneath the Western Canada sedimentary basin. *Bulletin of Canadian Petroleum Geology, 38*(1), 158-159.

Caldwell, W. G. E. (1984). Early Cretaceous transgressions and regressions in the southern Interior Plains. In: *The Mesozoic of Middle North America*. D. F. Stott and D. J. Glass (eds.). Canadian Society of Petroleum Geologists, Memoir 9, 173-203.

Collier, B. (2005). Sequence stratigraphy and its use for uranium exploration in the western Athabasca Basin of Alberta and Saskatchewan: Alberta Energy and Utilities Board, EUR/AGS Earth Report 2004-01.

Dawson, F. M., Evans, C., Marsh, R., and Power, B. (1990). Uppermost Cretaceous-Tertiary strata of the Western Canada Sedimentary Basin. *Bulletin of Canadian Petroleum Geology*, *38*(1), 160-161.

Edwards, D. E., Barclay, J. E., Gibson, D. W., Kvill, G., and Halton, E. (1990). Triassic strata of the Western Canada sedimentary basin. *Bulletin of Canadian Petroleum Geology*, *38*(1), 163-163.

Fenton, M. M., Pawlowicz, J. G., Schreiner, B. T., and Nielsen, E. (1990). Quaternary geology of the Western Plains. *Bulletin of Canadian Petroleum Geology*, *38*(1), 163-163.

Grasby, S. E., Chen, Z., Hamblin, A. P., Wozniak, P. R. J. and Sweet, A. R. (2008). Regional characterization of the Paskapoo bedrock aquifer system, southern Alberta. *Canadian Journal of Earth Sciences*, *45*(12): 1501–1516.

Grasby, S. E., Betcher, R. N., Maathuis, H., and Wozniak, P. R. J. (2014). Chapter 10: Plains Region. In: *Canada's Groundwater Resources.* Rivera, A. (ed.), 360-413.

Halbertsma, H. L, Mossop, G. D. and Shetsen, I. (1994). Devonian Wabamun Group of the western Canada sedimentary basin. In: *Geological atlas of the Western Canada Sedimentary Basin*. G. D. Mossop and I. Shetsen (comp.), Canadian Society of Petroleum Geologists and Alberta Research Council, pp. 203-220.

Hartman, G. M., Pawley, S. M., Utting, D. J., Atkinson, N., and Liggett, J. E. (2023). The Empress Group in Alberta, Canada. *Canadian Journal of Earth Sciences*, *61*(1), 86-101.

Hayes, B. J. R., Christopher, J. E., Rosenthal, L., Los, G., McKercher, B., Minken, D., DeWinton, Y. M., Fennell, J., and Smith, D. G. (1994). Cretaceous Mannville Group of the western Canada sedimentary basin. In: *Geological atlas of the Western Canada Sedimentary Basin*. G. D. Mossop and I. Shetsen (comp.), Canadian Society of Petroleum Geologists and Alberta Research Council, pp. 317-334.

Hein, F. J. (1987). Tidal/littoral offshore shelf deposits—Lower Cambrian Gog Group, Southern Rocky Mountains, Canada. *Sedimentary Geology*, *52*(3-4), 155-182.

Henderson, C. M. (1990). Permian strata of the Western Canada sedimentary basin. *Bulletin of Canadian Petroleum Geology*, *38*(1), 166-166.

Hughes, A. T., Smerdon, B. D., and Alessi, D. S. (2017). Hydraulic properties of the Paskapoo Formation in west-central Alberta. *Canadian Journal of Earth Sciences*, *54*(8), 883-892.

Kent, D. M., Mossop, G. D., and Shetsen, I. (1994). Paleogeographic evolution of the cratonic platform-Cambrian to Triassic. In: *Geological atlas of the Western Canada Sedimentary Basin*. G. D. Mossop and I. Shetsen (comp.), Canadian Society of Petroleum Geologists and Alberta Research Council, pp. 69-86.

Krebs, W. and Macqueen, R. W. (1984). Sequence of diagenetic and mineralization events, Pine Point lead-zinc property, Northwest Territories, Canada. *Bulletin of Canadian Petroleum Geology*, *32*, 434-464.

Kupsch, B. G. and Catuneanu, O. (2002). Preliminary results from a study of the geology and alteration at the Maybelle River uranium zone, Athabasca Basin, Alberta, EXTECH IV. In: *Summary of Investigations 2002, Volume 2*, Saskatchewan Geological Survey, Sask. Industry Resources, Misc. Rep. 2002-4.2, CD-ROM, Paper D-11, 8p.

Layer, D. B. (1949) Leduc Oil Field, Alberta, A Devonian Coral-Reef Discovery. *AAPG Bulletin 33*(4): 572–602.

Leckie D.A. (2006). Tertiary fluvial gravels and evolution of the Western Canadian Prairie Landscape. *Sedimentary Geology*, *190*: 139–158.

Meijer Drees, N. C., Mossop, G. D., and Shetsen, I. (1994). Devonian Elk point group of the western Canada sedimentary basin. In: *Geological atlas of the Western Canada Sedimentary Basin*. G. D. Mossop and I. Shetsen (comp.), Canadian Society of Petroleum Geologists and Alberta Research Council, pp.129-138.

Nguyen, N. and Pham, D. (2019). Tendencies of Mining Technology Development in Relation to Deep Mines. *Mining Science and Technology, 4*, 16-22.

Norford, B. S., Haidl, F. M., Bezys, R. K., Cecile, M. P., McCabe, H. R., Paterson, D. F. and Shetson, I. (1994). Middle Ordovician to lower Devonian strata of the western Canada sedimentary basin. In: *Geological atlas of the Western Canada Sedimentary Basin*. G. D. Mossop and I. Shetsen (comp.), Canadian Society of Petroleum Geologists and Alberta Research Council, pp. 109-127.

O'Connell, S. C., Dix, G. R., and Barclay, J. E. (1990). The origin, history, and regional structural development of the Peace River Arch, Western Canada. *Bulletin of Canadian Petroleum Geology, 38*(1), 4-24.

Oldale, H. S., Munday, R. J., Mossop, G. D., and Shetsen, I. (1994). Devonian Beaverhill Lake Group of the western Canada sedimentary basin. In: *Geological atlas of the Western Canada Sedimentary Basin*. G. D. Mossop and I. Shetsen (comp.), Canadian Society of Petroleum Geologists and Alberta Research Council, pp. 149-164.

Orr, R. G. (1989a): Assessment report for mineral exploration permits 6884120001-2, 6884120001, 6886050002-6 and 68887090002, July 1, 1986, to December 31, 1988; Alberta Geological Survey, Alberta Energy and Utilities Board, Assessment Report File 19890003.

Orr, R. G. (1989b): Assessment report for mineral exploration permits 6884120001-2, and 6884120001, January 1, 1989, to September 30, 1989; Alberta Geological Survey, Alberta Energy and Utilities Board, Assessment Report File 19890004.

Post, R. T. (2004): Stratigraphy and sedimentology of the Athabasca Group in the Net Lake-Maybelle River area, northeastern Alberta; Alberta Energy and Utilities Board, E*UB/AGS Earth Sciences Report* 2003-01, 103 p.

Poulton, T. P., Christopher, J. E., Hayes, B. J. R., Losert, J., Tittemore, J., Gilchrist, R. D., and Victoria, J. (1994). Jurassic and lowermost Cretaceous strata of the Western Canada sedimentary basin. In: *Geological atlas of the Western Canada Sedimentary Basin*. G. D. Mossop and I. Shetsen (comp.), Canadian Society of Petroleum Geologists and Alberta Research Council, pp. 297-316.

Ramaekers, P., Yeo, G., and Jefferson, C. (2001). Preliminary overview of regional stratigraphy in the late Paleoproterozoic Athabasca Basin, Saskatchewan and Alberta. *Summary of Investigations*, *2*, 2001-4.

Reinson, G. E., Warters, W. J., Cox, J., Price, P. R., Mossop, G. D., and Shetsen, I. (1994). Cretaceous Viking formation of the western Canada sedimentary basin. In: *Geological atlas of the Western Canada Sedimentary Basin*. G. D. Mossop and I. Shetsen (comp.), Canadian Society of Petroleum Geologists and Alberta Research Council, pp. 353-364.

Richards, B. C., Barclay, J. E., Osadetz, K. G., Trollope, F. H., and Hartling, A. (1990). Carboniferous strata of the Western Canada sedimentary basin. *Bulletin of Canadian Petroleum Geology*, *38*(1), 178-178.

Ramaekers, P. (2004). Development, stratigraphy and summary diagenetic history of the Athabasca Basin, early Proterozoic of Alberta, and its relation to uranium potential; Alberta Energy and Utilities Board, EUB/AGS Special Report 62. 85 p.

Slind, O. L., Andrews, G. D., Murray, D. L., Norford, B. S., Paterson, D. F., Salas, C. J., Tawadros, E.E., and Aitken J.D. (1994). Middle Cambrian to Lower Ordovician strata of the western Canada sedimentary basin. In: *Geological atlas of the Western Canada Sedimentary Basin*. G. D. Mossop and I. Shetsen (comp.), Canadian Society of Petroleum Geologists and Alberta Research Council, pp. 87-108.

Smith, D. G., and Leckie, D. A. (1990). The Paleogeographic Evolution of the Western Canada Foreland Basin. *Bulletin of Canadian Petroleum Geology, 38*(1), 181-181.

Stott, D. F. (1982). Lower Cretaceous Fort St. John Group and Upper Cretaceous Dunvegan Formation of the foothills and plains of Alberta, British Columbia, District of Mackenzie and Yukon Territory. *Geological Survey of Canada, Bulletin* 328, 124 p.

Taylor, G. C., Macqueen, R. W., and Thompson, R.I. (1975). Facies change, breccias, and mineralization in Devonian rocks of the Rocky Mountains, northeastern British Columbia (94B, G, K, N). In: Report of Activities, Part A, *Geological Survey of Canada, Paper* 75-1A, p. 577-585.

Teller, J. T. and Clayton, L. (1983). Glacial Lake Agassiz; *Geological Association of Canada, Special Paper* 26, 451 p.

Williams, G. D. and Stelck, C. R. (1975). Speculations on the Cretaceous palaeogeography of North America. In: *The Cretaceous System in the Western Interior of North America*. W. G. E. Caldwell (ed.). Geological Association of Canada, Special Paper 13, p. 1-20.

Wilson, J. A. (1986). Geology of the basement beneath the Athabasca Basin in Alberta. *Alberta Research Council, Bulletin* 55, 61 p.